



International Committee for Future Accelerators

Sponsored by the Particles and Fields Commission of IUPAP

Beam Dynamics Newsletter

No. 66

**Issue Editor:
R. Wanzenberg**

**Editor in Chief:
W. Chou**

April 2015

Contents

1	FOREWORD.....	7
1.1	FROM THE ICFA CHAIR.....	7
1.2	FROM THE PANEL CHAIR.....	8
1.3	FROM THE EDITOR.....	9
2	RADIATION DAMAGE OF ACCELERATOR COMPONENTS – DETECTION, MEASUREMENTS AND SIMULATIONS	10
2.1	ELECTRON BEAM HALO MONITORING USING DIAMOND-BASED DETECTORS TO PROTECT UNDULATOR PERMANENT MAGNETS FROM RADIATION DAMAGE.....	10
2.1.1	Introduction	10
2.1.2	Evaluation of Diamond-based Detectors.....	12
2.1.3	Mechanical Design of Beam Halo Monitor.....	13
2.1.3.1	<i>Diamond-based Detectors</i>	13
2.1.3.2	<i>Micro-stripline Structure</i>	14
2.1.3.3	<i>Rf fingers with Aluminum Windows</i>	15
2.1.3.4	<i>Final Design of Beam Halo Monitor</i>	17
2.1.4	Operational Results in SACLA	18
2.1.4.1	<i>Effect on Electron Beam Quality</i>	18
2.1.4.2	<i>Filtering of Residual High-Frequency Components</i>	19
2.1.4.3	<i>Scattering of Beam Core at RF Fingers</i>	20
2.1.4.4	<i>Measurement of Vertical Beam Halo Profile</i>	21
2.1.5	Conclusions	22
2.1.6	References	23
2.2	FAST BEAM LOSS DIAGNOSTIC TO QUANTIFY CHARGE DEPOSITION IN APS SUPERCONDUCTING UNDULATORS	24
2.2.1	Introduction and Motivation.....	24
2.2.2	Beam Loss Monitor Description	25
2.2.3	Calibration of FO BLM	26
2.2.3.1	<i>Relative Channel Gain</i>	27
2.2.3.2	<i>Beam-Based Calibration</i>	27
2.2.3.3	<i>Saturation Model Analysis</i>	28
2.2.3.4	<i>Calibration Beam Loss Measurements</i>	29
2.2.4	Beam Loss Measurements.....	29
2.2.4.1	<i>MPS Generated Beam Dumps</i>	29
2.2.4.2	<i>Injection Loss</i>	33
2.2.5	SCU0 Protection Studies	34
2.2.6	Discussion and Summary	35
2.2.7	Acknowledgments	35
2.2.8	References	35

2.3	DEMAGNETIZATION EFFECTS AT PETRA III UNDULATORS	37
2.3.1	Abstract	37
2.3.2	Introduction.....	37
2.3.3	Peak field Measurements in the Tunnel.....	39
2.3.4	Refurbishment of PU02	40
2.3.5	Dynamic Multipoles	42
2.3.6	Summary.....	43
2.3.7	References.....	44
2.4	RADIATION DAMAGE OF INSERTION DEVICES AT PETRA III – A PERSPECTIVE VIEW FROM OPTICS AND TRACKING STUDIES	45
2.4.1	Introduction.....	45
2.4.2	Observation of Radiation Damage of Insertion Devices	46
2.4.3	Diagnostic Tools.....	49
2.4.3.1	TLDs	49
2.4.3.1	Beam Loss Monitors	49
2.4.3.1	Cherenkov Fibers	50
2.4.3.1	PANDORAS.....	51
2.4.4	Measurements	51
2.4.4.1	TLD Measurements.....	51
2.4.4.2	Beam Loss Monitor Studies	52
2.4.4.3	960 Bunch Mode.....	55
2.4.4.4	40 Bunch Mode.....	56
2.4.4.5	Comparison with BLM 14 (PU090 : Exit end of PU09).....	57
2.4.4.6	First Tests with Cherenkov Fibers.....	58
2.4.5	Simulations Introduction	59
2.4.5.1	On Momentum Tracking.....	60
2.4.5.2	Off Momentum Tracking.....	62
2.4.6	Conclusions.....	71
2.4.7	Acknowledgements.....	72
2.4.8	References.....	72
3	WORKSHOP AND CONFERENCE REPORTS	73
3.1	ICFA ADVANCED BEAM DYNAMICS WORKSHOP “AOC2015” ENABLES ACCELERATOR EXPERTS TO MEET OPTICS CHALLENGES OF FUTURE MACHINES	73
4	RECENT DOCTORIAL THESES.....	77
4.1	OPTICS DESIGN AND OPTIMIZATION OF ELECTRON BUNCH COMPRESSOR TRANSFER LINE (WITH A CASE STUDY OF CTF3 BUNCH COMPRESSOR)	77
5	FORTHCOMING BEAM DYNAMICS EVENTS	78
5.1	THE 9 TH INTERNATIONAL ACCELERATOR SCHOOL FOR LINEAR COLLIDERS.....	78
5.2	ICFA MINI-WORKSHOP ON "HIGH FIELD SUPERCONDUCTING MAGNETS FOR PP COLLIDERS"	84

5.3	THE 37TH INTERNATIONAL FREE ELECTRON LASER (FEL) CONFERENCE	84
5.4	13TH INTERNATIONAL CONFERENCE ON HEAVY ION ACCELERATOR TECHNOLOGY (HIAT2015)	85
5.5	4TH INTERNATIONAL BEAM INSTRUMENTATION CONFERENCE (IBIC 2015)	85
5.6	THE 17TH INTERNATIONAL CONFERENCE ON RF SUPERCONDUCTIVITY (SRF2015)	86
5.7	INTERNATIONAL WORKSHOP ON BEAM COOLING AND RELATED TOPICS (COOL'15)	86
5.8	12TH INTERNATIONAL COMPUTATIONAL ACCELERATOR PHYSICS CONFERENCE (ICAP'15)	87
6	ANNOUNCEMENTS OF THE BEAM DYNAMICS PANEL.....	88
6.1	ICFA BEAM DYNAMICS NEWSLETTER.....	88
6.1.1	Aim of the Newsletter	88
6.1.2	Categories of Articles	88
6.1.3	How to Prepare a Manuscript.....	88
6.1.4	Distribution.....	89
6.1.5	Regular Correspondents	89
6.2	ICFA BEAM DYNAMICS PANEL MEMBERS	91

1 Foreword

1.1 From the ICFA Chair

Joachim Mnich, DESY
Mail to: joachim.mnich@desy.de

It is my pleasure to thank Nigel Lockyer for his leadership of the International Committee for Future Accelerators (ICFA). Nigel's tenure covers several events of high significance for our field of research, e.g. the 2013 Nobel Prize in Physics to Englert and Higgs, and the vote of our Japanese colleagues for a potential construction site for the International Linear Collider (ILC). The first event marks the end of a decade-long quest – and the other hopefully is the beginning of a new worldwide project! Another very remarkable event under Nigel's leadership was the ICFA seminar held in October 2014 in Beijing, during which the enormous progress made in the past few years became very clear. Hopes are high that with the upcoming start of LHC Run 2 at full energy, of SuperKEKB, and in the future hopefully also of the ILC, the rate of progress will stay as high as it was during the past few years.

The agenda for this is set: The recent strategy updates from all world regions show a remarkable consensus concerning future projects. Although there are different regional flavours, all roadmaps and strategies are coherent, and together show a clear global strategy of particle physics. The highest priority is the full exploitation of the LHC, which will resume operation close to its design energy in summer 2015. We expect many more beautiful results in Higgs physics from the LHC, but we certainly hope for the unknown – for the discovery of new physics, be it in direct searches or in precision measurements. The LHC will thus remain the main international particle physics project for the coming years, with a physics programme sketched for as far as 2035. Meanwhile, however, post-LHC collider projects are discussed in ICFA and elsewhere:

After the preparation of the ILC TDR, the linear collider community has adopted a new organisational form, the Linear Collider Collaboration (LCC). The Linear Collider Board (LCB) is the main body to promote and oversee activities on linear colliders and their detectors as worldwide collaborative projects. We all hope that the ILC review process currently ongoing in Japan will soon conclude with a positive statement. Japan could then make a big step towards realising the ILC as a truly global project.

Meanwhile, other major projects come onto the agenda: CERN pursues the case of CLIC and investigates the options of a Future Circular Collider (FCC) for both hadrons (a 100 TeV pp machine) and leptons in an approximately 100 km tunnel in the Geneva area. The Chinese CEPC study is of a similar size (a ring of 50 - 70 km circumference), foreseeing as a first step an electron-positron machine with 250 GeV centre-of-mass energy and, at a later stage, with a proton-proton option. The most relevant development in accelerator-based neutrino physics is the Long Baseline Neutrino Facility (LBNF) project in the US that ultimately – like HyperK – might establish a CP-violating phase.

Especially for projects beyond our current concrete planning, accelerator R&D is vital. Various directions are being pursued, with high gradients being the most

important objective. Efforts focus on new materials for superconducting cavities and on new acceleration concepts like CLIC or plasma-wakefield acceleration. Also high-field magnets and materials for them are being investigated, like NbTi or Nb₃Sn, which will already be employed at the high-luminosity LHC. Further topics of crucial importance are cost reduction and the reduction of power consumption.

ICFA will follow the large projects sketched above, playing an active role in the ever more global field of research in particle physics with accelerators. We are clearly up to very exciting times!

1.2 From the Panel Chair

Weiren Chou, Fermilab
Mail to: chou@fnal.gov

The new ICFA chair and DESY Research Director Joachim Mnich wrote a column in Section 1.1 of this newsletter, in which he discusses the status of high-energy physics (HEP) around the world and gives a clear vision of its future.

The International Committee for Future Accelerators (ICFA) met on February 26-27, 2015 at Jlab, USA. Joachim chaired the meeting.

An important discussion at the meeting was on the proposed new IUPAP Commission (or Working Group) on accelerator science. As ICFA's mission is "*to promote international collaboration in all phases of the construction and exploitation of very high energy accelerators,*" there are many accelerator communities that do not feel represented by ICFA. The discussion came to the agreement that ICFA would welcome a new IUPAP working group which covers a broader area of accelerators than ICFA itself does; but the new group should have links to ICFA and duplication should be avoided. Some ICFA panels (e.g., this Beam Dynamics Panel) cover subjects much broader than HEP (such as beam dynamics studies for light sources, neutron sources, FEL, ERL, high intensity hadron beams, ADS, FFAG, etc.) and can be a bridge to connect to the new group.

The Funding Agencies for Large Colliders (FALC) welcomed John Womersley as its new chair on January 1st, 2015. It discussed a possible ILC cost model, with 50% provided by the host country (conventional facilities and 33% of the SRF) and the remainder by international partners. The Japanese funding agency MEXT is in the process to evaluate the costs and human resources needs of the ILC in order to make a decision on whether or not Japan will host the construction of the ILC. MEXT has set up an expert committee for advice and hired the private company Nomura to collect information from around the world on current trends in accelerator technology and the spin-offs of accelerator technology. An interim report from the expert committee was expected in June, 2015.

ICFA discussed a proposal for a new ICFA panel on sustainable accelerators and colliders. The goal is to improve the power efficiency of every accelerator component; to have energy recovery from the accelerator; to re-use the recovered energy; and to have a stand-alone system to provide all or part of the accelerator power needs. ICFA formed a small group to study this proposal before making a decision.

An important event in March 2015 was the FCC Week Conference in Washington, D.C., U.S.A. (<http://indico.cern.ch/event/340703/>) It was co-sponsored by the US Department of Energy (DOE), IEEE and CERN. The focus was on circular colliders in

the post-LHC era. More than 300 people participated, including a large attendance from the US universities and laboratories showing strong interest in a future proton-proton collider with an energy much higher than the LHC. A large size ring (~100 km) is also ideal for an e⁺e⁻ collider as a Higgs factory or Super Z factory. In the meantime, China also completed and published a preliminary conceptual design report for a ring collider CEPC-SPPC (<http://cepc.ihep.ac.cn/preCDR/volume.html>) with a size of 54 km. These two newly proposed machines – FCC and CEPC – are like “twins.” Both have our best wishes and support for growing up together healthy and strong.

The 2015 Linear Collider School will be in Whistler, BC, Canada on 26 October to 6 November 2015. An announcement can be found in Section 5.1 of this newsletter.

The editor of this issue is Dr. Rainer Wanzenberg, a senior scientist at DESY, Germany, and a member of the ICFA Beam Dynamics Panel. The theme is “*Radiation Damage of Accelerator Components – Detection, Measurements and Simulations.*” He collected four well-written articles on this theme and gives a comprehensive review of this important field in beam dynamics.

In this issue there are also a workshop report (*Advanced Optics Control: AOC2015*), one doctoral thesis abstract (Amalendu Sharma, RRCAT, India) and seven workshop announcements (*ICFA mini-workshop on high-field superconducting magnets for pp colliders, 37th FEL conference, HIAT2015, IBIC2015, SRF2015, COOL2015 and ICAP2015*). I want to thank Rainer for editing a high quality and valuable newsletter for the accelerator community.

1.3 From the Editor

Rainer Wanzenberg
Deutsches Elektronen-Synchrotron, Notkestraße 85, 22607 Hamburg, Germany
Mail to: rainer.wanzenberg@desy.de

First and foremost I would like to thank all authors who have contributed to this issue of the ICFA Beam Dynamics Newsletter. The theme of this newsletter is “*Radiation Damage of Accelerator Components*”, with an emphasis on detection, measurements and simulations. In my view this is an interesting theme which is important not only for high energy accelerators but also for light sources, and other specialized accelerators. I really appreciate the positive response of my colleagues to my proposal to focus on this subject in this edition of the newsletter. I received four well written contributions for the theme section covering several important issues of the subject, including a report on beam halo monitoring using a diamond-based detector to protect the undulators of SACLA, a report on fast beam loss diagnostic to quantify charge deposition in the APS superconducting undulators, a report on demagnetization effects at the PETRA III undulators, and a report with an perspective view from optics and tracking studies on the insertion devices at PETRA III.

The contribution to the section on workshop and conference reports, namely about an ICFA beam dynamics workshop on “Advanced Optics Control (AOC)”, hosted at CERN in Feb. 2015, is closely related to frontiers and future directions of accelerator optics control for colliders, light sources, and other specialized storage rings. The workshop covered lessons from LHC Run-1 and interesting new diagnostics and modelling approaches from various state-of-the-art light sources, demonstrating the close relation between optics issues of accelerators from different research areas.

An abstract of a recently finished doctoral theses are in section 4 of the newsletter and several forthcoming beam dynamics events can be found in section 5. Reports from these conferences and workshops are expected for the forthcoming issues of the Beam Dynamics Newsletter.

2 Radiation Damage of Accelerator Components – Detection, Measurements and Simulations

2.1 Electron Beam Halo Monitoring using Diamond-based Detectors to Protect Undulator Permanent Magnets from Radiation Damage

Hideki Aoyagi

Mail to: aoyagi@spring8.or.jp

Japan Synchrotron Radiation Research Institute (JASRI/SPring-8),
1-1-1, Kouto, Sayo-cho, Sayo-gun, Hyogo 679-5198 Japan

2.1.1 Introduction

In high-energy particle accelerators, unintended beam loss results not only in radio activation of the apparatus but also in radiation damage to it. In particular, in X-ray free-electron laser (XFEL) facilities and synchrotron radiation facilities, where undulators are used, even if a small part of the halo of the electron beam is continuously irradiated to permanent magnets of the undulator, the magnets may be demagnetized, resulting in a fatal problem [1].

NdFeB becomes used as a material of permanent magnets of undulators in various facilities, because it possesses high intrinsic coercivity and high maximum magnetic energy product. However, the remanent field decreases by suffering radiation damage. It is very difficult to quantify demagnetization caused by radiation damage, because it depends on various conditions such as a kind of a particle, energy of it, manufacturing process, magnet shape and environmental conditions (temperature, clamp material and shape etc.). To solve this problem, Bizen et al. measured quantitatively demagnetization of the magnet with the same material and the same shape as that used in actual undulators under the condition equal to actual use conditions [1]. The measurement has been carried out by changing the energy of the incident electron beam and the intensity systematically as shown in Fig.1. The quantity of demagnetization is proportional to the number of electrons and it increases as the energy becomes high.

Assuming the tolerance of demagnetization rate of undulator magnets of 1% in 10 years, the tolerance of incident electron on the undulator magnets is estimated to be 4×10^{14} electrons/10 year, which is based on the experimental results as shown in Fig 1. In the case of the 60 Hz operation for 24 hours and 365 days, the required lower detection limit corresponds to 2×10^4 electron/pulse.

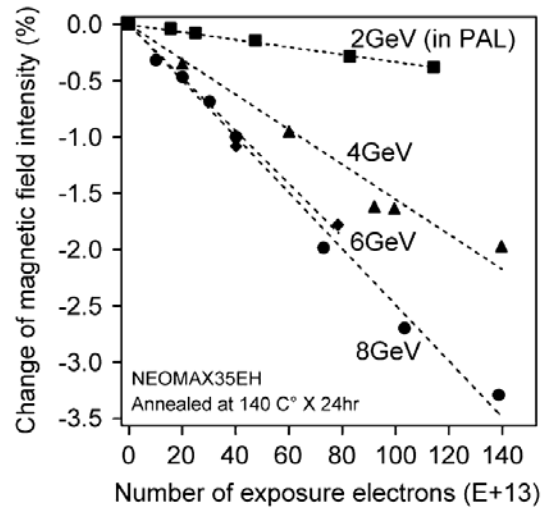


Figure 1: Dependence of magnetic field loss on the electron-beam. Magnetic field intensities decrease with the number of electrons. The experimental data for 2GeV had been performed previously at the Pohan Accelerator Laboratory [2].

Diamond-based detectors, which operate in the ionization mode as shown in Fig. 2, possess high radiation hardness [3,4], high heat resistance, high insulation resistance, and so on [5]. Demonstrations of the observation of charged particles using a diamond-based detector have already been carried out at some facilities [5], and such detectors have been used operationally at the Large Hadron Collider (LHC) at CERN for a wide variety of beam instruments, such as particle counters, phase monitors, beam-loss monitors, and spectrometers [6, 7].

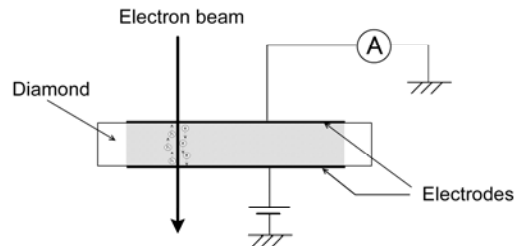


Figure 2: Principle of the diamond-based detector.

We have designed and fabricated a prototype beam halo monitor using diamond-based detectors made of chemical vapor deposition diamond [8] to protect the SPring-8 Angstrom compact free-electron laser (SACLA) undulators [9]. Pulse mode measurement is adopted to avoid the background noise efficiently, since 1 fC/pulse with 60 Hz, for example, corresponds to 60 fA in current mode measurement, which could be buried under the background noise. The detectors are directly inserted in the beam duct to measure the intensity of the beam halo. The two diamond-based detectors mounted in the prototype are arranged to measure the halo that passes over the upper and lower sides of the core of the electron beam.

2.1.2 Evaluation of Diamond-based Detectors

To evaluate the basic characteristics of the diamond-based detectors, such as detection sensitivity to an electron beam and linearity, beam tests were performed at the beam dump of the 8 GeV SPring-8 booster synchrotron [9]. A schematic diagram of the experimental setup is shown in Fig. 3.

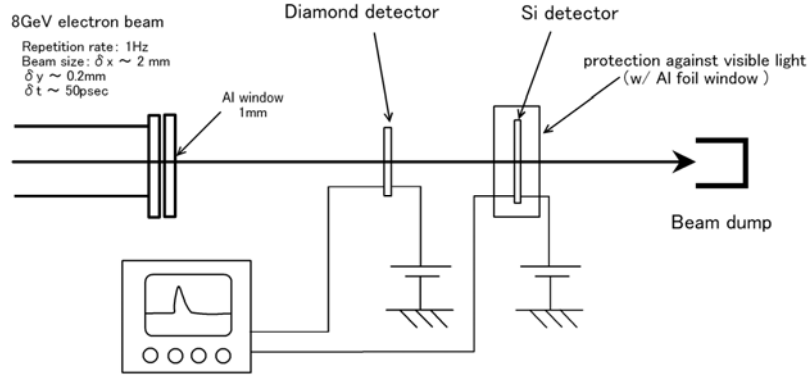


Figure 3: Setup of the electron beam tests performed in the SPring-8 synchrotron beam dump area. An oscilloscope with a sampling rate of 20 GS/s and an analogue bandwidth of 4 GHz was used.

The typical pulse shape of the output signal is shown in Fig. 4. One-shot measurements were performed in the tests. The bias voltage was +100 V. The number of electrons per pulse was about 10^4 . A pulse length with a full width at half maximum (FWHM) of 0.33 ns was obtained. The pulse width of the output signal can be shortened by using a detector with lower electrical capacitance. The rms noise signal level (σ_n) was suppressed to about 0.5 mV for the one-shot measurements.

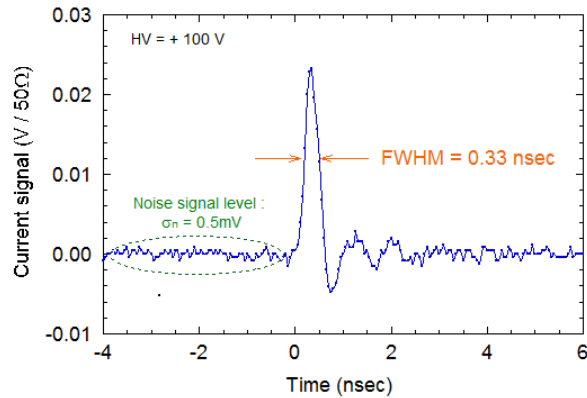


Figure 4: Pulse shape of current signal of the diamond-based detector.

The linearity of the output signal of the injected beam was also demonstrated as shown in Fig. 5. The number of incident electrons per pulse was estimated using the output charge from the silicon PIN photodiode (Hamamatsu S5377-05). The output charge from the diamond-based detector is proportional to the number of incident

electrons per pulse in the range of approximately 10^3 to 10^7 electrons/pulse. The lower detection limit for a single shot is about 2×10^3 electrons/pulse, which is equivalent to a charge signal of 25 fC when the bias voltage is +100 V. Here, we define the pulse height at which the output signal corresponds to $10\sigma_n$ as the lower detection limit.

In the literature the number of electron-hole pairs created by a MIP in diamond is assumed to be 36 per μm . In the above case, it is 78 electron-hole pairs per 300 μm with the bias voltage of +100 V, which corresponds to 0.26 electron-hole pairs per μm . This result originates the fact that the collection distance in the diamond detector used in this experiment is extremely suppressed. The collection distance can be described as $d = \mu\tau E$, where d , μ , T , and E are the collection distance, the mobility, the life time of carriers, and the applied bias voltage, respectively [10]. Increasing the bias voltage, the charge signal of diamond can be enhanced by a factor of several. However, to avoid the surface discharge, and to guarantee steady operation, the electrode bias is set to +100 V in our experiments.

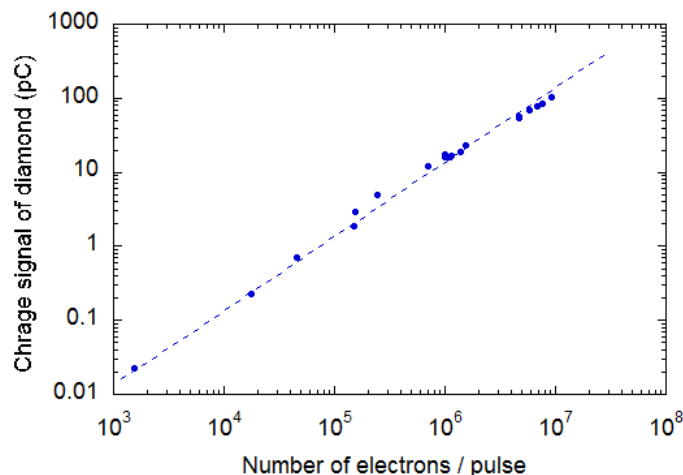


Figure 5: Linearity of output signal.

2.1.3 Mechanical Design of Beam Halo Monitor

2.1.3.1 Diamond-based Detectors

The diamond-based detectors were newly designed [11], as shown in Fig. 6. The diamond crystal was miniaturized from the prototype to adopt the microstripline structure and rf fingers easily. It was 12 mm (H) \times 8 mm (V) with a thickness of 0.3 mm. The size of the active area, which was sandwiched between electrodes, was 1 mm (H) \times 10 mm (W) with a thickness of 0.3 mm. The height of the active layer was chosen to be 1 mm. By having this narrow active area, the monitor can be also used for the profile measurement of a beam halo.

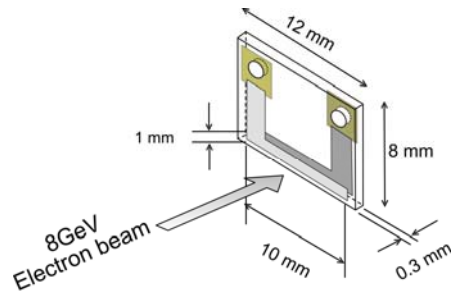


Figure 6: Dimensions of newly designed diamond-based detector.

2.1.3.2 Micro-stripline Structure

The pulse signal originating from the ionization by induced electrons typically had a length of 0.33 ns FWHM [9]. The waveform of the pulse would be deformed if an open-wire line was used in the vacuum chamber of the monitor. Therefore, we applied a microstripline structure [12] in the vacuum chamber to improve the high-frequency property. Figure 7 shows microstripline structure mounted on an ICF70 flange. The microstripline structure is composed of a strip conductor (Cu), a dielectric substrate (ceramic), and a ground plate (stainless steel). The width of the strip conductor and the thickness of the dielectric substrate were designed to give an impedance of 50Ω . High-frequency SMA feedthrough connectors, fabricated by Kyocera Corporation, are used to prevent the generation of ringing between the SMA feedthrough connector and the diamond-based detectors. The SMA feedthrough connector has a cutoff frequency of more than 10 GHz, which satisfies the requirements of the monitor. A demonstration of the transmission of a pulse having a length of 200 ps FWHM using the microstripline structure and the SMA feedthrough connector has been described previously [12].

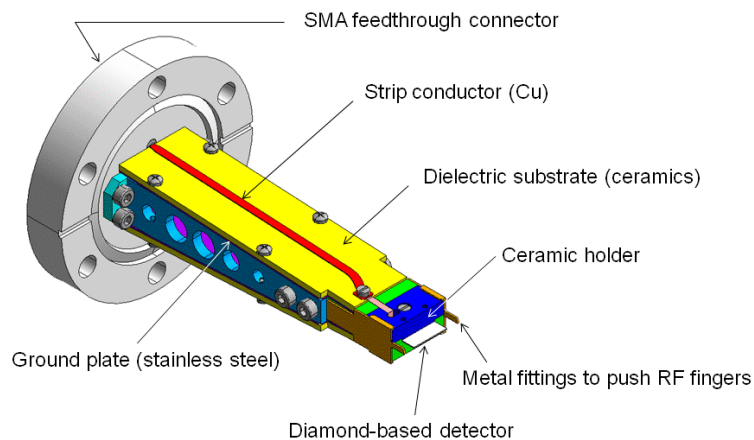


Figure 7: Microstripline structure with SMA feedthrough connectors on an ICF70 flange. The diamond-based detector is clamped on a ceramic holder.

2.1.3.3 Rf fingers with Aluminum Windows

There is a possibility that the electron beam quality will degrade when the detectors approach the core of the electron beam. Therefore, we attempted to cover the detectors with rf fingers to completely exclude this factor, which deteriorates the stability of the XFEL lasing in SACLA, and we adopted these rf fingers in the actual monitor for SACLA [11]. The main purpose of the rf fingers is to remove the wakefield to preserve the electron beam quality. We found that, as a by-product, high-frequency components that emerge in the signal of the diamond-based detectors can be reduced in intensity.

We evaluated the effects of the type 1 and type 2 configurations of rf fingers, as shown in Fig. 8, on reducing the wakefield in the detector signal. Measurements have been carried out at the 250 MeV SCSS test accelerator. Figure 9 shows the output current signal with the high-frequency components resulting from the wakefield generated when the beam core passes between the diamond detectors. Using the rf finger structure with the type 2 configuration, we succeeded in reducing the wakefield generated by the resonance in the vacuum chamber of the monitor without any intrinsic drawbacks. It is, rather, an advantage at the point of view of the signal processing that the high-frequency component was reduced.

Beryllium copper alloy (BeCu), which has good spring characteristics, is usually used for rf fingers. However, BeCu has a high atomic number. Thus, if the rf fingers are placed in front of the detectors, secondary electrons and bremsstrahlung will radiate from the rf fingers and the output signal of the detectors will be contaminated by them. Beam tests and simulation studies have been carried out, and we found that the increase in the energy deposition from these materials is not significant, if we adopt Al windows with a thickness of 0.1 mm in front of the active areas of the diamond-based detectors.

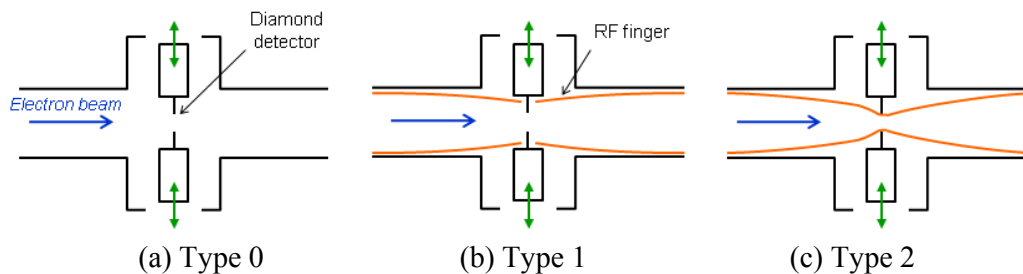


Figure 8: Configurations of the RF fingers: (a) type 0, without fingers; (b) type 1, with fingers (the active areas of the detectors are not covered); (c) type 2, with fingers (fully covered).

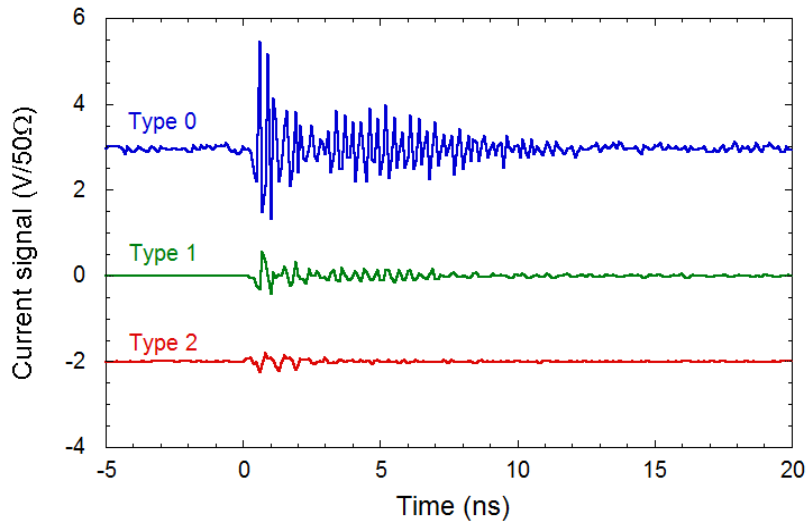


Figure 9: Effect of configuration on reducing the wake field.

A schematic view of the rf fingers with the Al windows [11] is shown in Fig. 10. The thickness of the Al windows is 0.1 mm to minimize the effect of radiation. The base material of the rf fingers is BeCu ($t = 0.1$ mm). To form the Al windows, plates of Al are attached to the frame of the BeCu fingers by spot welding. Four rf fingers are used to cover the pair of diamond-based detectors. Only the fingers on the upstream side have Al windows. The outside edges of four fingers are fixed on the top and bottom walls of the beam duct, which have a square cross section. The inside edges overlap each other and undergo sliding motion immediately after the diamond-based detectors, so that each detector can be actuated independently. There are two modes of operation for the beam halo monitor. In the active mode, the rf fingers are pushed inward by metal fittings, which are attached beside the detectors, to measure the beam halo close to the beam core [Fig. 11(a)]. In the shelter mode, the diamond detectors are pulled fully outward, and the size of the aperture of the beam duct is maximized [Fig. 11(b)].

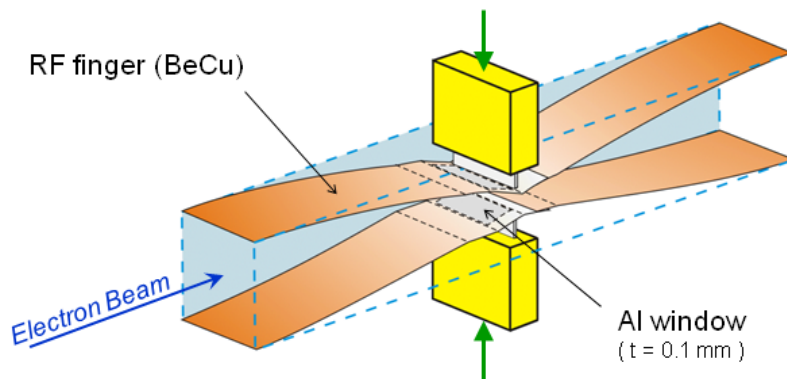


Figure 10: Schematic view of the RF fingers with aluminum windows.



Figure 11: Photograph of the RF fingers with Al windows in (a) active mode and (b) shelter mode. The beam direction is from right to left.

2.1.3.4 Final Design of Beam Halo Monitor

Figure 12 shows the final mechanical design of the beam halo monitor employed in SACLA [11]. The beam halo monitor is equipped with rf fingers with Al windows, which have the type 2 configuration as mentioned earlier. Beam pipe adaptors are connected to the upstream and downstream sides of the vacuum chamber of the monitor in order to suppress the reflection of the wakefield. Inside the beam pipe adapter, the circular cross section on one side is smoothly and continuously converted into the square cross section on the other side. The diamond-based detectors on both the upper and lower ports can be independently manipulated using stepping motors. The vacuum chamber and beam pipe adaptors are fixed during the manipulation of the detectors. Thus, there is no transverse offset that causes mechanical stress on the bellows attached to both beam pipe adaptors. Because the monitor is used under an ultrahigh-vacuum condition, it is designed to be baked in vacuum.

The beam halo monitor is installed about 1 m upstream of the undulators to monitor the intensity of the beam halo that irradiates the undulator permanent magnets. In the area several meters upstream of the undulators, it is necessary to decrease the geomagnetic field of 0.4 G by about 100-fold for the electron beam to propagate in a straight line in this area. Therefore, the beam halo monitor is covered by a geomagnetic shield box so as to attenuate the magnetic field on the beam axis [13].

As a data acquisition system, the preamplifier prepared for the evaluation of the prototype is combined with an event-synchronized data acquisition system in SACLA. The preamplifier was originally developed for the current transformer (CT) in the SCSS test accelerator [14]. The time constant of the amplifier was adjusted to about 40 ns to match the event-synchronized data acquisition system and to effectively suppress the ringing noise caused by the wakefield of the electron beam. This system can record every set of output signals that are synchronized with electron beam shots [15]. We also prepared a system to manipulate the diamond-based detectors from a central control room.

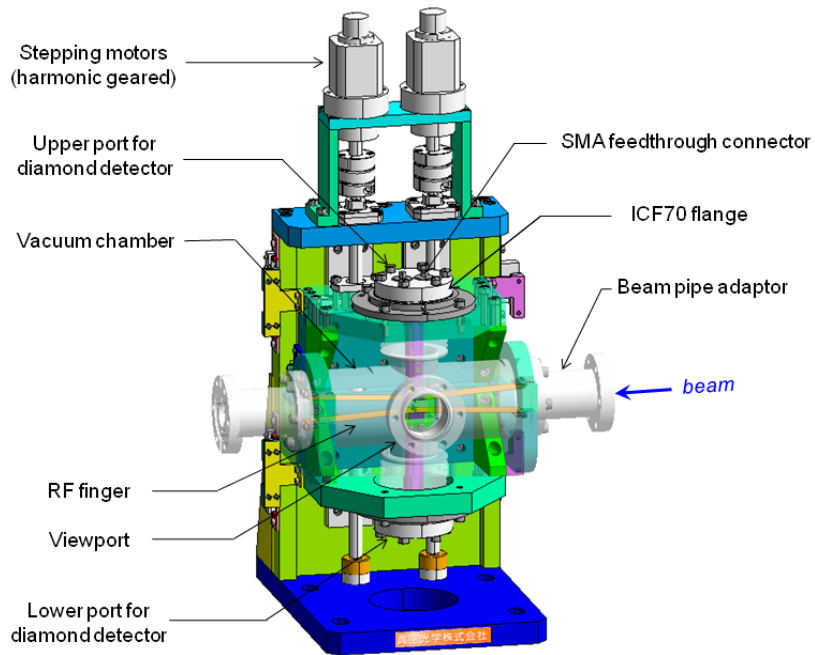


Figure 12: Illustration of the beam halo monitor employed in SACLA.

2.1.4 Operational Results in SACLA

2.1.4.1 Effect on Electron Beam Quality

In order for the beam halo monitor to be continually used in SACLA, the degradation of the electron beam must be avoided, even when the diamond detectors covered with the rf fingers approach the beam axis. Figure 13 shows the behavior of the laser power when the distance from the edges of the rf fingers to the beam axis is changed [11]. The laser power does not change significantly even when the gap between the rf fingers is 0.4 mm. This result means either that the quality of the electron beam is not degraded as a result of reducing the wake field by the RF fingers.

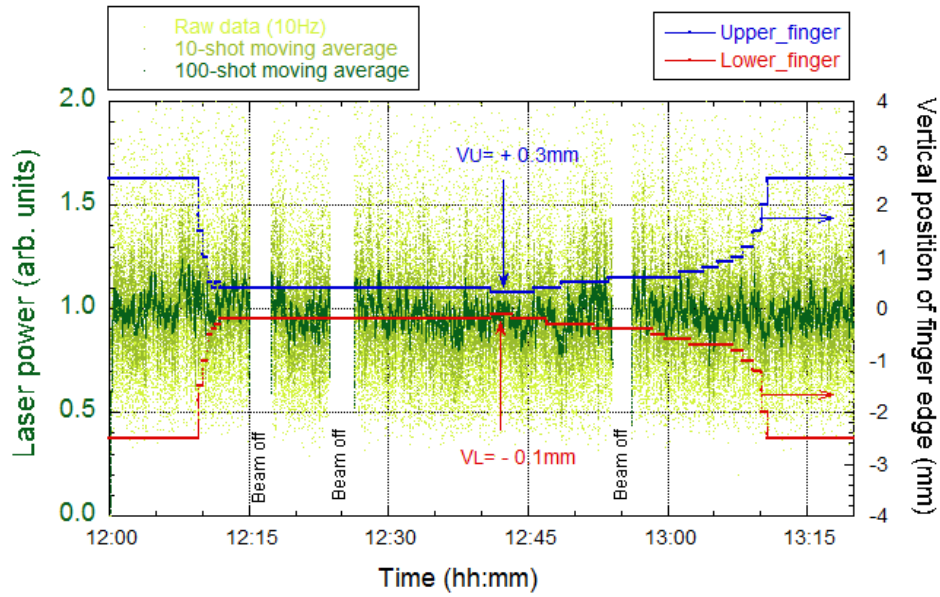


Figure 13: Behavior of laser power (left axis) and vertical position of edges of RF fingers (right axis) over time. The minimum gap is 0.4 mm at approximately 12:42.

2.1.4.2 Filtering of Residual High-Frequency Components

We adopt low pass filters (LPFs) to suppress the effect of residual high-frequency components, which originate from the induction current of the beam core. Figure 14 shows the effect of the residual high-frequency components before and after filtering. The cutoff frequency of the LPFs was set at 117 MHz, which is the same as that in the prototype [9]. In the case that the original current signal originating from ionization by induced electrons is larger than the residual high-frequency components, one can clearly observe that the residual high-frequency components are filtered and the original current signal is enhanced, as shown in Figs. 14(a) and 14(b). In the case that the original current signal is very small compared with the residual high-frequency components, one can also observe that the original current signal is enhanced and the residual high-frequency components are filtered, as shown in Figs. 14(c) and 14(d). We conclude that the reduction in the intensity of high-frequency components becomes possible by adopting the rf fingers with aluminum windows and that the residual high-frequency components are efficiently suppressed by the LPFs.

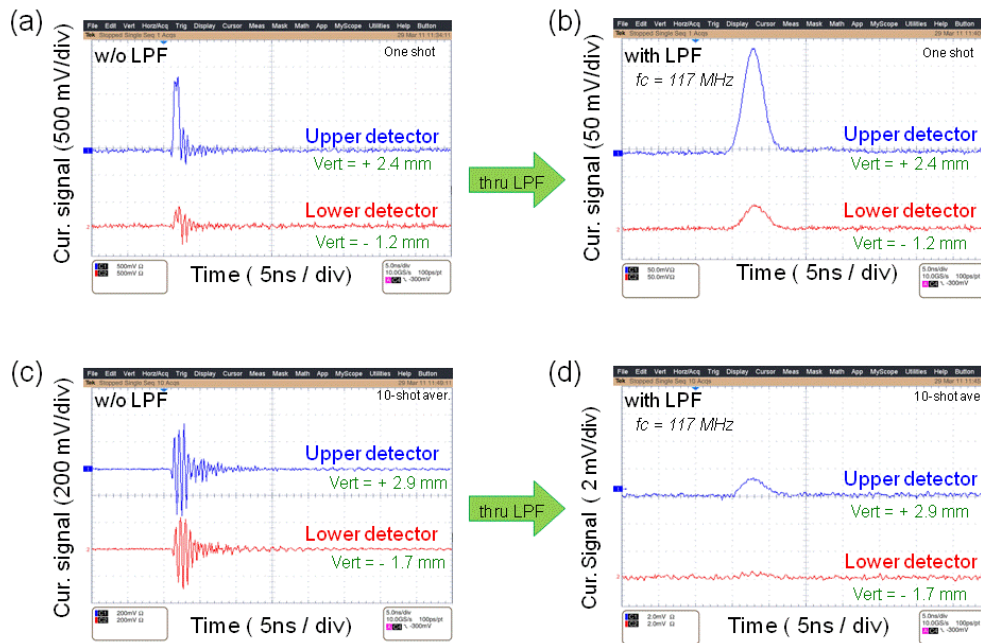


Figure 14: Filtering of residual high-frequency components without (w/o) or with LPFs. (a) Large original current signal w/o LPFs, (b) large original current signal with LPFs, (c) small original current signal w/o LPFs, and (d) small original current signal with LPFs.

2.1.4.3 Scattering of Beam Core at RF Fingers

The rf fingers with aluminum windows were adopted for the beam halo monitor employed in SACLA. The fingers expanded by 1 mm from the detector tip toward the beam core. When the edges of the rf fingers are irradiated by the beam core, scattering radiation is generated, resulting in an increase in the output signal of the diamond detectors. To evaluate this effect, we observed the output signal of the diamond detectors when either of the upper or lower diamond detectors was moved from the position at which the gap between the upper and lower rf fingers was 0.4 mm [11]. The experimental result is shown in Fig. 15. L1 and L2 (U1 and U2) indicate that only the lower (upper) finger was moved. The output signal of the upper (lower) detector also changed especially at L1 (U1). This result suggests that the core of the beam is scattered at the edge of the rf fingers when the gap is under about 0.6mm.

Figure 16 shows the charge signal of the diamond-based detectors versus the vertical position of the edge of the rf fingers [11]. The solid lines indicate the data measured after the XFEL lasing of SACLA. When the edges of the rf fingers are near the beam core, the charge signals of the diamond detectors increase in intensity because of scattering. On the other hand, when the absolute value of the vertical position of the rf finger edge is 1 mm or higher, the charge signal decreases in intensity to below the lower detection limit of 2×10^3 electrons/pulse [9]. Therefore, we conclude that a charge signal originating from a beam halo with a distance from the beam axis of 2 mm or more is below the lower detection limit. In other words, there are no effects of the dark current, secondary electrons, or bremsstrahlung generated in the accelerator on the charge signal. This result

means that the permanent magnets of the undulators are not demagnetized by the irradiation of the beam halo when the gap between the undulator magnets is more than 4 mm.

In Fig. 16, the following features can also be observed. The dashed lines indicate the data measured during the early stage of the commissioning of the linear accelerator of SACLA. The effect of scattering at the edge of the rf fingers can be seen in a larger area than that after XFEL lasing. This observation suggests that the size of the beam core decreased during the commissioning, and that the position of the beam core approached the center. In this way, the beam halo monitor can be used as a beam diagnostic tool during the accelerator commissioning as well as during regular accelerator tuning.

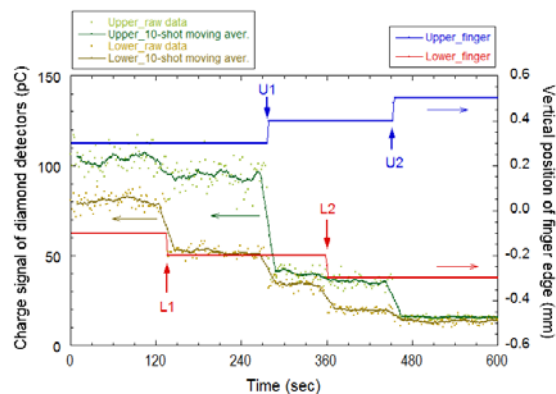


Figure 15: Behavior of charge signal of diamond-based detectors when the vertical position of the finger edge is changed. The gap was varied from 0.4 mm to 0.8 mm.

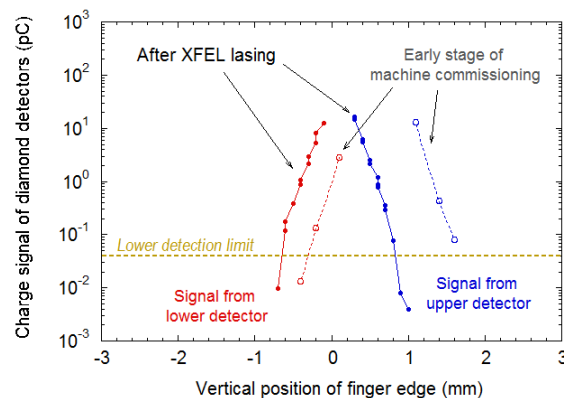


Figure 16: Effect of rf finger edge position on charge signal of diamond-based detectors. Solid lines were obtained after XFEL lasing. Dashed lines were obtained during the early stage of machine commissioning. The lower detection limit of 2×10^3 electrons/pulse, which corresponds to 0.04 pC, is indicated.

2.1.4.4 Measurement of Vertical Beam Halo Profile

An optical transition radiation (OTR) screen monitor is usually used for profile measurement of an electron beam core, which has relatively strong intensity. However, it is impossible to detect the weak intensity of the halo part of the beam. To overcome

this problem, Oshima et al. have tried to measure vertical beam profile of the whole beam in large dynamic range using with the halo monitor and the OTR screen monitor [16]. Figure 17 shows the result of the profile measurement. Measurement data with the OTR screen monitor is indicated by red points. The detection efficiency for each pixel of a CCD camera is calibrated by a CT. This result suggests that the lower detection limit is about 100pC/mm of the charge density. Measurement data with the halo monitor is indicated by blue and green dots. Knife edge method, where upper and lower detectors are scanned, has been adopted. A solid line indicates a Gaussian fit of significant data with the OTR screen monitor. The fitting curve is also suitable to the data with the halo monitor. This proves the calibration of the detection efficiency of the halo monitor is feasible for an absolute measurement. In this way, it has been demonstrated that the vertical profile measurement of the electron beam in a wide dynamic range of 7 digits is able to be done by combining the halo monitor with the OTR screen monitor.

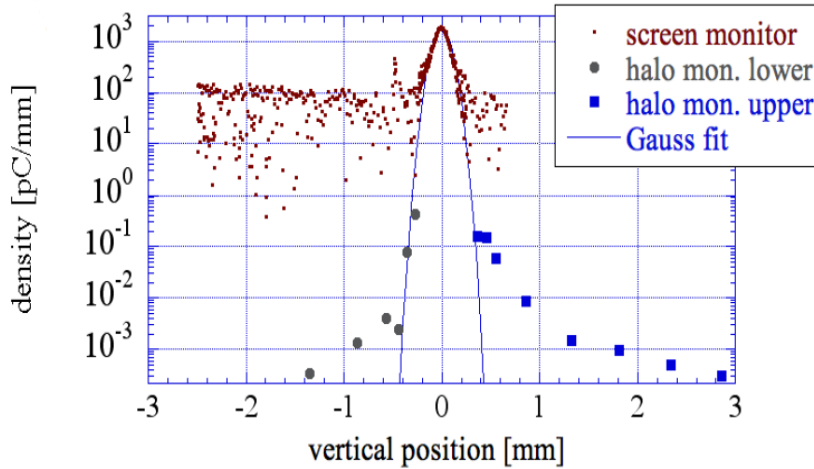


Figure 17: Vertical beam profile measurement by using the halo monitor and the screen monitor.

2.1.5 Conclusions

The electron beam halo monitor using diamond-based detectors for SACLA has been designed and fabricated. The rf fingers with Al windows were designed to fully cover the diamond-based detectors. The monitor has been installed upstream of the undulators to prevent the demagnetization of the permanent magnets of the undulators by the irradiation of the beam halo. We demonstrated the performance of the monitor during the machine commissioning of SACLA and the early stage of the user operation. We have been monitoring the intensity of the beam halo continually using the data acquisition system, and we found that the intensity of the beam halo is always below the detection limit during the normal user operation. The lower detection limit of the monitor is very low and scanning measurement can be done, so it can be used as not only the interlock sensor for machine protection but also the beam diagnostic tool.

2.1.6 References

1. T. Bizen et al., Nucl. Instrum. Methods Phys. Res., Sect. A 574, 401(2007).
2. T. Bizen, Y. Asano, T. Hara, X. Marechal, T. Seike, T. Tanaka, H.S. Lee, D.E. Kim, C.W. Chung, H. Kitamura, Nucl. Instr. and Meth. A 515 (2003) 850.
3. C. Bauer et al., Nucl. Instrum. Methods Phys. Res., Sect. A 367, 207 (1995).
4. T. Behnke, M. Doucet, N. Ghodbane, A. Imhof, C. Martnez, and W. Zeuner, Nucl. Instrum. Methods Phys. Res., Sect. A, 489, 230 (2002).
5. R. J. Tapper, Rep. Prog. Phys. 63, 1273 (2000).
6. L. Fernandez-Hernando, D. Chong, R. Gray, C. Ilgner, A. Macpherson, A. Oh, T. Pritchard, R. Stone, and S. Worm, Nucl. Instrum. Methods Phys. Res., Sect. A 552, 183 (2005).
7. E. Griesmayer, B. Dehning, E. Effinger, and D. Dobos, in Proceedings of the 14th Beam Instrumentation Workshop, Santa Fe, New Mexico (LANL, Los Alamos, 2010), MOCNB02.
8. H. Aoyagi, T. Kudo, H. Tanida, and H. Kitamura, in Proceedings of the 8th International Conference on Synchrotron Radiation Instrumentation, San Francisco, California, AIP Conf. Proc. No. 705 (AIP, New York, 2004), p.933.
9. H. Aoyagi, Y. Asano, T. Itoga, N. Nariyama, T. Bizen, T. Tanaka, and H. Kitamura, Phys. Rev. ST Accel. Beams 15, 022801 (2012).
10. L. S. Pan et al., J. Appl. Phys. 74, 1086 (1993).
11. H. Aoyagi, Y. Asano, T. Itoga, N. Nariyama, T. Bizen, K. Fukami, T. Aoki, S. Suzuki, M. Yamaga, T. Otake, T. Tanaka, and H. Kitamura, Phys. Rev. ST Accel. Beams 16, 032801 (2013).
12. H. Aoyagi, S. Takahashi, and H. Kitamura, in Proceedings of the 10th European Workshop on Beam Diagnostics and Instrumentation for Particle Accelerators, Hamburg, Germany (DESY, Hamburg, 2011), MOPD91.
13. H. Aoyagi, T. Hasegawa, T. Bizen, and Y. Asano, in Proceedings of the 8th Annual Meeting of the Particle Accelerator Society of Japan, Tsukuba, Japan (PASJ, Japan, 2011), TUPS161.
14. A. Higashiya, H. Maesaka, and Y. Otake, in Proceedings of the 29th Free Electron Laser Conference, Novosibirsk, Russia (BINP, Novosibirsk, 2007), WEPPH051.
15. M. Yamaga, Y. Furukawa, T. Hirono, M. Ishii, T. Masuda, T. Ohata, R. Tanaka, A. Yamashita, T. Fukui, and N. Hosoda, in Proceedings of the 12th International Conference on Accelerator and Large Experimental Physics Control Systems, Kobe, Japan (SPRING-8, Japan, 2009), TUB003.
16. T. Oshima, H. Maesaka, S. Matsubara, S. Inoue and Y. Otake, in Proceedings of the 10th Annual Meeting of the Particle Accelerator Society of Japan, Nagoya, Japan (PASJ, Japan, 2013), SAP087.

2.2 Fast Beam Loss Diagnostic to Quantify Charge Deposition in APS Superconducting Undulators

Jeffrey C. Dooling, Katherine C. Harkay and Yury Ivanyushenkov
Argonne National Laboratory, 9700 S. Cass Ave, Lemont, IL 60439
Mail to: dooling@aps.anl.gov

2.2.1 Introduction and Motivation

Protection against beam-loss-induced quenches is a well-known issue in high-energy proton accelerators, where superconducting magnets have been used for several decades [1-4]. Machine protection interlocks typically include beam loss monitoring [5] and beam abort systems. For almost as long, but mostly in the past 10-12 years, superconducting magnets – wigglers [6-13] and superbends [14] – have been employed for the generation of high-energy photons in electron synchrotron light sources. There are presently only two light sources that employ superconducting undulators (SCUs): ANKA [15] and Advanced Photon Source (APS) [16]. While all the superconducting wigglers and SCUs have quench-detection interlocks to protect the magnet, very little has been written about characterizing and preventing beam-loss induced quenches. Notable exceptions are at the Canadian Light Source, where injection kickers have recently been implemented to also serve as an abort system to prevent such quenches [17], and at the APS, where a dedicated abort kicker system has been developed, guided by simulations and beam loss monitor (BLM) studies, and is ready for installation [18,19].

We report on the calibration and use of fast fiber-optic (FO) BLMs in the APS storage ring (SR) as a diagnostic [19,20]. SCU quenching can interrupt x-ray user operation and potentially leads to magnet damage. To address the requirements of a beam abort system that will prevent beam-loss induced quenches, we are interested in quantifying losses locally near the SCU.

A superconducting undulator SCU0 has been operating in APS Sector 6 (“ID6”) since the beginning of 2013 [16], and a second, longer superconducting undulator SCU1 is scheduled for installation in Sector 1 (“ID1”) in 2015 [21]. SCU0 often quenches during beam dumps triggered by the Machine Protection System (MPS) (SCU0 is powered off during manual beam dumps). Quench recovery is typically fast enough to allow SCU0 to be operated once the beam is restored. However, SCU1 may require longer recovery time, which could impact user operation. To characterize local beam losses, high-purity fused-silica FO cables were installed in ID6 on the SCU0 vacuum chamber (warm) transitions and in ID1 where SCU1 will be installed. These BLMs aid in the search for operating modes that protect both SCUs from beam-loss-induced quenching.

Calibration of the BLMs allows us to compare lost charge with simulations of energy deposition and subsequent temperature excursions in the SCU; this information can be used to determine permissible loss rates that will avoid quenching both during beam dumps as well as possibly during injection (to date, no injection-loss induced quenches have been observed with SCU0). MARS [22] simulations have shown that relatively small beam loss (<1 nC) can lead to temperature excursions sufficient to cause quenching when the NbTi windings are near critical current [20].

In this paper, we describe the BLM calibration process that included deliberate beam dumps at locations of BLMs. We also compare operational beam dump events where SCU0 did and did not quench. First, we describe the fast FO BLMs installed in ID6 and compare them with the Čerenkov radiation detection system distributed around the SR. Next, the analysis used to calibrate the FO BLMs is presented. We discuss the experimental method, including simulations, used in the calibration measurements. The calibration model is then applied to beam loss events including beam dumps and injection.

2.2.2 Beam Loss Monitor Description

Loss of primary, 7-GeV electrons leads to an electromagnetic (EM) shower composed of photons, electrons, and positrons. High-purity, fused-silica FO cable bundles are sensitive to all three of these EM shower components (in the case of photons, via pair production). Light is generated within the fibers from both Čerenkov radiation and optical transition radiation (OTR). OTR tends to be much weaker than Čerenkov radiation. However, OTR is generated at the fiber surface, and fibers can have high surface-to-volume ratios in the radiator region depending on bundle orientation relative to the direction of beam and beam loss. OTR intensity favors the detection of higher-energy electrons with emission at small angles from the direction of electron propagation. On the other hand, Čerenkov radiation is emitted at a cone of angle $\theta_c = \cos^{-1}(1/n) \approx 47^\circ$ in fused silica at the middle of the visible spectrum (n is refractive index). If the fiber bundle is oriented such that its axis is parallel to the electron beam trajectory, θ_c will be outside of the numerical aperture of most fibers; however, as the fiber bends away from its radiator end, some length of the fiber will be at angles capable of accepting Čerenkov-generated light.

Four fast FO BLMs are mounted adjacent to the SCU0 cryostat, as shown in Fig. 1. The FO BLMs are positioned in pairs with one pair upstream (US) of the SCU0 and the other pair downstream (DS) on the vacuum chamber transitions. The radiator ends of each bundle (protected by a red cap, seen in the figure) are placed parallel to the beam trajectory at the nominal beam centerline: one bundle above and the other below the chamber midplane. Vertical separation between the individual bundles and beam centerline is ± 5.4 cm on the US side and ± 2.8 cm at the DS side.

The FO cable is composed of 61 200- μm -diameter, fused-silica fibers with step-index-cladding yielding an outside diameter of 220 μm . The fibers are arranged close-packed for an effective bundle diameter of 2 mm, with a packing efficiency $\eta_{cp} = \pi/(2\sqrt{3}) = 0.907$. Each fiber is 4 m in length, with the signal ends coupled into four Hamamatsu “sub-miniature” R7400 photomultiplier tubes (PMTs) mounted within Pb shielding on the SR tunnel floor. The PMT waveforms are acquired using a digital scope.

Response times of the FO BLMs are determined by the PMT and the length of the FO exposed to the electromagnetic shower. PMT rise time for the R7400 units are given as 0.78 ns [23]; this is sufficiently fast to observe most multi-bunch loss patterns within a single turn of 3.68 μs . The two most-used operational bunch patterns are 24 and 324 uniformly-spaced bunches [24].

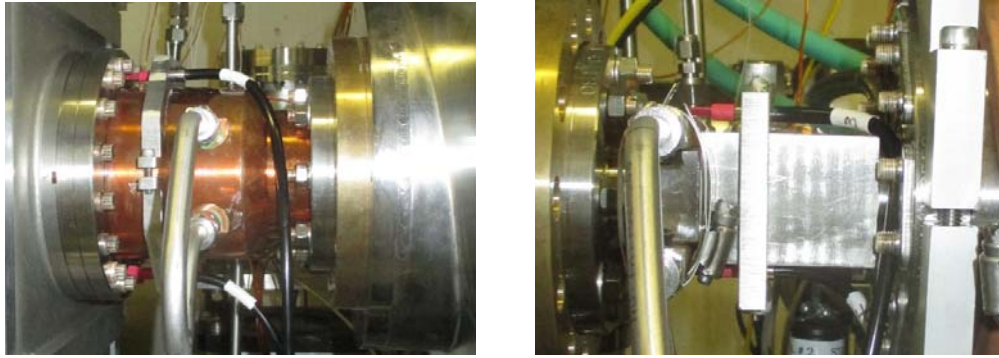


Figure 1: FO BLMs positioned on the SCU0 chamber upstream (left) and downstream (right) transition. The top and bottom pairs are mounted at ± 5.4 cm with respect to beam height on the US side and ± 2.8 cm on the DS side.

The APS Čerenkov radiation detection system consists of Čerenkov detector (CD) BLMs distributed around the SR, in particular, near small-gap ID chambers, injection region, and near scrapers [25]. The CD BLMs are used in counting mode for the detection of Bremsstrahlung radiation and Touschek scattered electrons and, therefore, do not accurately register beam dump losses. The system is intended for monitoring and measuring steady-state localized loss rates during beam operations. Also composed of fused-silica, the CD radiator is a minimum surface-to-volume ($h=2r$) cylinder with radius $r=4$ mm. The PMT photocathode is close-coupled vertically to the top plane of the radiator cylinder, as seen in Fig. 2. The barrel and bottom surfaces of the radiator are mirror-coated to improve coupling efficiency to the PMT. Calibration of the CDs was carried out separately [26] and is not discussed here. Rather than change the configuration of the existing operational CD diagnostic, the FO prototype detectors are employed to observe the fast losses associated with beam dumps and injection.



Figure 2: Čerenkov detector radiator and PMT

2.2.3 Calibration of FO BLM

Calibration is carried out in two steps. First, relative signal gains are determined by separately exposing the radiator ends of each of the four fiber channels to the same

pulsed LED signal. Second, a beam-based calibration is performed using known amounts of lost charge.

2.2.3.1 Relative Channel Gain

We want the four channels to respond equally to the same input signal. The channels are labelled according to their location in ID6 near SCU0 as upstream top (UT), upstream bottom (UB), downstream top (DT), and downstream bottom (DB). The integrated PMT output charge and scale factors are given in Table 1. The scale factors k_{pmt} are used to equalize the response of each channel. We want $Q_j = Q_T / N_{\text{ch}}$ and $\sum f_{\text{pmt},j} k_{\text{pmt},j} = 1$, where Q_T is the total measured (uncorrected) charge from all channels, $f_{\text{pmt},j}$ is the measured fraction, and $N_{\text{ch}} = 4$. We set $f_{\text{pmt},j} = Q_{\text{pmt},j} / Q_T$, where $Q_{\text{pmt},j}$ is the uncorrected output charge on channel j . Also, $\sum Q_{\text{pmt},j} k_{\text{pmt},j} = Q_T$ and $Q_{\text{pmt},j} k_{\text{pmt},j} = Q_j$; therefore, $k_{\text{pmt},j} = Q_T / N_{\text{ch}} Q_{\text{pmt},j} = 1 / N_{\text{ch}} f_{\text{pmt},j}$.

Table 1: PMT response and relative gain using a 1- μs amber LED pulse.

ID6 FO channel, j	Q_{pmt} (nC)	f_{pmt}	k_{pmt}
UT	64.62	0.189	1.322
UB	75.52	0.221	1.131
DT	94.32	0.276	0.905
DB	107.11	0.314	0.797
Σ	341.57	1.000	—

2.2.3.2 Beam-Based Calibration

We deposit a known beam charge at ID6 using an injection kicker, and measure the BLM response. We make two assumptions: 1) PMT response does not change during the loss event except as described by the saturation described in the following section; 2) total calibrated charge deposited in ID6 is the average of the four independently calibrated channels.

The spatial charge distribution in ID6 is not known *a priori* during a beam loss event. Though each channel is calibrated independently for a give charge, we want the sum of the individual loss pulses for each of the channels to represent the total charge; therefore, we take the average of four channels as the total charge.

Using multiparticle tracking in *elegant* [27], a single-bunch solution was found using injection kicker IK2 (located in Sector 39) that results in virtually all charge being lost in ID6. The top panel in Fig. 3 shows the horizontal bunch centroid trajectory versus longitudinal position over one third of the SR circumference, comparing beam position monitor (BPM) turn-by-turn data (black) with *elegant* (red). The trajectories < 10 mm are in good agreement, but the trajectory maxima are not matched because the large-amplitude nonlinear BPM response was not corrected. The bottom panel in the figure shows the BPM sum signal, which shows that the losses occur in ID6. This agrees well with the simulated loss location (cyan). The simulation shows that the beam is lost on the ID chamber transition. For reference, the location of ID4 is also marked, which has the smallest-gap insertion device (ID) chamber of 5 mm full vertical aperture. In comparison, ID6 has a 7.2-7.5 mm full vertical aperture chamber. The beam losses occur mostly on the transition to the small ID chamber.

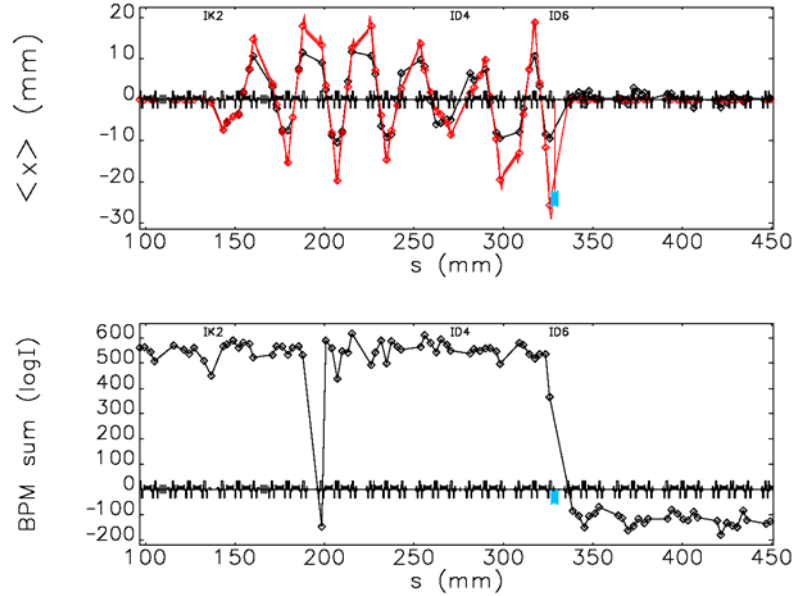


Figure 3: Deliberate beam loss in ID6 using injection kicker IK2 at ~ 1 mrad kick. Top: Horizontal bunch centroid trajectories, comparing measurements (black) and simulation (red). Bottom: BPM sum signal and simulated loss location (cyan).

2.2.3.3 Saturation Model Analysis

The integrated PMT output charge on channel j is calculated as,

$$Q_{pmt,j} = \sum_{i=1}^{N_s} \frac{V_{i,j}}{R} \Delta t,$$

where N_s is the total number of samples, $R=50 \Omega$, Δt is the sample period (typically 400-800 ps), and the PMT output voltage is defined as,

$$V_{i,j} = \begin{cases} V_{pmt,i,j}, & V_{pmt,i,j} \geq V_{thresh} \\ 0, & V_{pmt,i,j} < V_{thresh} \end{cases},$$

with threshold voltage, V_{thresh} . Typically, $V_{thresh} = -50$ mV.

We use the following model that includes linear and saturation components [28],

$$Q_{pmt,j} = \frac{A_j I_j}{(1 + B_j I_j^{\alpha_j})^{1/\alpha_j}}$$

where A , B , and α are determined from data fits, and I_j represents the known charge circulating in the SR per unit time at detector j . The fits are forced to include the origin, ($I_j=0$, $Q_{pmt,j}=0$). This model accounts for the nonlinear response of the PMT detectors at

high signal levels. When α^{-1} is an integer, $Q_{pmt,j}$ can be expressed as a polynomial. Making the substitution $u=BI^\alpha$,

$$Q(1+u)^{1/\alpha} = A \left(\frac{u}{B} \right)^{1/\alpha}.$$

For example, assuming $\alpha^{-1}=3$, we obtain the cubic expression,

$$au^3 + bu^2 + cu + d = 0$$

where,

$$a = 1, b = c = 3 \left(\frac{QB^3}{QB^3 - A} \right), d = \left(\frac{QB^3}{QB^3 - A} \right)$$

For a given calibration data set, we first fit all three parameters A, B, and α using the `sddsstoolkit` command `sddsgenericfit` [29,30] and select the closest integer value for α^{-1} . The data are then fit again keeping α constant to find the best values for A and B. Having solved for I, the average calibrated charge is expressed as,

$$\langle Q_{cal} \rangle = \frac{1}{N_{ch}} \sum_{j=1}^{N_{ch}} Q_{cal,j} = \frac{1}{N_{ch}} \sum_{j=1}^{N_{ch}} k_{pmt,j} \tau_{QI} \sum_{p=1}^{N_p} I_{f,j,p}$$

where the index p represents each loss pulse, $k_{pmt,j}$ is the PMT correction factor from Table 1, τ_{QI} is the conversion of current to charge for one turn ($=3.68$ nC/mA= 3.68 μ s), $I_{f,j,p}$ is the intercepted beam current from the fit associated with pulse p on channel j , and N_p is the total number of pulses.

2.2.3.4 Calibration Beam Loss Measurements

The calibration data and saturation fits are presented in Fig. 4 for the four detector locations in ID6 mentioned above. Note that the data fits indicate a quadratic form for the upstream detector pair, but a cubic dependence for the downstream pair. In anticipation of the installation of SCU1 in ID1, similar calibration measurements were conducted for FO BLMs in both US and DS locations in the ID straight section.

2.2.4 Beam Loss Measurements

2.2.4.1 MPS Generated Beam Dumps

The calibration was used to analyze specific beam losses recorded during beam operations. In Table 2, ID6 losses associated with MPS trips are presented. In all but one case shown, the SCU0 main coil windings experienced a quench. Calibrated charge detected by each BLM, as well as the average calibrated charge are also presented in the table. The total stored charge is nominally 376 nC (102 mA); ID6 losses range from 0.7-2% of the total with the average loss from Table 2 of 4.2 nC. Thirty-three small-gap ID chambers exist around the SR. If the losses were uniformly distributed, then 11 nC would be lost at each ID. However, elegant simulations indicate 77% of the beam in a hybrid fill pattern is lost on the smallest aperture at ID4 [31,32], with the rest is distributed among the remaining ID chambers. The hybrid mode consists of one high-charge bunch with approximately 15% of the total circulating charge and eight 7-bunch

trains on the opposite side of the SR with the remaining charge; there is a 1.6- μ s gap on either side of the singlet with a gap of 51 ns between each bunch train. The BLM results here are consistent with that picture. If we naively take the average charge from ID6 to be the same for all 32 small gap chambers except ID4, this accounts for 134 nC or 36% of the stored charge. The remaining 64% of the charge is presumably lost in ID4. More work is needed to understand both the quantitative loss distribution and variability at ID6.

The beam dump that did not result in an SCU0 quench took place during the hybrid-mode fill pattern [24]. There does not appear to be any correlation of quench or no quench with bunch pattern. Rather, these sample beam dumps were chosen because it is instructive to compare the loss associated with BLM indices 735 and 736. These loss events occurred within 5 h of each other in the same bunch pattern and with the same SCU0 main coil current. The BLM waveform time structure is also very similar (not shown). It appears that the quench threshold for these conditions may be between 2.66 and 2.87 nC average loss charge.

It is also interesting to study why the loss associated with BLM index 691 causes the SCU0 to quench while the 735 beam dump did not, even though both events deposited approximately equal amounts of charge. The four waveforms from each BLM are presented in Figs. 5 and 6 for both beam dumps. The loss from the 24-bunch fill pattern occurs over a shorter number of turns and, therefore, has higher peak intensity. Perhaps more significantly, the coil current is over 100 A higher in the 24-bunch case, meaning the coil is operating closer to its critical current. For the same deposited energy, a smaller temperature excursion within the coils can lead to a quench in the 24-bunch case.

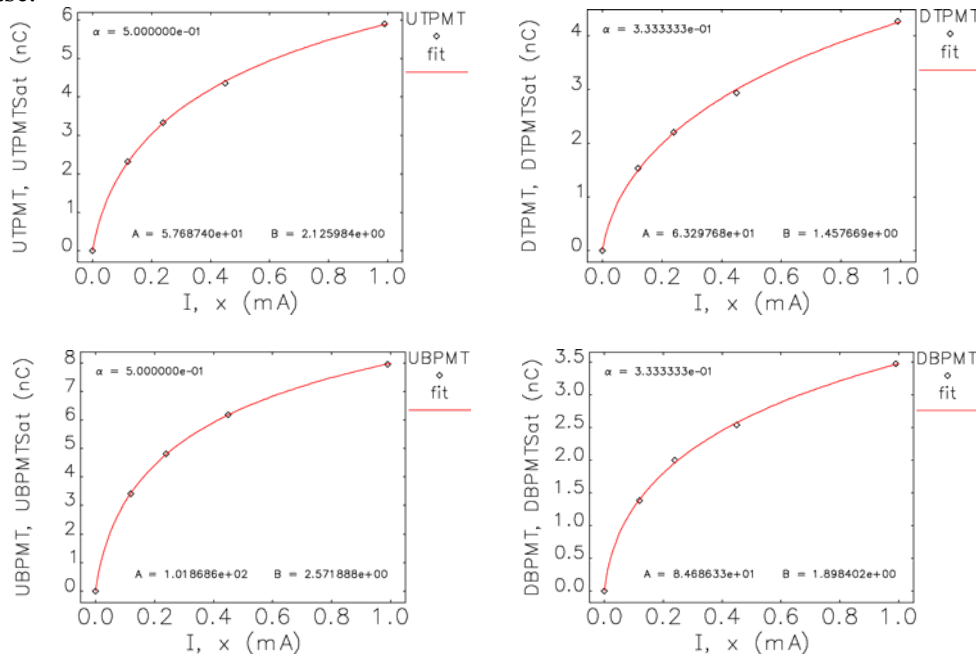


Figure 4: Direct ID6 beam deposition data with saturation model fits.

Preliminary simulations with the particle-matter interaction program MARS [22] have shown that 1 nC of 7-GeV electrons directly striking the beam chamber at the upstream end of the SCU0 undulator is more than sufficient to cause temperature

excursions that can lead to quenching at normal operating currents [19]. Calibrated BLM measurements indicate that beam losses greater than 1 nC may not always cause SCU0 to quench, suggesting that energy deposition may be more diffuse than in the simple, directed beam loss scenario described. `Elegant` modeling shown in Fig. 3 shows that lost beam is first incident on the upstream ID chamber transition, which is about 3.8 m upstream of the SCU0 undulator. More work is planned.

Table 2: Beam dumps initiated by MPS, with corresponding SCU0 operating current, ID6 BLM index, total uncalibrated output PMT charge, calibrated, and average charge.

Bunches	Main coil current (A)	BLM index	Total uncalibrated charge (nC)	UT (nC)	UB (nC)	DT (nC)	DB (nC)	Average calibrated charge (nC)
57*	577	735	149.48	1.08	0.35	5.78	3.43	2.66
57	577	736	161.55	1.36	0.46	6.06	3.59	2.87
24	658	784	346.45	2.04	0.52	17.33	11.17	7.77
24	661	720	108.36	1.01	0.34	6.20	3.31	2.72
24	661	723	146.48	1.47	0.51	9.08	4.77	3.96
24	661	721	148.62	1.46	0.50	9.31	4.84	4.03
24	661	722	153.26	1.50	0.52	9.77	5.04	4.21
24	686	691	100.72	0.63	0.17	6.00	3.35	2.54
24	686	692	128.87	0.81	0.23	8.98	4.51	3.63
24	686	693	199.21	1.22	0.31	11.74	6.70	4.99
24	687	729	230.79	1.40	0.37	16.39	8.44	6.65

* Did not quench.

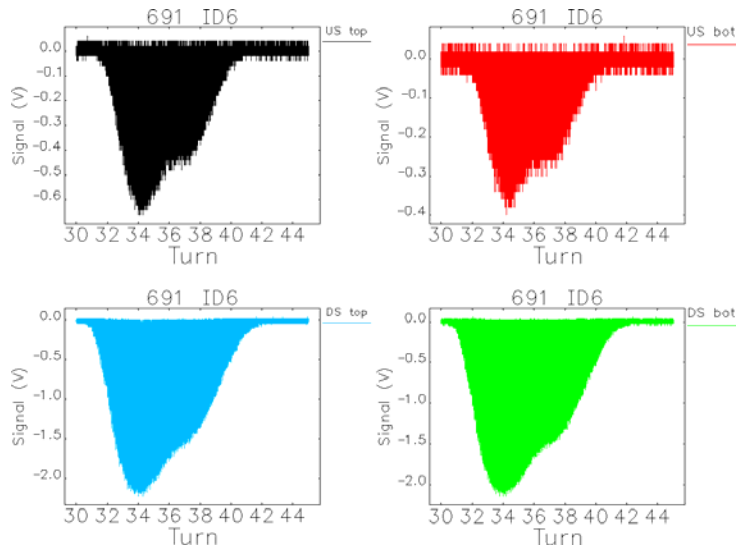


Figure 5: ID6 beam loss from 24-bunch fill pattern (index 691) which caused a quench.

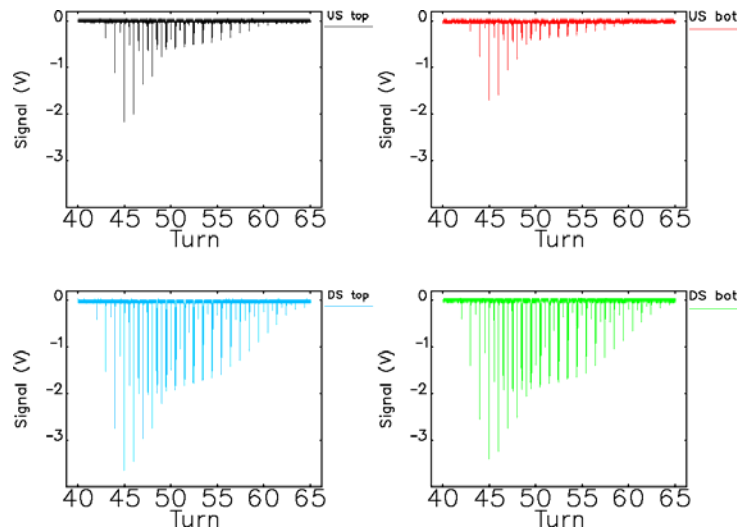


Figure 6: ID6 beam loss from hybrid fill pattern (index 735) which did not cause a quench.

ID1 has been chosen as the location for the longer SCU1; thus, characterizing the loss there is important. Prior to SCU1's installation in May 2015, a pair of fast FO BLMs were installed in ID1. Each FO bundle was run parallel to the beam axis for a length of 1.4 m near beam elevation. One bundle was placed on the upstream (US) ID and the other on the downstream (DS) ID. Horizontally, the bundles are located 10 cm from the vacuum chamber inboard edge. An example of a recent beam dump is presented in Figure 7. Plotting the US/DS waveforms in the same panel and zooming in on a single loss pulse, time-of-flight time differences are evident as shown in Figure 8; also variations in the shape of each pulse indicate spatial distribution of loss along the fiber bundles. This is an ongoing area of investigation. The average calibrated charge is less than 0.5 nC.

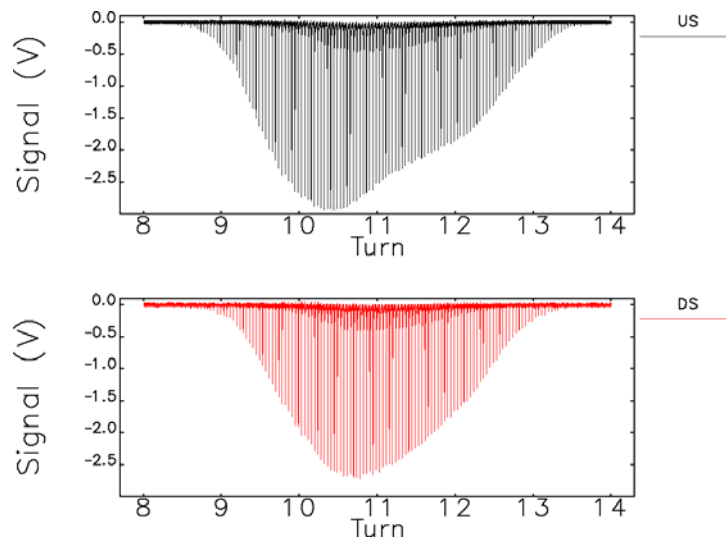


Figure 7: ID1 beam dump signals from a 24-bunch fill pattern.

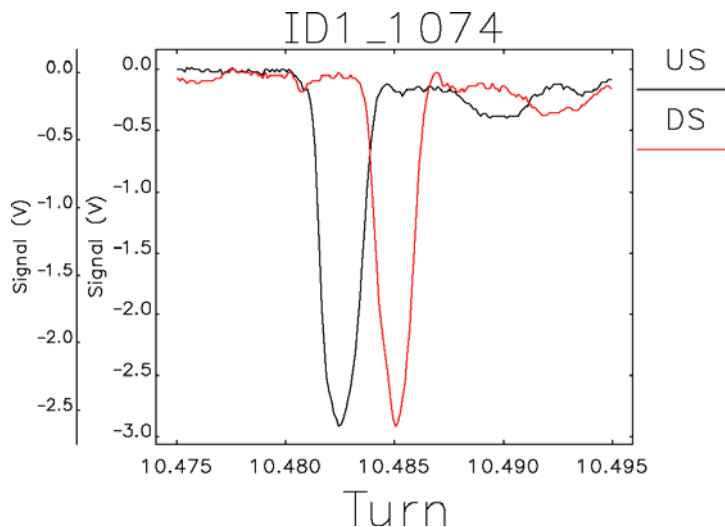


Figure 8: Zooming in on a single loss pulse pair of the event shown in Fig. 7. Time-of-flight distinguishes upstream and downstream signals; variations between the pulses reflect spatial variations in the loss.

2.2.4.2 Injection Loss

Though not the smallest ID vacuum chamber in the SR, ID1 is the first ID straight section after injection and four sectors of larger-aperture chambers associated with the rf cavities. Shortly after the start of Fall 2014 user operations, the FO BLM installed in the upstream end of ID1 indicated elevated injection loss signals. The SR was operating in standard 24-bunch top-up mode. A sample of these data is presented in Fig. 9 (left); the losses are multi-bunch, single turn events. Calibration measurements indicated $\alpha^{-1}=4$ provided the best fit for ID1 BLM data set. With calibration, Fig. 9 represents a lost charge of 32 pC (0.23 J at 7 GeV). Injection tuning reduced this number to approximately 10 pC per injection. Typically 2 nC (~ 0.5 mA) are injected into the SR per top-up cycle [33]. MARS simulations suggest 32 pC would be roughly an order of magnitude below the quench point at nominal operating current; however, more simulations including realistic loss distributions are required. Other injected loss distributions are generally lower than that shown in Fig. 9 (left); for example, a typical 324-bunch injected-loss waveform is presented in Fig. 9 (right). The waveform again shows multi-bunch single-turn loss, but at a greatly reduced signal intensity relative to the 24-bunch case. Total calibrated losses here are < 1 pC.

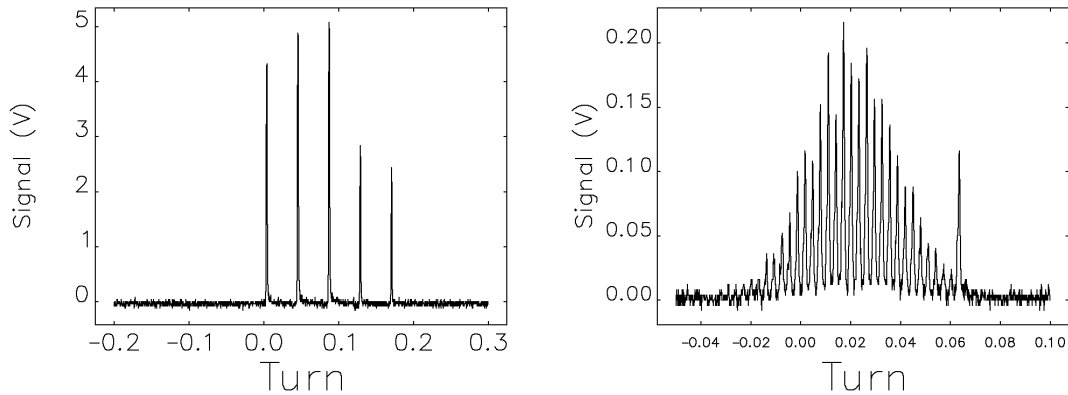


Figure 9: Uncalibrated injection loss in ID1 for 24-bunch top-up (left) and 324-bunch non-top-up (right) (signals inverted).

2.2.5 SCU0 Protection Studies

The horizontal injection kickers (IK) were used to test a beam abort system. The injector kicker pulse waveform is $\sim 2 \mu\text{s}$ FWHM [34]. In order to kick out a full turn, which is $3.68\text{-}\mu\text{s}$ long, two horizontal injection kickers were used as a pair, with the second kicker timing shifted by half a turn [35]. We used IK1 (in Sector 38) and IK4 (in Sector 40) as a pair, and IK2 and IK3 (both in Sector 39) as another pair. The kickers were set to their maximum peak kicks of $\sim 1.5 \text{ mrad}$ and it was verified that the entire beam was lost. The studies were repeated for the nominal 102 mA stored in 24 and 324 uniformly-spaced bunches. In Table 3, the BLM integrated loss charge for a normal MPS beam dump is compared to that using the kickers. For loss events 833 and 836, a combination of IK1 and IK4 dramatically reduces beam losses in ID6.

To test whether lower ID6 beam losses can prevent a quench, 102 mA were stored in 24 bunches and SCU0 was powered to a typical main coil current of 650 A . IK1 and IK4 were fired, dumping the entire beam, and SCU0 did not quench. In this case, the losses at SCU0 were below the BLM measurement threshold.

While the injection kicker tests were a successful proof of principle, the loss distribution is not ideal, in that beam is lost in ID1, the planned location of SCU1. The beam abort system should limit losses at both SCU0 and SCU1. Also, injection kicker abort configurations are incompatible with top-up operation. The new beam abort system will use a dedicated horizontal kicker in Sector 36. More details can be found in [18].

Table 3: Beam dump studies using injection kickers; ID6 (SCU0) BLM signals and total calibrated deposited charge. The SCU0 is de-energized.

<i>Dump type</i>	<i>24 bunches Total integrated output charge (nC)</i>	<i>Ave. dep. charge (nC)</i>	<i>BLM index</i>	<i>324 bunches Total integrated output charge (nC)</i>	<i>Ave. dep. charge (nC)</i>	<i>BLM index</i>
MPS only	444	11.42	830	480	7.93	835
IK1 & IK4 @ 14 kV	1	0.011	833	6	0.095	836
IK2 & IK3 @ 14 kV	30	1.52	834	44	0.90	837

2.2.6 Discussion and Summary

Fast FO beam loss monitors have proven to be a useful tool for the characterization of local beam losses, in particular, beam dump-induced losses at SCU0. They have also been used to guide the design of a beam abort kicker system to minimize beam losses both at SCU0 and the future SCU1, with the goal of mitigating quenches. Dedicated FO BLMs have been installed inside the SCU1 cryostat and will be calibrated later this year. More work is needed to quantify the SCU quench threshold, which will involve analysis and more realistic beam loss modeling with MARS.

2.2.7 Acknowledgments

Thanks to Michael Borland, Louis Emery, Vadim Sajaev, Nicholas Sereno, Aimin Xiao, and Alexander Zholents for discussions and suggestions, and to Albert Hillman for providing IK waveforms. Thanks also to Adam Brill, Chuck Doose, John Grimmer and his staff for installation of the FO BLMs. The work was supported by U. S. Department of Energy, Office of Science, under Contract No. DE-AC02-06CH11357.

2.2.8 References

1. H.T. Edwards, "The Tevatron Energy Doubler: A Superconducting Accelerator," *Ann. Rev. Nucl. Part. Sci.* 35, 605 (1985).
2. J.B. Jeanneret, D. Leroy, L. Oberli, T. Trenkler, "Quench levels and transient beam losses in LHC magnets," LHC Project Report 44 (1996).
3. D. Bocian, B. Dehning, A. Siemko, "Modeling of Quench Limit for Steady State Heat Deposits in LHC Magnets," *IEEE Trans. Applied Superconductivity* 18, 112 (2008).
4. Y. Iwamoto et al., "Quench Stability Against Beam-Loss in Superconducting Magnets at the 50 GeV Proton Beam Line for the J-PARC Neutrino Experiment," *IEEE Trans. Applied Superconductivity* 14, 592 (2004).
5. E. B. Holzer et al., "Beam Loss Monitoring System for the LHC," 2005 IEEE Nucl. Science Symposium Conf., 1052 (2005).
6. N. Marks et al., "Initial operation of a 5T superconducting wiggler magnet in the SRS," *Nucl. Instrum. Meth.* 208, 97 (1983).
7. M. Poole et al., "A second superconducting wiggler magnet for the Daresbury SRS," *Proc. 1989 Part. Accel. Conf.*, 1250 (1989).
8. K. Soutome et al., "Generation of high-energy synchrotron radiation with a 10-T

- superconducting wiggler installed in the SPring-8 storage ring,” Proc. 2003 Part. Accel. Conf., 250 (2003).
9. A. Temnykh, J. Crittenden, D. Rice, and D. Rubin, “Beam based characterization of a new 7-pole superconducting wiggler at CESR,” Proc 2003 Part. Accel Conf, 3425 (2003).
 10. L. Tosi, C. Knapic, and D. Zangrando, “The ELETTRA superconducting wiggler,” Proc. 9th European Part. Accel. Conf., 390 (2004).
 11. C. H. Chang et al., “In-achromatic superconducting wiggler in Taiwan Light Source: installation and test results, Proc. 10th European Part. Accel. Conf., 3613 (2006).
 12. S. V. Khrushev et al, “Superconducting 63-pole 2-T wiggler for Canadian Light Source, Nucl. Instrum. Methods Phys. Res., Sect. A 575, 38 (2007).
 13. J. C. Schouten and E. C.M. Rial, “Electron beam heating and operation of the cryogenic undulator and superconducting wiggler at Diamond,” Proc. 2nd Int’l Part. Accel. Conf., 3323 (2011).
 14. D. Robin et al., “Superbend upgrade on the Advanced Light Source,” Nucl. Instrum. Methods Phys. Res., Sect. A 538, 65 (2005).
 15. S. Casalbuoni et al, “Generation of x-ray radiation in a storage ring by a superconductive cold-bore in-vacuum undulator, Phys. Rev. ST Accel. Beams 9, 010702 (2006).
 16. Y. Ivanyushenkov, et al., “Development and operating experience of a short-period superconducting undulator at the Advanced Photon Source,” Phys, Rev. ST Accel. Beams, **18**, 040703 (2015).
 17. W.A. Wurtz et al, “Preventing Superconducting Wiggler Quench During Beam Loss at the Canadian Light Source,” Proc. 2014 Int’l Part. Accel. Conf., 1992 (2014).
 18. K. Harkay et al., “Development of an abort kicker at APS to mitigate beam loss-induced quenches of the superconducting undulator,” to be published in Proc. 6th Int’l Part. Accel. Conf., TUPJE066 (2015).
 19. J. Dooling et al., “Calibration of fast fiber-optic beam loss monitors for the Advanced Photon Source storage ring superconducting undulators,” to be published in Proc. 6th Int’l Part. Accel. Conf., TUPJE064 (2015).
 20. J. Dooling et al, “Development of a fiber-optic beam loss position monitor for the Advanced Photon Source storage ring,” Proc. 2009 Part. Accel. Conf., 3438 (2009).
 21. Y. Ivanyushenkov et al., “Development and performance of 1.1-m long superconducting undulator at the Advanced Photon Source,” to be published in Proc. 6th Int’l Part. Accel. Conf., TUPJE068 (2015).
 22. N. V. Mokhov et al., AIP Conf. Proc. 896 (2007).
 23. Metal Package Photomultiplier Tube R7400U Series, TPMH1204E07 (2004). http://ctf3-tbts.web.cern.ch/ctf3-tbts/instr/PMT/R7400U_TPMH1204E07.pdf.
 24. http://www.aps.anl.gov/Accelerator_Systems_Division/Accelerator_Operations_Physics/SRparameters/SRparameters.html
 25. A. Pietryla, W. Berg, R. Merl, “A Cerenkov radiation detection system for the Advanced Photon Source storage ring,” Proc. 2001 Part. Accel. Conf., 1622 (2001).
 26. B.-X. Yang, private communication September, 2008.
 27. M. Borland, “elegant: A Flexible SDDS-Compliant Code for Accelerator Simulation,” Technical Report LS-287, Advanced Photon Source, Sep 2000.
 28. L. Emery, private communication, August 2014.
 29. M. Borland et al., “User’s Guide for SDDS Toolkit Version 2.8” (Jan. 28, 2014). http://www.aps.anl.gov/Accelerator_Systems_Division/Accelerator_Operations_Physics/manuals/SDDStoolkit/SDDStoolkit.html
 30. R. Soliday et al., “New Features in the SDDS Toolkit,” Proc. 2003 Part. Accel. Conf., 3473 (2003).
 31. M. Borland and L. Emery, “Touschek Lifetime and Undulator Damage in the Advanced Photon Source,” Proc. 2005 Part. Accel. Conf., 3835 (2005).

32. J. C. Dooling and M. Borland, "Simulation and Measurement of Beam Loss in the Narrow-Gap Undulator Straight Section of the Advanced Photon Source Storage Ring," Proc. IPAC2012, 106 (2012).
33. L. Emery, "Optimization and Modeling Studies For Obtaining High Injection Efficiency At The Advanced Photon Source," Proc. 2005 Part. Accel. Conf., 871 (2005).
34. W.W. Frey, "Single-bunch Kicker Pulsar," Proc. IEEE 4th Intl. Pulsed Power Conf., Albuquerque, NM (1983).
35. V. Sajaev, private communication, July 2014.

2.3 Demagnetization Effects at PETRA III Undulators

Markus Tischer, Pavel Vagin

Deutsches Elektronen-Synchrotron, Notkestraße 85, 22607, Hamburg, Germany

Mail to: markus.tischer@desy.de

2.3.1 Abstract

In the PETRA III storage ring light source at DESY, 15 undulators are presently operated together with 20 damping wigglers. All of these devices are built in permanent magnet technology and are therefore subject of potential demagnetization, especially as the straight sections for insertion devices usually provide the smallest aperture in the storage ring. Even though beam collimators are installed in the machine, the general radiation background in the tunnel is high which can also be anticipated from a beam life time in the order of only a few hours. Signs of radiation damage of some undulators have already been indicated for several years in a systematic long-term decrease of the magnet gap for tuning at particular photon energy and a growing distortion of the spectral distribution of the undulator harmonics. Finally, magnetic measurements in the tunnel confirmed the demagnetization problem at several undulators; two devices were meanwhile removed from the storage ring and were carefully characterized before refurbishment. We report on magnetic measurements of these undulators and discuss operation restrictions due to the damage.

2.3.2 Introduction

PETRA III is a 3rd generation light source operating since 2009. By that time, one octant of the machine had been reconstructed to a DBA-lattice with 5m long straight sections. In total, 15 undulators are installed in these straights, partly 5m long undulators but in majority two 2m long insertion devices (IDs) in a canted configuration (5mrad). Additionally, two times 40m of damping wigglers are in operation in the long straight sections in the West and North of the machine in order to reduce the beam emittance down to 1nmrad.

The smallest apertures for the electron beam in such machines are usually found in the straight sections for undulators and wigglers which makes these locations likely for the occurrence of beam losses. During the last five years of operation, thermoluminescent dosimeters (TLDs) were routinely placed and read out to monitor the overall radiation exposure of the IDs in all straight sections. A generally very high radiation background level was found from the beginning on and it was observed that the radiation level varies significantly for the different locations. Substantial variations

could also be seen over time, which might have been caused by temporary operation difficulties. For a few ID positions, a total dose of up to several hundred kGy has been accumulated up to now. Besides, visible corrosion was observed at several undulators; it turned out however, that this is a surface effect which does not deteriorate the magnetic properties significantly and could be caused by radio-chemical reactions initiated by the synchrotron radiation background in the tunnel.

Radiation damage problems had previously also been reported from other synchrotron radiation facilities where both corrosion by synchrotron radiation and also damage of various components and permanent magnet structures due to particle losses were observed [1-3]. In particular at the APS, demagnetization of IDs was experienced in the past which required a repeated refurbishment and retuning of undulator magnet structures [4, 5]. Also for the sFLASH seeding section, a damaged undulator, previously used during the booster operation of PETRA in the early days, was successfully refurbished and retuned [6].

At PETRA III, first hints on a degradation of the undulator performance appeared already in the first years of operation. It was found at some beamlines that tuning the photon energy to always the same value (with otherwise same experimental conditions) required a continuously smaller undulator gap over long time [7]. In particular, a severe operation restriction was foreseeable for the high resolution powder diffraction beamline P02.1 operating at a fixed energy of 60keV which could be reached on the 7th harmonics only very close and closer to the minimum magnetic gap. Together with a continuous gap change, an increasing distortion of the spectral distribution of the undulator harmonics had been observed accompanied by a substantial intensity reduction. This problem could be partly corrected by tapering the undulator gap, however the demagnetization profile is usually not linear along the device [8].

The demagnetization problems were finally confirmed by a direct measurement of the peak field distribution of the IDs while installed in the tunnel. Two of the undulators which were proven to show significant demagnetization effects were brought back to the magnet measurement lab for retuning during the long shutdown period of PETRA in 2014. One of the undulators, a U29 at beamline P08, was retuned after disassembling the magnet structure and flipping all magnets. For the other device, a U23 at beamline P02, larger demagnetization effects had been found as will be discussed in the next sections. Finally, all magnets needed to be remagnetized to bring the undulator back to specifications.

Also the damping wigglers in the long straight sections in the West and North of the machine are generally susceptible to radiation damage. As these closed-box devices cannot be measured in the installed state, two prominent wigglers had been uninstalled for that purpose: the first wiggler in the West which is located behind a beam trap and secondly the last wiggler in this straight which is exposed to the full synchrotron radiation background of all the upstream wigglers; for the latter, no demagnetization could be detected. The first wiggler did show only a small peak field degradation of about 0.3% [7] but no changes in the field integrals besides a small variation in the multipole distribution of the horizontal field which had been retuned.

Collimators are usually installed in storage rings to confine the beam and prevent from beam loss at ID straights. At PETRA, a second pair of vertical collimators has recently been installed to improve the situation. Along with this, detailed tracking studies have been pursued to get a deeper understanding of observed locations with pronounced radiation damage effects [9]. While the additional collimators shall reduce

the long-term damage of particular magnet structures, the overall problem is based on the generally very short beam life time at PETRA which has been about 15 hours in the 960-bunch operation mode but not more than a few hours in timing mode operation with 40 bunches.

2.3.3 Peak field Measurements in the Tunnel

To confirm that the observed spectral changes were caused by radiation demagnetization of the permanent magnets, the undulators' magnetic field was remeasured in the tunnel. It is not possible to measure the field on the beam axis with closed undulator gap because of the vacuum chamber. Therefore top and bottom magnet modules were measured separately at fully opened gap and then averaged. Also due to space constraints in the tunnel, the Hall probes were moved manually along the structure using the undulator itself as a mechanical reference. Without proper longitudinal positioning only the peakfield values could be measured. Despite of such a manual way of measurement the non-reproducibility is below 0.1%, and the absolute accuracy in comparison to the measurements in the lab with closed gap is better than 1%, which is caused mostly by a gain error due to the limited vertical positioning accuracy in the vertical field gradient of a single module at open gap.

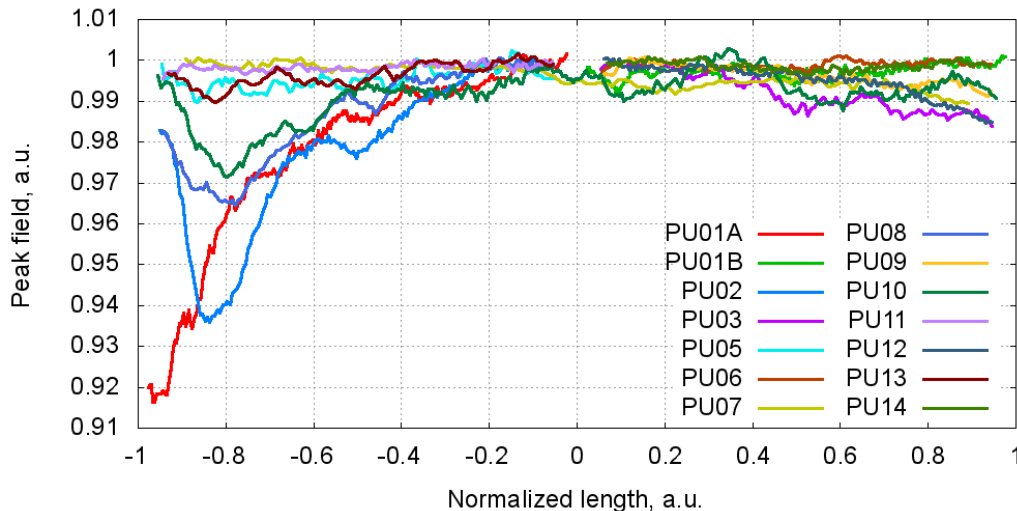


Figure 1: Demagnetization of PETRA III undulators. The horizontal axis is normalized to the length of a straight section. Most of the devices are 2m long and installed in pairs, except for PU10 (5m) and PU07 (2m) which are single in a straight. PU01A,B are two 5m devices installed in the first long straight.

There are 9 straight sections in the rededicated PETRA III octant with 14 undulator beamlines installed. Some devices are paired in a canted straight section. The first ones of these show a stronger demagnetization, mainly at their upstream part. The second devices show generally less demagnetization, which is found mainly at the downstream end (Fig. 1). This pattern corresponds to the beta function and beam size being minimal at the center of the straight section and increasing towards both ends while the beam aperture given by the undulator vacuum chamber remains constant over its entire length which makes beam losses most likely at the ends of the small gap undulator chamber. Related beam loss pattern have also been calculated in theoretical investigations [9, 10].

The largest demagnetization effects in Fig. 1 are seen for undulator PU01A, which represents the first narrow gap aperture in the machine behind the injection point, and PU02 which is the upstream undulator in the first DBA cell of the remodelled octant of PETRA III.

2.3.4 Refurbishment of PU02

During the last shutdown a few devices were removed from the tunnel and properly remeasured in the lab. Measurements show a transverse non-uniformity of the demagnetization (higher at "ring-outside", i.e. negative Z), which is also different for top and bottom magnet modules (Fig. 2).

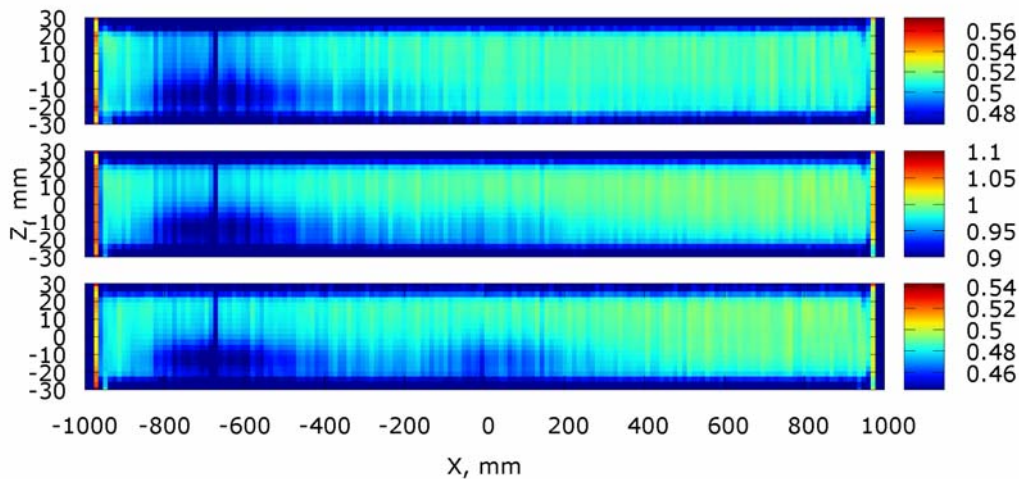


Figure 2: 2D-field map of undulator PU02 for top module (top) at open gap, closed gap of 10mm (center), and bottom module at open gap (bottom), normalized to the initial field amplitude. The demagnetization is non-uniform and localized in the upstream part towards "ring outside" (negative Z). Also, the demagnetization of top and bottom modules is different.

Despite the strong field losses of $\sim 6\%$, the trajectory straightness was not really affected, as a significant number of poles were demagnetized. Thus, field changes on neighboring poles with opposite signs were similar, having only minor impact on the field integrals as it can be seen in Fig. 4.

In contrast to that, the effect of demagnetization on the phase error is much more severe, since different parts of the undulator have different field amplitude and thus correspond to different emitted wavelengths (Fig. 5).

The damage to the magnets is localized to the part which is close to the beam axis. Therefore flipping of the magnets upside down could, for some time, have fully corrected all field errors due to demagnetization, since the magnet parts far away from the beam axis contribute much less to the peakfield. For this particular device it was finally decided to completely refurbish and remagnetize the magnets. The coercivity of the magnets was enhanced by a rare earth diffusion process treatment to strengthen the grain boundaries, and after all an additional coating was applied to prevent them from corrosion by exposure to synchrotron radiation.

Before disassembly of the magnet structure for refurbishing the magnets, there was an attempt to retune the undulator poles and correct for the field errors resulting in a

2D-field map shown in Fig. 3. By that means, the phase error on-axis could be brought down to 5° RMS (Fig. 5) within a single tuning iteration. However, because of the transverse non-uniformity of the field errors it was only possible to correct the field on-axis and at one particular gap (Fig. 4, 5). Off-axis errors as well as their gap dependence could not be corrected just by pole tuning. That would also have resulted in a strong sensitivity of the spectral performance on the actual orbit.

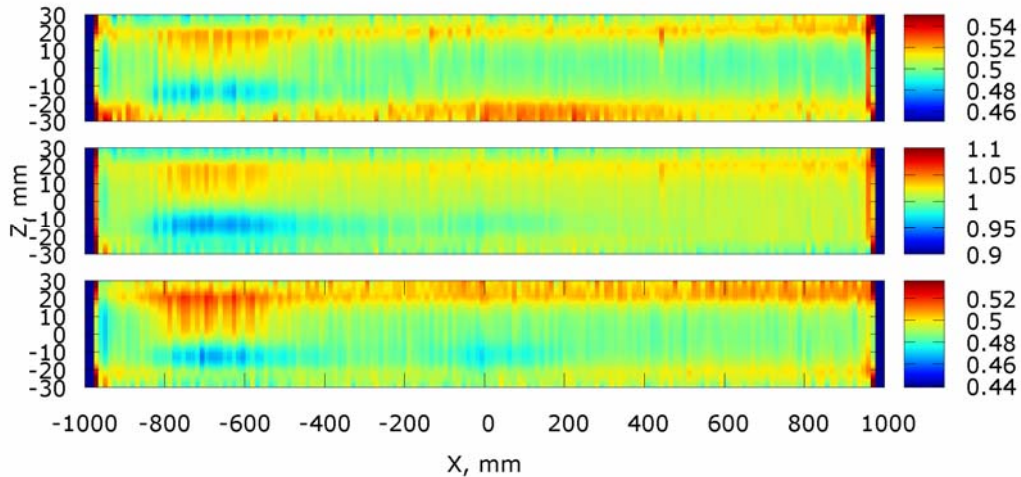


Figure 3: 2D-field map of undulator PU02 after retuning for top module (top) at open gap, closed gap of 10mm (center), and bottom module at open gap (bottom), normalized to the initial field amplitude. Pole tuning for proper field amplitude on-axis could not correct the transverse non-uniformity of the field.

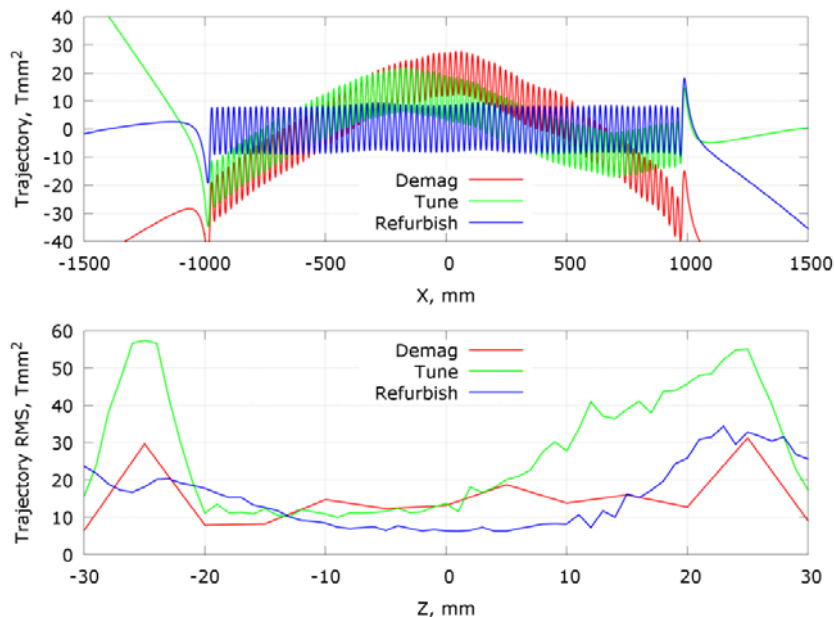


Figure 4: PU02 trajectory on-axis along the structure (top) and transverse dependence of the RMS 2nd field integral value (bottom) in the damaged state, after retuning and after refurbishing. As the demagnetization spreads over a large number of poles, the neighbored opposite magnets are demagnetized similarly with almost no change of the field integrals.

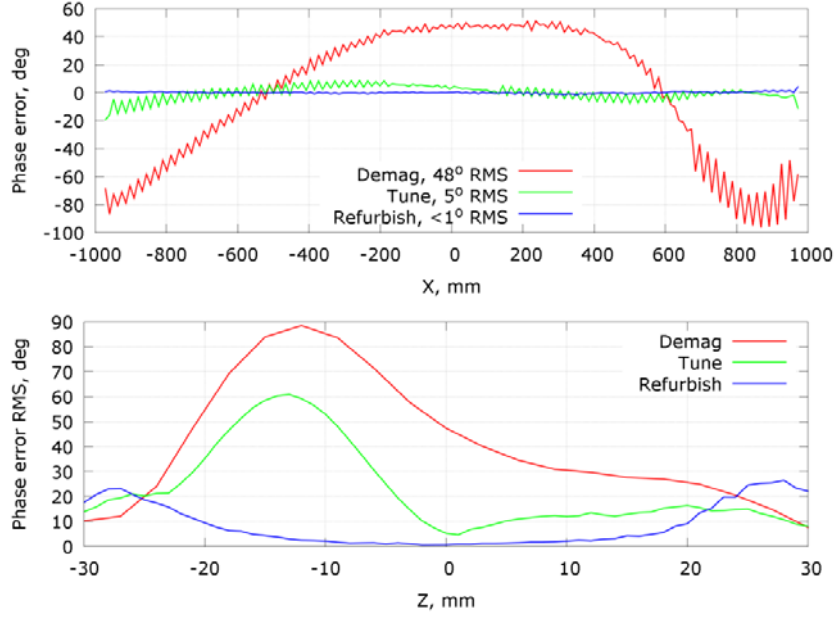


Figure 5: PU02 phase error on-axis along the structure (top) and transverse dependence of the RMS phase error value (bottom) in the damaged state, after retuning and after refurbishing. Retuning could correct the phase error on-axis but not the transverse non-uniformity.

2.3.5 Dynamic Multipoles

Demagnetization, being non-uniform in the transverse direction, creates field gradients that could create dynamic multipoles. When moving in the vertical field along the undulator, the electron oscillates in horizontal plane. For an electron displacement in a transverse field gradient, the positive half period of the trajectory is passing through a higher field than the negative half period. With the field amplitude B_0 and period length λ_u , the first field integral of a half period is $B_0\lambda_u/\pi$. The trajectory oscillation amplitude is $Z_0 = B_0(\lambda_u/2\pi)^2 c/E$, where E is the electron energy. The field amplitude in presence of a transverse field gradient can be written as $B(\mathbf{z}) = B_0 + (dB/dz) \cdot \mathbf{z}$. Then, the additional kick obtained per half period in a field $B(Z_0)$ for a beam displaced by Z_0 is $I = (B(Z_0) - B_0)\lambda_u/\pi = 2B_0(dB/dz)(\lambda_u/2\pi)^3 c/E$.

Deriving the transverse field gradients from the measured 2D-map (Fig. 2) and integrating the dynamic multipoles along the structure results in a dynamic field integral shown in Fig. 6. It can be seen that for such a short period 2m long device like PU02, with 23mm period length, the dynamic multipoles are negligible in a field gradient of only a few mT/mm caused by radiation demagnetization. This holds even at the transverse position of ± 25 mm where the pole ends and field gradients have a maximum (Fig. 6). However for longer devices with a long period length, like the 4m damping wigglers with 200mm period length, this could be as issue as the dynamic kick is proportional to the 3rd power of the period length.

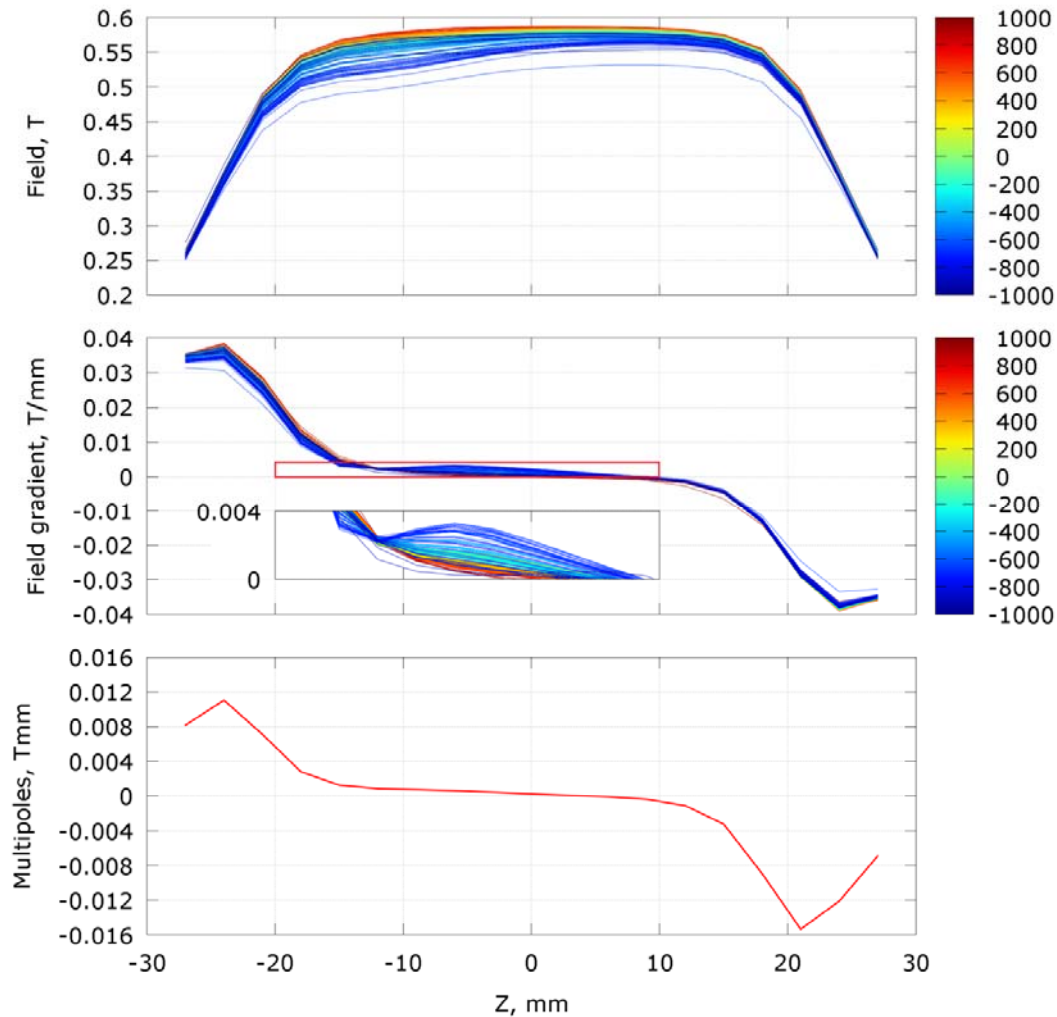


Figure 6: Top: Transverse profiles of the vertical field of undulator PU02; the longitudinal position along the undulator is color-coded. Center: Related transverse field gradients. Bottom: Dynamic multipoles integrated along the undulator.

2.3.6 Summary

Synchrotron radiation in the PETRA III storage ring aggravates radio chemistry which leads to corrosion of magnet structures; this is however not the cause for the observed demagnetization. Demagnetization of several magnet structures and their corrosion are not correlated.

For the undulators installed in pairs in straight sections, the first IDs show demagnetization from the upstream side, while the second ones are damaged from downstream side. This indicates demagnetization by particle losses. At these positions the vertical beam size is largest in each undulator cell, since the vertical beta function has its minimum in the center of straight section, between two paired undulators. Losses are higher at the upstream end of the first undulators, where the aperture is decreasing for the straight section.

In order to compensate for the demagnetization of the PU02 undulator, gap settings to reach the same wavelength were decreasing over time until reaching the minimum value defined by the vacuum chamber. Retuning of the undulator by shifting poles could correct the field amplitude only on-axis; however the transverse non-uniformity of the field errors makes the trajectory and phase errors off-axis too big. To make the matter worse, there is only a single U23 undulator at PETRA so that a spare magnet structure for a future quick replacement cannot be considered. Therefore it was finally decided to refurbish the magnets and improve their radiation resistance during the recent one-year shutdown for building PETRA III Extension. Otherwise, the magnets are usually damaged only from one side, the one which faces the beam. If they are shaped symmetrically, it is then possible in some cases to flip them and to retrieve nearly the initial magnetic field level; this approach was followed for the repair of the U29 undulator for beamline PU08.

2.3.7 References

1. M. Petra, P. Den Hartog, E. Moog, S. Sasaki, N. Sereno, I. Vasserman, "Radiation effects studies at the Advanced Photon Source", Proceedings of FEL02, Nucl. Instr. and Meth. A 507 (2003) 422
2. T. Bizen, et al., "Demagnetization of undulator magnets irradiated high energy electrons", Nucl. Inst. & Meth. A 467, (2001) 185
3. P. Van Vaerenbergh, "Radiation damage issues at the ESRF", Proceedings of Accelerator Reliability Workshop, Grenoble, France (2002)
4. S. Sasaki, M. Petra, I. Vasserman, C. Doose, E. Moog, "Radiation damage to Advanced Photon Source undulators", Proceedings of PAC05, Knoxville, Tennessee USA (2005)
5. I. Vasserman, S. Sasaki, M. Petra, "Retuning of radiation-damaged undulators at APS", IMM13, Stanford, California USA (2003)
6. H. Delsim-Hashemi, J. Rossbach, M. Tischer, A. Schöps, Y. Holler, "Undulator system for a seeded FEL experiment at FLASH", Proceedings of PAC09, Vancouver, BC, Canada (2009)
7. P. Vagin, O. Bilani, A. Schöps, S. Tripathi, T. Vielitz, M. Tischer, "Radiation Damage of Undulators at PETRA III", WEPRO35, pp. 2019, Proceeding of IPAC2014, Dresden, Germany (2014)
8. P. Vagin, S. Francoual, J. Keil, O.H. Seeck, J. Stempfer, A. Schöps, M. Tischer, "Commissioning Experience with Undulators at PETRA III", Proceedings of SRI2012, Lyon, France (2012)
9. M. Bieler et al., "Radiation Damage of Insertion Devices at PETRA III – A Perspective View from Optics and Tracking Studies", this Newsletter
10. N. Simos, P.K. Job, N. Mokhov, "An experimental study of radiation-induced demagnetization of insertion device permanent magnets", WEPC053, Proceedings of EPAC08, Genoa, Italy (2008)

2.4 Radiation Damage of Insertion Devices at PETRA III – A Perspective View from Optics and Tracking Studies

M. Bieler, J. Keil, G. Kube, G.K. Sahoo, M. Tischer, R. Wanzenberg
Deutsches Elektronen Synchrotron, Notkestraße 85, Hamburg, Germany.

Mail to: gajendra.kumar.sahoo@desy.de

A. Kling

Institute of Dual Cooperative Studies, Osnabrück University of Applied Sciences,
Kaiserstraße 10b, Lingen, Germany.

Mail to: A.Kling@hs-osnabrueck.de

2.4.1 Introduction

PETRA III [1, 2] is a 3rd generation synchrotron light source operating with electrons at a beam energy of 6 GeV. PETRA was originally built in 1976 as an electron - positron collider and was used as a preaccelerator for the HERA lepton hadron collider ring from 1988 to 2007 (PETRA II). After the end of the HERA collider physics program PETRA II was converted into a dedicated synchrotron radiation facility (PETRA III). It has a large circumference of 2304 m which is considerably larger than any existing light source. The machine consists of arcs and several straight sections. The so-called long straights which have a length of 108 m are located in the North, East, South and West. In between two long straights are two arcs and short straight sections with a length of 64.8 m. The magnetic structure of the arcs is a simple FODO lattice. The part that extends from the middle of one long straight to the middle of the adjacent short straight is the basic building block of the machine. Since this section is just one eighths of the machine it is called an octant. The magnetic arrangement of one octant is mirror reflected at the middle of the short straight. Electrons are injected in the South-East (SE) and travel clockwise around the machine. The octant extending from North-East to East was modified breaking the fourfold symmetry and is called as new octant (built in the building Max von Laue Hall). It consists of eight double bend achromat cells (DBA). The DBA-cells provide space for one 5 m or two 2 m long insertion devices (ID). The two 2 m IDs are inclined towards each other by 5 mrad. This scheme allows operating two independently tunable undulators in a single straight section with beam paths sufficiently separated for individual beam line optics. In the North-East a ninth straight section is suitable for the installation of an insertion device up to a length of 10 to 20 m. The horizontal beam emittance is 1 nm rad while a coupling of 1% amounts to a vertical emittance of 10 pm rad. The machine is dedicated to users at 14 beam lines with 30 end-stations. Parts of the storage ring [3] have recently been reconstructed to accommodate 10 new beamlines and additionally a super luminescence near UV beamline providing bending magnet radiation. PETRA III operates with several filling modes, such as 40, 60, 240, 480 and 960 equally spaced bunches with a total beam current of 100 mA.

The IDs and other accelerator components are expected to experience extreme radiation in synchrotron light sources especially where higher beam energies, beam currents and smaller gaps are in place. It is worth to mention that, permanent magnets operating under conditions of high radiation are especially susceptible to

demagnetization [4] caused by direct and scattered radiation induced by electrons, positrons, high-energy photons and neutrons. Serious demagnetization has been observed in some of the operating light sources such as ESRF, where insertion devices experienced field losses of as much as 8% [5] and at the APS [6]. Here we report on partial demagnetization profiles, which are not linear along the device [7, 8, 9]. Similar loss patterns are also clearly seen in tracking results. To protect the IDs additional collimators have been recently installed at PETRA III.

2.4.2 Observation of Radiation Damage of Insertion Devices

Radiation damage of machine hardware, electronics and magnet structures have been observed for some time in PETRA III. First signs of radiation damage were observed in the damping wiggler sections and in the form of rust on undulators as shown in Figure 1. On the other hand, performance losses have been observed at several beam lines. The gaps operated at some beam lines have to be decreased or tapers introduced over time and distortions of higher harmonics have been observed, as depicted in Figures 2 and 3. Beam lines suffering from performance losses are in most cases not affected by the appearance of rust on their IDs, as can be seen in Figure 1. PU08 (PETRA Undulator 08) shows significant loss in performance but essentially no sign of rust, while PU09 (located in the same canted straight section) shows essentially no sign of field deterioration of the insertion device but significant signs of rust. In the following, we will focus on the aspect of performance losses. Different measures have been taken to mitigate the rust problem (i.e., better control of tunnel humidity, improved orbit control in upstream dipoles, etc.).

Inspection of the magnetic structures and in-situ magnetic measurements revealed a partial demagnetization of devices exhibiting performance losses. Some results of these measurements are summarized in Figures 4, 5 and 6. Devices located upstream in canted straight sections as PU02 and PU08 are damaged at the upstream end of the magnet structure while the downstream located device PU03 is damaged at the downstream end (see Figures 4 and 5). The measured decrease of the peak field is attributed to radiation damage and is most likely caused by particle losses.

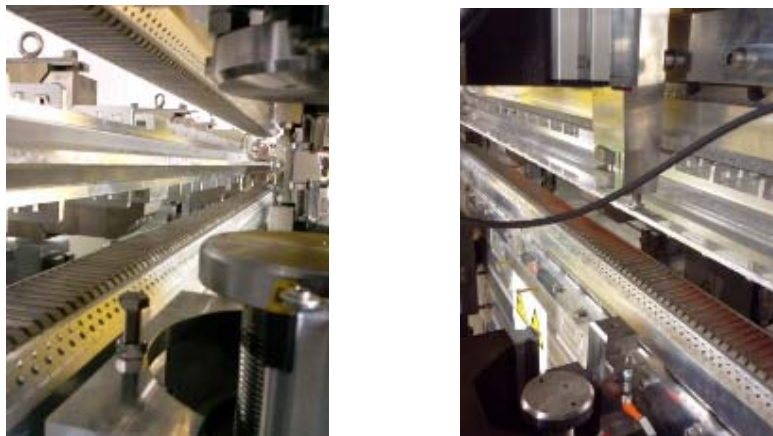


Figure 1: The magnetic structure of undulators PU08 (left) and PU09 (right). On PU09 significant signs of rust are clearly visible.

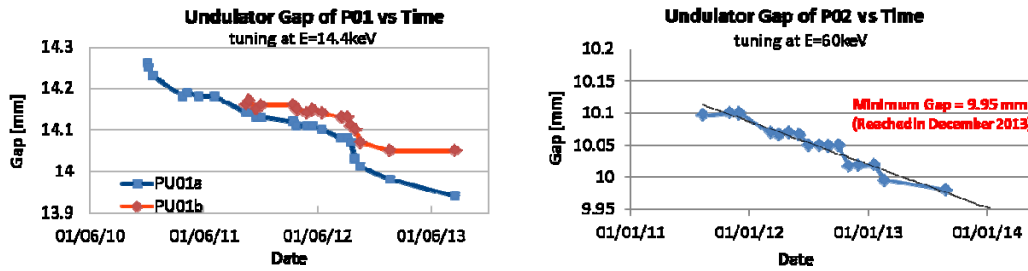


Figure 2: Gap vs. operation time of undulators PU01 and PU02. Both undulators observe performance losses.

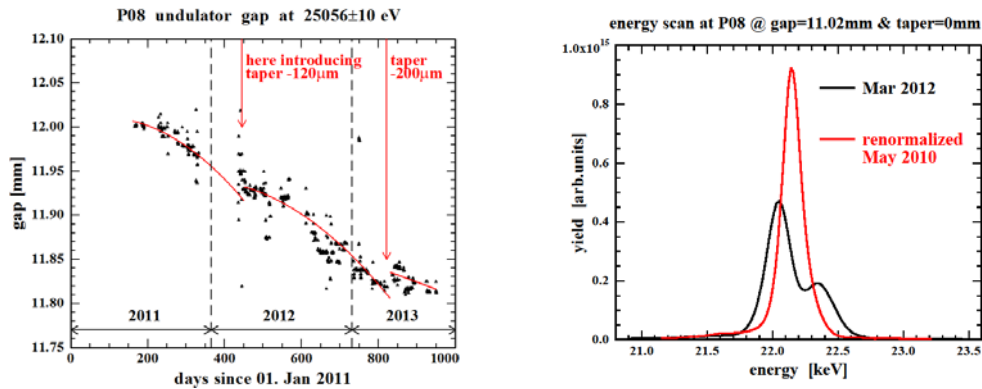


Figure 3: Left: Gap vs. operation time of undulator PU08. The introduction of tapers partially compensates the performance loss by accounting for the linear part of the demagnetization. Right : Distortion of the 5th harmonic at PU08 due to radiation damage of the ID.

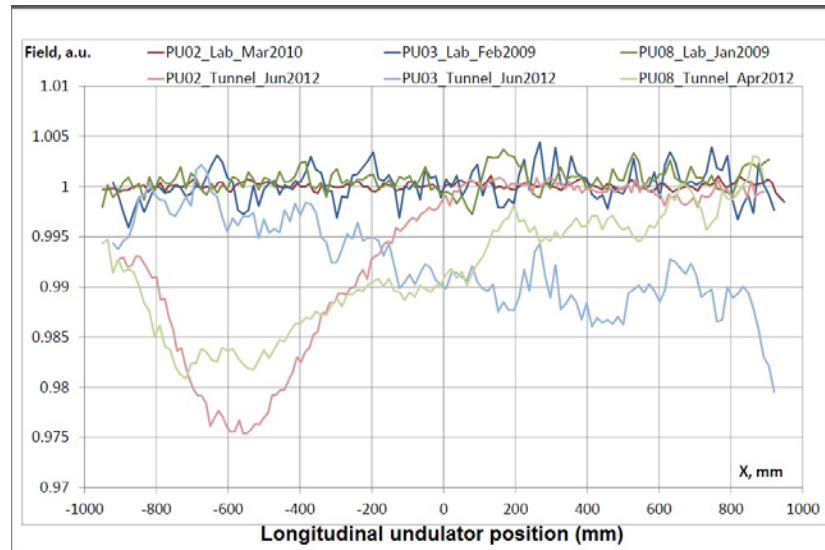


Figure 4: In-situ magnetic measurements reveal a loss of up to 2.5% in peak field at certain insertion devices. Devices located upstream in canted straight section as PU02 and PU08 are damaged at the upstream end of the magnet structure while the downstream located device PU03 is damaged at the downstream end.

The rationale behind this hypothesis is that in particular PU01 is affected. PU01 is located at the center of an almost 70 meters long straight section in north east. The upstream and downstream dipoles are comparatively far away. Moreover, the upstream dipole is a weak 5.3 meters long standard old octant dipole. The background of synchrotron radiation is most likely low at PU01. However, PU01 has the first low gap chamber at the entrance to the experimental hall. Particles with large vertical amplitude are likely to be intercepted at this point. The same refers to PU02 where the vertical aperture is even smaller (7 mm at PU02 vs. 10.5 mm at PU01). PU08 is most likely affected because it was the first beam line to be commissioned in early stages of PETRA III operation and probably has accumulated radiation doses, possible also in less controlled machine states.

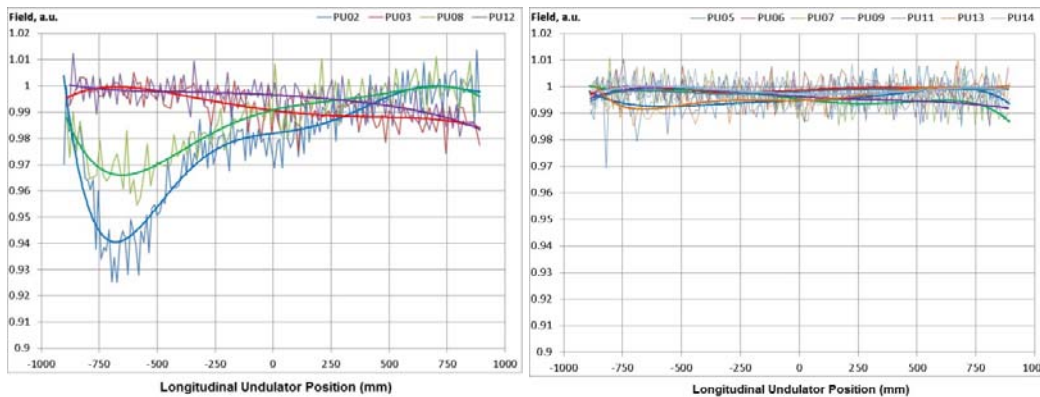


Figure 5: Measured longitudinal peak field variation of the 2 m devices installed in PETRA III. The left picture shows devices with signs of damage while the right picture shows devices with essentially no sign of demagnetization.

A similar situation as for the 2 m devices located in canted straight sections is observed for the 5 m long devices installed in PETRA III (Figure 6). In sector 1 the 5m undulators PU01a and PU01b are installed side by side. The upstream device PU01a is strongly damaged at the upstream end. The downstream located device PU01b shows no sign of demagnetization. This is somewhat surprising because anticipating results from beam loss monitor (BLM) measurements the downstream end of sector 1, where PU01b is installed, shows high loss rates as measured by the BLMs. The undulators PU01a and PU01b are usually operated together, nevertheless these undulators seem not been exposed to beam losses in a comparable way. Data taken for the 5 m device PU10 also confirm the damage pattern observed at the 2 m devices installed in the canted straight sections. The undulator is installed in a standard (not canted) straight section. PU10 shows signs of demagnetization at the entrance and the exit of the device. Moreover, a comparison of data taken in 2012 and 2013 shows that in spite of the decreasing total dose measured with thermo-luminescent dosimeters (TLDs) the damage seems to continue unabatedly.

In the Figure 6, data plotted in green show the situation at PU10 which is a 5m device located in a standard straight section (not canted). The characteristics of the magnetic damage follow the pattern of the 2m devices in the canted straights. The damage occurs at the entrance and the exit of the straight section and the damage of the upstream part are more severe than the damage of the downstream part. The figure on

the right compares measurements of PU01a from 2012 and 2013 to the measurement of PU01b. From the shown data it is clear that the magnetic deterioration continues, although the total radiation dose measured by TLDs is reduced from year to year.

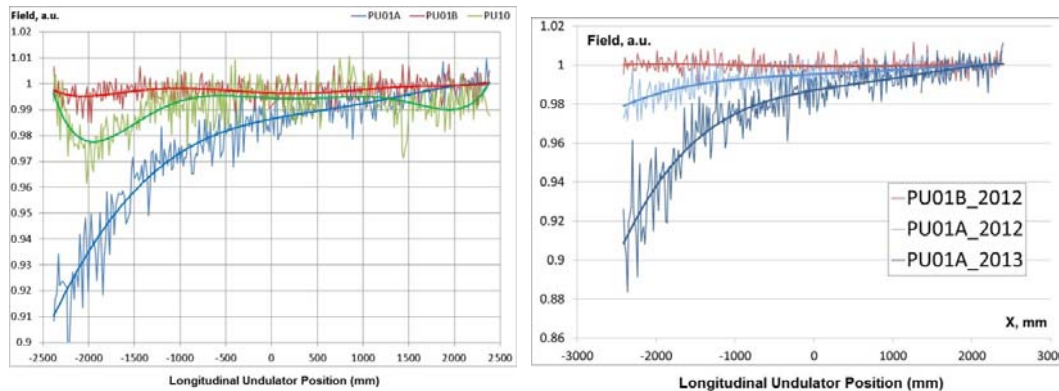


Figure 6: Left: Previously measured 5 m devices installed in PETRA III. PU01a and PU01b are located in sector 1 and both serve beamline P01. The upstream device PU01a shows strong signs of demagnetization, while the downstream device PU01b is not affected.

In summary, radiation damage of insertion devices is observed at several places of the PETRA III undulator sections. It follows a general pattern that devices located at the entrance of a straight section are damaged at the entrance end while undulators installed at the exit of a straight section show signs of demagnetization at the exit end. This seems to indicate that particle losses occur in the vertical plane at locations where the beta functions become large while the physical aperture limits are still very small.

2.4.3 Diagnostic Tools

In the following section, a number of diagnostic tools available for the detection of radiation in PETRA III are described. Some of them were originally not intended to detect sources of radiation damage.

2.4.3.1 TLDs

The insertion devices group at the photon science department regularly installs thermo luminescent dosimeters (TLDs) and evaluates the measured radiation doses.

2.4.3.1 Beam Loss Monitors

Originally, no beam loss monitors (BLMs) were foreseen in PETRA III. Already at an early stage of the commissioning phase, a BLM system has been installed which was previously used in the HERA electron accelerator. The monitors as shown in Figure 7 consist of two reversely biased PIN-photodiodes, mounted face-to-face with a 300 μm thin copper layer in between. Charged particles which cross both diodes produce coincidence signals with a high efficiency, while the efficiency of coincident signals from photons from synchrotron radiation is very small. The copper layer additionally helps to reduce spurious coincidence signals from Photo- or Compton-electrons, generated by synchrotron radiation in one diode, which may reach the other one. While the coincidence mode is mainly sensitive on charged particle losses, it can remotely be

switched off such that it is also possible to measure the count rate of a single diode which is dominated by synchrotron radiation background. With this system it is possible to count beam losses up to the maximum frequency of 10.4 MHz. More details can be found e.g. in Ref. [17].

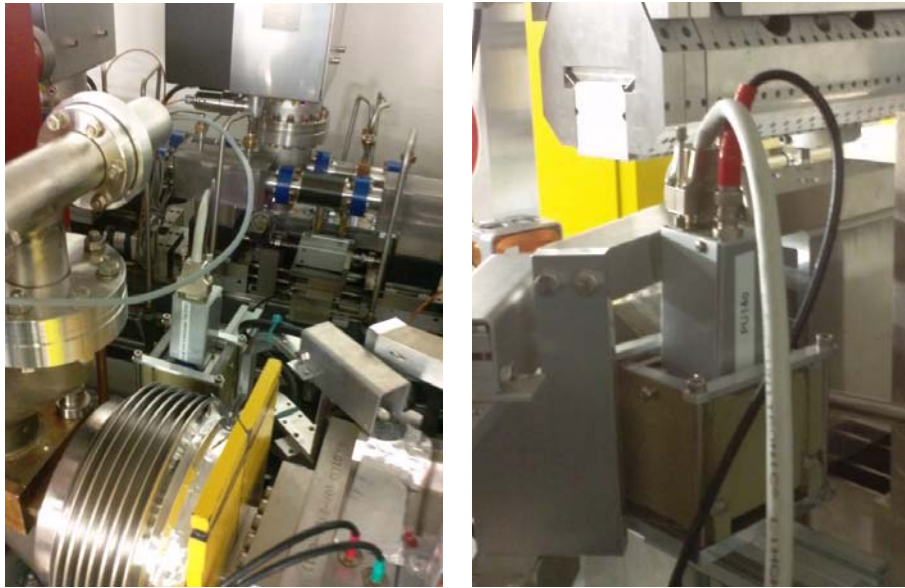


Figure 7: Beam loss monitors in PETRA III. Each section is now equipped with an upstream and a downstream BLM.

2.4.3.1 *Cherenkov Fibers*

The BLM system is a counting system and therefore not sensitive on the amplitude of the particle losses. Therefore, as a test, a “Cherenkov fiber”-based loss monitor system has been temporarily installed in sector 1 and sector 2, along the most affected insertion devices PU01(A, B), PU02 and PU03 as shown in Figure 8. This system is originally designed to monitor beam losses in the undulator section of the VUV-FEL FLASH [18] and was temporarily installed at PETRA III for test experiments.

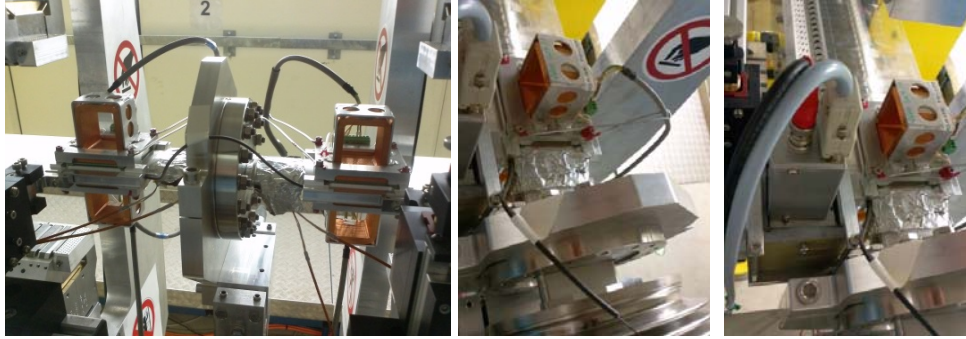


Figure 8: Temporarily installed Cherenkov fibers in sections 1 and 2 along beamlines P01, P02 and P03.

2.4.3.1 PANDORAS

A number of radiation detection devices called PANDORA (**Photon And Neutron Dose Rate meter for Accelerators**) [20] sensitive to different types of radiation are installed outside the tunnel for radiation protection. Several measurements using those types of devices have been performed to cross-check results obtained by other means of detection.

2.4.4 Measurements

The diagnostics tools are used to detect the exposure of the insertion devices to radiation. The results from the TLD measurements, the beam loss monitors and first test of the Cherenkov fibers are reported.

2.4.4.1 TLD Measurements

Every insertion device installed in PETRA III (including the damping wigglers) is monitored with respect to its exposure to radiation using TLDs. From the first day of installation of the devices TLDs are directly mounted to the devices (upstream and downstream) and regularly replaced and evaluated. The integrated dose accumulated of every device is showed in Figure 9.

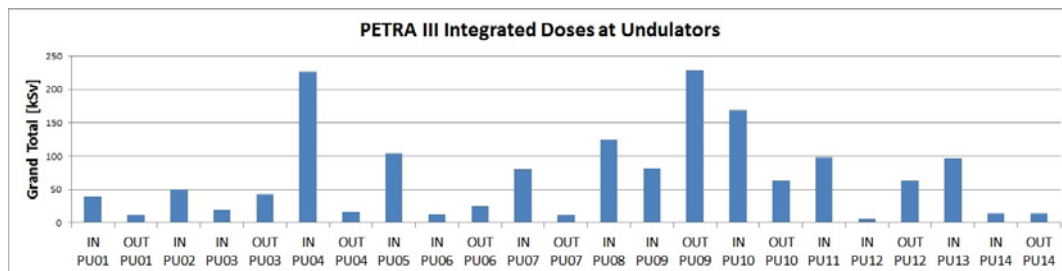


Figure 9: Integrated radiation dose accumulated at every insertion device from the first day of its installation as measured by TLDs.

The integrated dose as measured by the TLDs varies strongly from device to device and does not show any regular pattern. Even from run period to run period the

accumulated dose may vary over orders of magnitude as can be seen in Figure 10, where the integrated dose for the first four run periods of 2013 is shown. In Figure 11, the yearly integrated dose accumulated at all TLDs from 2011 to 2013 normalized to the integrated current stored is shown. The integrated dose has been reduced by almost a factor of 3. Since TLDs are sensitive to particle losses and synchrotron radiation it is hard to distinguish relevant from 'harmless' parts of the measured radiation. Moreover, it is known from beam loss monitor measurements that the synchrotron radiation background strongly varies with closed orbit distortions in upstream dipoles. As stated earlier, the appearance of rust on some of the devices is attributed to unfavorable steering in upstream dipoles. Although a (long term) damage of insertion devices due to this mechanism is not ruled out the observed demagnetization effects are most likely not caused by synchrotron radiation.

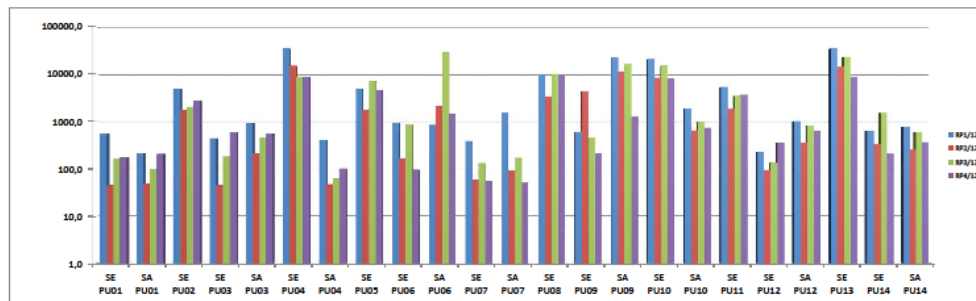


Figure 10: TLD measurement of the integrated radiation dose for the first four run periods in 2013.

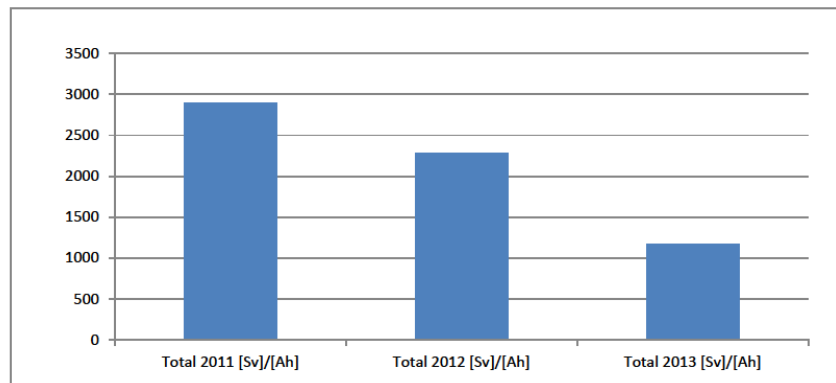


Figure 11: Yearly integrated dose accumulated at all TLDs from 2011 to 2013 normalized to the integrated current stored. The integrated dose has been reduced by almost a factor of 3.

2.4.4.2 Beam Loss Monitor Studies

In order to obtain a clearer picture of the particle losses causing radiation damage, studies have been performed using the beam loss monitors installed at the entrance and the exit of each straight section. The studies compare BLM signals recorded in the 960 bunch mode (standard continuous mode) and signals collected in the 40 bunch mode (standard timing mode). In order to quantify the effect of the collimators on different loss modes, the set points of the collimators are varied during the measurements from

the nominal value applied during user operation to fully open. The measurements have been performed in Top-Up operation in order to quantify the injection losses. The current and lifetime during the measurements are depicted in Figure 12. A comparison of the integrated count rates during injection (see Figure 13, 14) and standard stored current operation (see Figure 15) shows that in both cases the integrated count rate is high in the first part of the undulator section of PETRA III. In particular, BLM 1 corresponds to the entrance of PU01a and BLM 2 corresponding to the exit of PU01b show high count numbers.

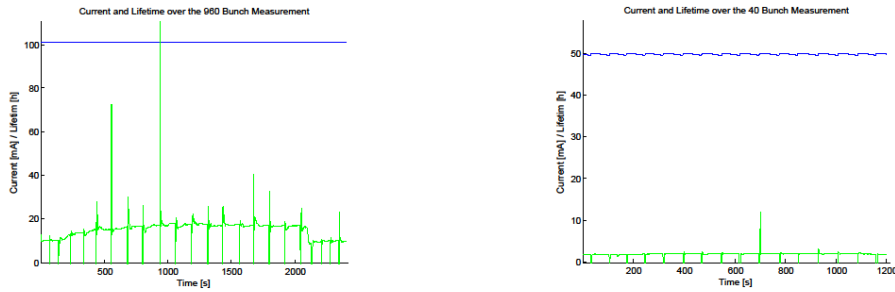


Figure 12: Current and lifetime during the beam loss monitor studies. The left picture shows the measurement using the 960 bunch mode with 100 mA; while the right picture shows the 40 bunch mode measurement with 50 mA.

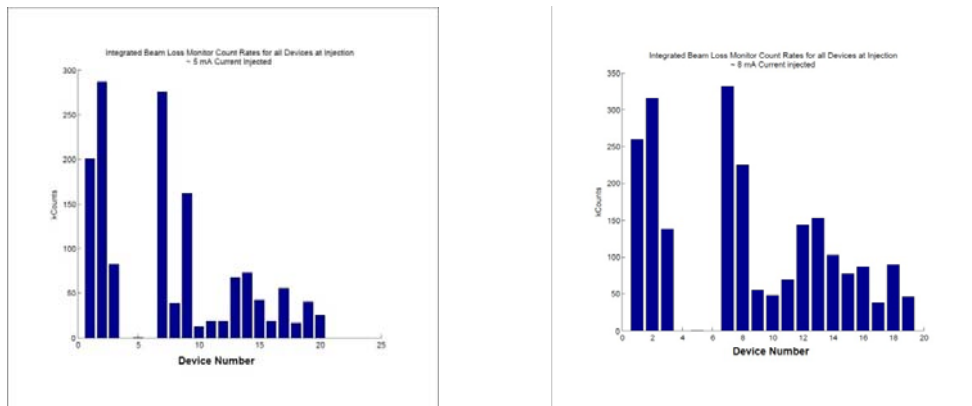


Figure 13: Integrated count rates measured during injection in the 960 (left) and 40 (right) bunch mode. The total injected current is approximately 5 mA (in ~25 injections) in the 960 bunch mode and around 8 mA (in ~16 injections) in the 40 bunch mode. Data from the BLMs 4 to 6 were not available due to technical reasons.

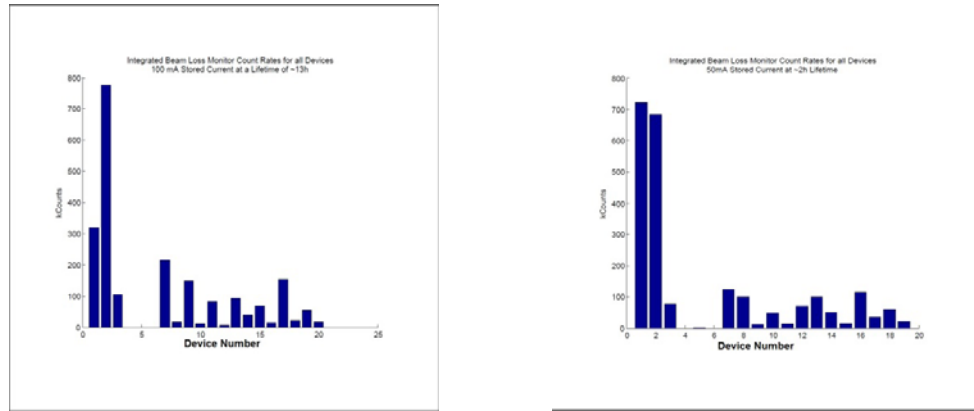


Figure 14: Integrated count rates measured during stored current operation in the 960 (left) bunch mode at 100 mA and a life time of ~10 to 15 hours and 40 (right) bunch mode at 50 mA and a lifetime of ~2 hours.

During injection the integrated rates can be significant also at other insertion devices. The integrated rates during normal stored beam operation are strongly peaked at BLM 1 and BLM 2 located in sector 1 housing beamline P01. Interestingly, the highest rates are measured at the downstream end of PU01b. However, that device does not show any signal of radiation damage!

While the measured count rates during injection are directly comparable in both operation modes, the count rates during stored current operation have to be scaled for the 40 bunch mode. During timing mode user operation usually a current of 80 mA (or even 100 mA in some run periods) is stored in 40 bunches. In the 40 bunch mode the lifetime and therefore the loss rate is dominated by Touschek scattering and scales approximately linear with the stored current. Moreover the total loss rate is proportional to the stored current. Therefore the integrated count rate at the BLMs has to be scaled by at least a factor of 3-4 to be in correspondence with standard user operation in timing mode. The total time of measurement is two times longer in the 960 bunch case, which has to be compensated by an additional factor of 2 in the 40 bunch case.

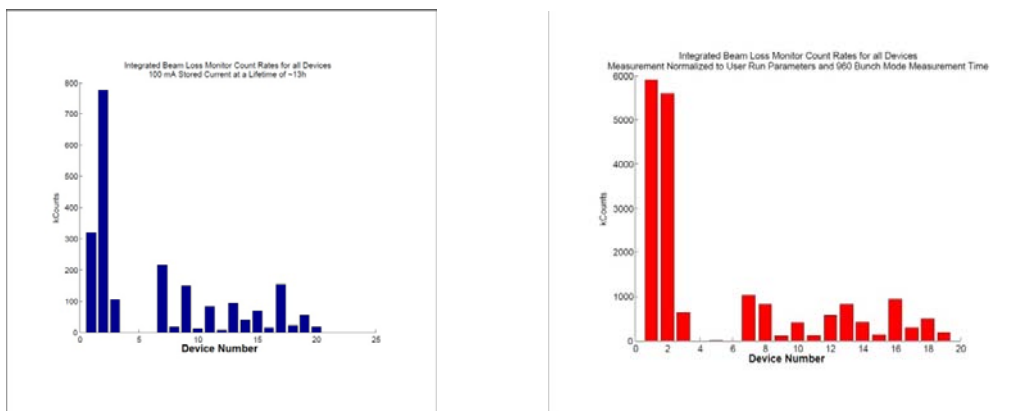


Figure 15: Integrated count rates measured during stored current operation in the 960 (left) bunch mode at 100 mA and a life time of ~10 to 15 hours and 40 bunch mode at 50 mA and a lifetime of ~2 hours taking into account the scaling to standard user operation parameters and normalized.

2.4.4.3 960 Bunch Mode

Looking at the dependency on the collimator settings for particular devices in the 960 bunch mode the effect of the collimators is clearly visible although they are located almost exactly half the ring upstream in the short straight section south-west, see Figures 16 and 17. However, while in the case of injection losses the count rates can be reduced by almost two orders of magnitude, the count rate during normal stored current operation is reduced by a factor of 3-5. Moreover, the injection losses could be further reduced by closing the collimators beyond their nominal set points, of course on the cost of reducing the injection efficiency severely, which renders this step questionable. Losses in stable beam operation are hardly further reduced already several millimeters before the collimators reach their nominal set points.

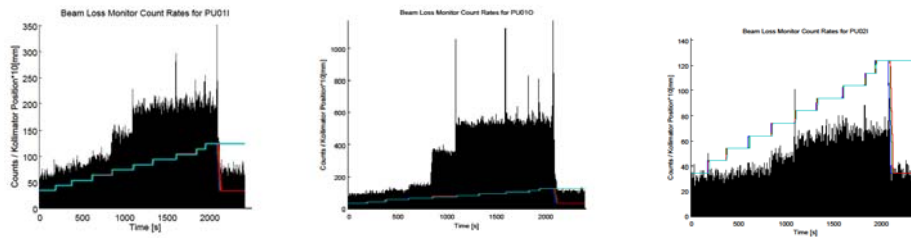


Figure 16: Count rates measured at BLM 1 (PU01a), BLM 2 (PU01b) and BLM 3 (PU02) during stable beam operation with 100 mA in 960 bunches. When opening the collimators stepwise the count rates increase by a factor of 3-5.

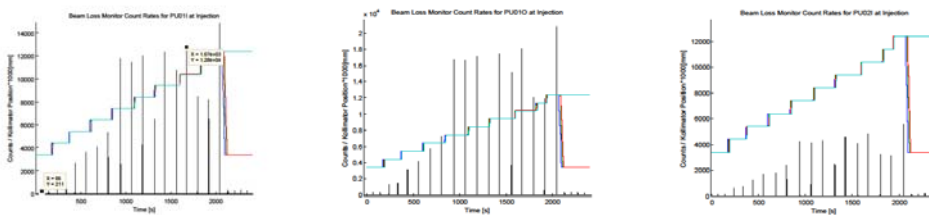


Figure 17: Count rates measured at BLM 1 (PU01a), BLM 2 (PU01b) and BLM 3 (PU02) during injection at 100 mA in 960 bunches. At every injection approximately 0.2mA was injected. When opening the collimators step wise the count rates increase by almost 2 orders of magnitude.

A comparison of the integrated losses during injection and during stable beam operation over time at 100 mA in 960 bunches shows that at (almost) all BLMs the accumulated counts during stable beam operation outbalance the counts accumulated during injection. This statement has to be taken with care since the BLMs do not provide amplitude information of the losses. This means in turn that the true losses during injection could be larger by some (unknown) factor and the measurement only provides a kind of lower limit.

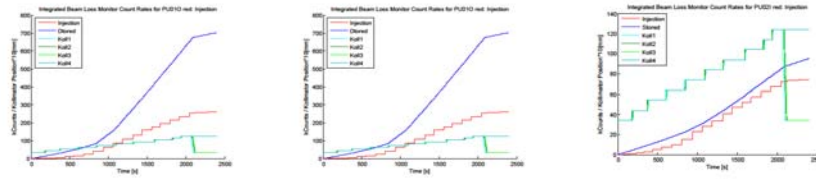


Figure 18: Comparison of the integrated losses during injection and during stable beam operation over time at 100 mA in 960 bunches. At all shown BLMs the accumulated counts during stable beam operation outbalance the counts accumulated during injection.

2.4.4.4 40 Bunch Mode

In the timing mode the situation is essentially the same as in the 960 bunch mode with the only important difference that the count rates are considerably higher due to low lifetime by Touschek dominated scattering. The count rates during stable beam operation have still to be scaled to standard user run parameters which amounts to a factor of ~ 4 .

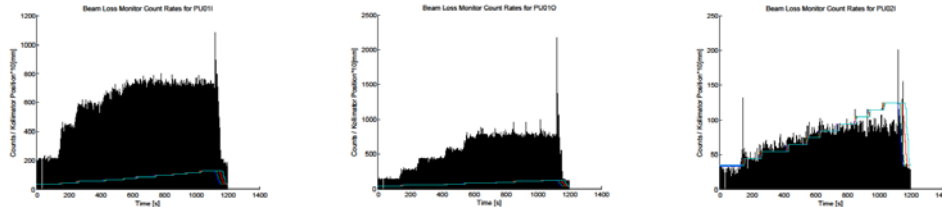


Figure 19: Count rates measured at BLM 1 (PU01a), BLM 2 (PU01b) and BLM 3 (PU02) during stable beam operation with 50 mA in 40 bunches. When opening the collimators stepwise the count rates increase by a factor of 3-5.

Interestingly, the stable beam count rates are significantly reduced also at collimator set points close to nominal values. This could be an indication that the dominating loss mechanism is different in the 960 and 40 bunch mode.

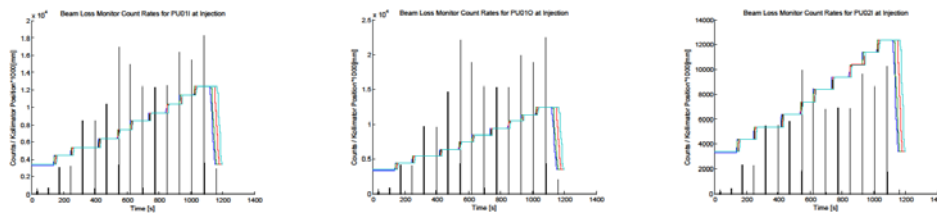


Figure 20: Count rates measured at BLM 1 (PU01a), BLM 2 (PU01b) and BLM 3 (PU02) during injection at 50 mA in 40 bunches. At every injection approximately 0.5 A are injected. When opening the collimators stepwise the count rates increase by almost 2 orders of magnitude.

A comparison of the integrated losses during injection and during stable beam operation over time at 50 mA in 40 bunches shows the same characteristics as in the 960 bunch mode. At (almost) all BLMs the accumulated counts during stable beam operation outbalance the counts accumulated during injection. This situation becomes

even more clear when one takes into account that the stable beam losses have to be scaled by at least a factor of 3 to 4 while the injection losses not. However, the weight factor of the injection losses is still an unknown (see above).

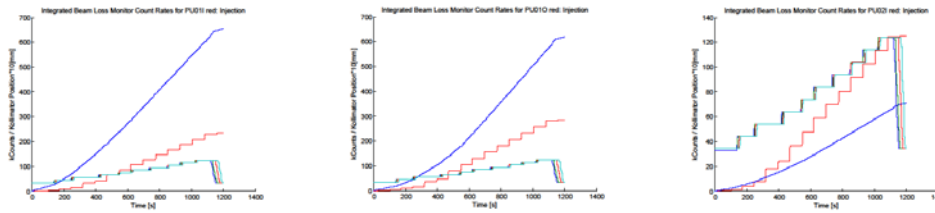


Figure 21: Comparison of the integrated losses during injection and during stable beam operation over time at 50mA in 40 bunches. At all BLMs shown the accumulated counts during stable beam operation outbalance the counts accumulated during injection. This becomes even more prominent if the scaling to standard user operation parameters is taken into account (see text).

2.4.4.5 Comparison with BLM 14 (PU090 : Exit end of PU09)

It is interesting to compare the results for devices exhibiting signs of damage presented above with measured data at BLM 14 corresponding to the downstream end of PU09. P09 was also one of the first beam lines to be commissioned so that one could expect sign of damage also from early periods with less controlled beam operation. However, this is not the case. The corresponding measurements are shown in Figures 22 and 23.

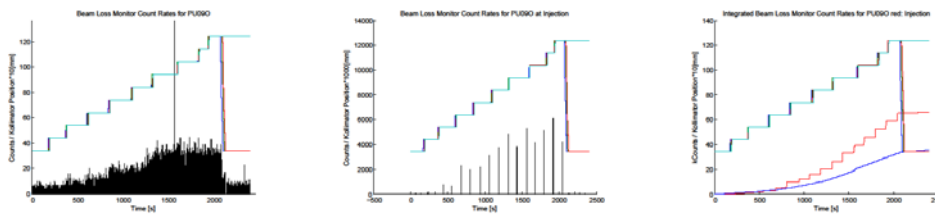


Figure 22: Count rates during stable beam operation (left), injection (center) and integrated over time for both (right) at 100mA in 960 bunches. The rates are somewhat lower (approximately a factor of 2) than those measured at PU02.

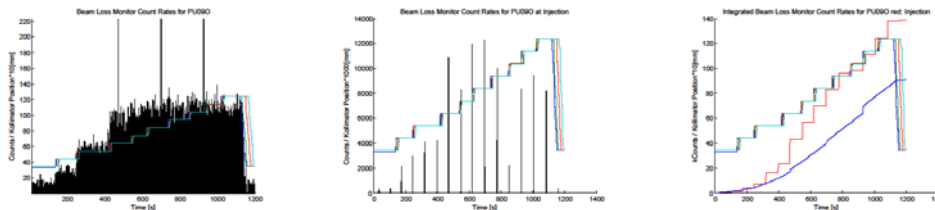


Figure 23: Count rates during stable beam operation (left), injection (center) and integrated over time for both (right) at 50mA in 40 bunches. The rates are somewhat lower (approximately a factor of 2) than those measured at PU02.

The count rates measured at PU09 are only slightly higher than those measured at PU02. A somewhat extraordinary feature of PU09 is that the cumulated rates of the injection exceed the ones for stable beam operation. That is likely to be an artefact of the way the measurement is executed. The injection losses are affected stronger by the collimator settings than the stable beam losses. The measurement integrates over quite some time with (almost) open collimators which leads to a distortion of the result.

2.4.4.6 First Tests with Cherenkov Fibers

Cherenkov fibers have been installed temporarily in sectors 1 and 2 along the undulators PU01a, PU01b, PU02 and PU03, and a series of test experiments have been performed. Figure 24 shows signals of a beam loss occurring during injection. The measurement has turn-by-turn resolution capabilities and provides additional amplitude information for the observed losses. However, the test experiments indicated that the measurement is not sensitive to stored beam losses, and only losses in the orbit plane could be observed. Nevertheless, an interesting result has been obtained from the measurements using the fiber. The signals appear typically with a frequency of 13 kHz which seems to correspond to the detuned horizontal tune for large amplitudes at injection. This indicates that the losses occur at large horizontal betatron amplitudes, where the vertical aperture is even more restricted due to the elliptic shape of the chambers.

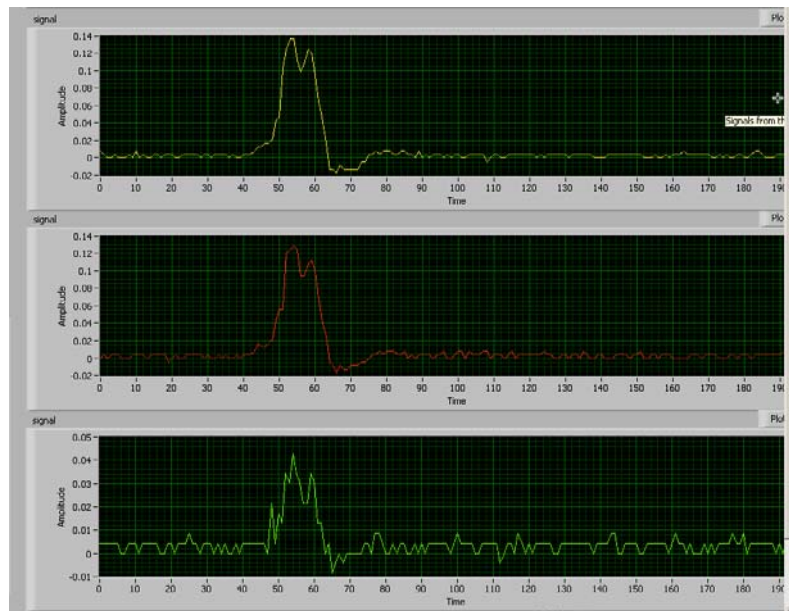


Figure 24: First signals of beam loss using the Cherenkov fiber installed in sector 1. Signal appearing in turn 1, 2 and 10.

Due to the insensitivity on the losses caused by the circulating beam which even could be observed with the PIN-photodiode based BLM system, in the future it is planned to increase the active detection volume and to test a Cherenkov based system which was originally designed for the European XFEL [19]. First test experiments which were performed at the ESRF look very promising.

2.4.5 Simulations Introduction

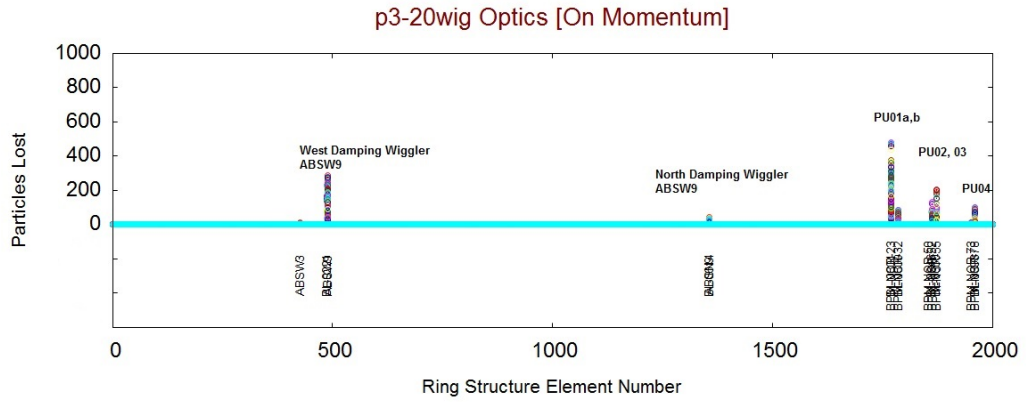
In the previous sections we have shown that radiation damage of insertion devices is observed in several places of the PETRA III undulator sections. It follows a general pattern that devices located at the entrance of a straight section are damaged at the upstream part while undulators installed at the exit of a straight section show signs of demagnetization at the downstream part. This seems to indicate that particle losses occur in the vertical plane at locations where the beta functions become large while the physical aperture limits are still very small. Whether these particle losses occur during injection; or are mainly caused by off-momentum particles remains to be clarified.

In order to gain more insight into the mechanism causing the radiation damage of the insertion devices, we embarked on a series of tracking studies using the tracking code SixTrack [10]. This code tracks particles through a magnetic lattice over large number of turns taking into account the full six-dimensional phase space including synchrotron oscillations in a simplistic manner. The systematic and random multipole measured field errors for each type of dipoles, quadrupoles, sextupoles, wigglers and correctors etc. are introduced to these magnets as thin nonlinear element at the center. The studies are performed for on energy as well as off-energy particles. Tracking studies were of course already performed during the design and commissioning phase of PETRA III [2, 11]. In those studies however, only the resulting dynamic and momentum aperture were recorded. No investigation on the loss patterns has been done. Actually, the presently used rather old version 1.1a of SixTrack does not generate separate output files for such a purpose. Therefore, we had to modify the code to get more direct access to the loss pattern.

The tracking studies are based on the standard PETRA III optics (p3_20wig) used during user operation containing the damping wigglers modeled in terms of a numerical generating function [12]. The model of the accelerator is put together by constructing a sequence of blocks of linear elements, nonlinear elements, observation points and possibly an RF cavity. The linear magnetic elements (dipoles, quadrupoles) are split into two linear parts and a thin nonlinear elements containing the multipole field errors. Consecutive linear elements are blocked together for fast tracking using a single transfer matrix. The particle trajectories are recorded at the 227 BPMs and several other particular longitudinal positions along the ring. The aperture limitations are introduced at several longitudinal positions in horizontal and vertical planes imposed by the physical aperture limitations of the vacuum system. For example, the absorbers in west (ABSW1-ABSW10)/north (ABSN1-ABSN10) damping wiggler section are elliptic in size with half apertures of 30 mm in the horizontal and 4.50/8.5 mm in the vertical plane. The undulator vacuum chambers have lower gaps than the absorbers in double bend achromat sections in the Max von Laue Hall. The beam position monitors (BPMs) in undulator sections have an elliptic vacuum chamber with half apertures of 30 mm in the horizontal and 5.25/3.5 mm in the vertical plane. Nonlinear elements such as sextupoles are modeled with half apertures of 40 mm in horizontal and 20 mm in the vertical plane. On top of that there is a general rectangular aperture check at each non-zero length elements. During tracking the particle is lost if the tracked orbit exceeds the physical aperture.

2.4.5.1 *On Momentum Tracking*

The on momentum tracking mainly aims at a better understanding of particle losses during injection. This is necessary to reduce the particle losses in the process of injection so that the radiation detectors (Pandoras) are at low rates to protect the activation at venerable locations. This also helps in finding the locations where the particles are lost due to unclosed kicker bumps. For the simulation particles are tracked with initial horizontal amplitudes increased from 0 mm to 55 mm in 111 steps. For every horizontal initial condition the vertical amplitude is varied in 81 steps starting from 0 mm using in step of 0.1 mm. The results of these tracking using 30 different error sets are shown in Figures 26(a, b). Depicted are the results for the tracking of 8991 on momentum particles. The color code is used to present the loss of particles for the aforesaid initial conditions tracked at 360 different block positions starting from South West of the ring. The two collimators (COLL1 in South West Right (SWR)), COLL2 in South West Left (SWL)) are open with half gaps of 40 mm, 20 mm. A maximum of 482 particles are lost out of 8991 near PU1a, b, which is 5.36%. The simulation shows that the losses are localized and independent of tracking starting block position and independent of random error sets, only the numbers of loss particles are changed. This means the loss of particles at local position PU01a is fixed for any random sets or any start point of tracking, but only different number of particles lost are seen. As anticipated from the experiments during machine studies, the referred location of particle loss is at PU01a and PU01b. A comparable number of particles are lost in the damping wiggler section west at absorber ABSW9 (and/or damping wiggler section north at absorber ABSN9). It may be mentioned that the vertical aperture limitations are imposed first 4.5mm in west damping wiggler section followed by 4.5 mm in north damping wiggler section, 5.25 mm at PU01a,b and 3.5 mm at PU02 etc. The tracking shows that the particles are lost in vertical plane at those locations.



31/03/2015 15:35

Collimators are open with elliptic aperture [40mm, 20mm].
Tracking results for initial conditions at first 360 Blocks from mid of South West shown in different color codes.

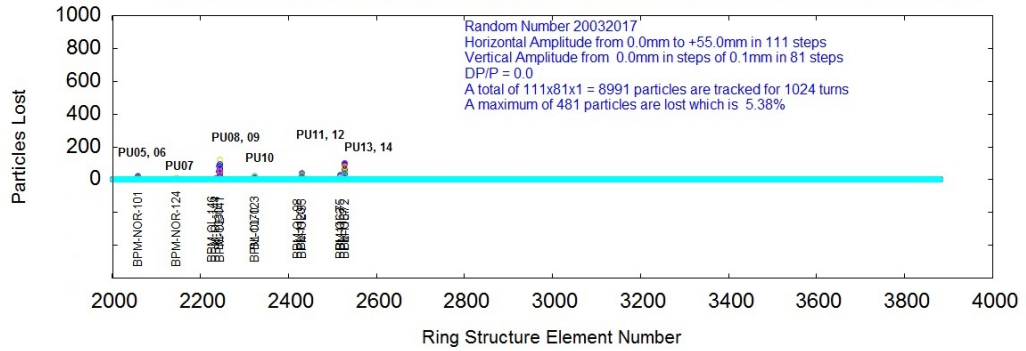


Figure 26a: Tracking results for on momentum particles with magnetic field errors tracked at 360 different structure element positions starting from South West for a single random number (Collimators are with elliptic aperture of 40mm, 20mm). A maximum of 482 particles are lost out of 8991 near PU1a, b, which is 5.36%.

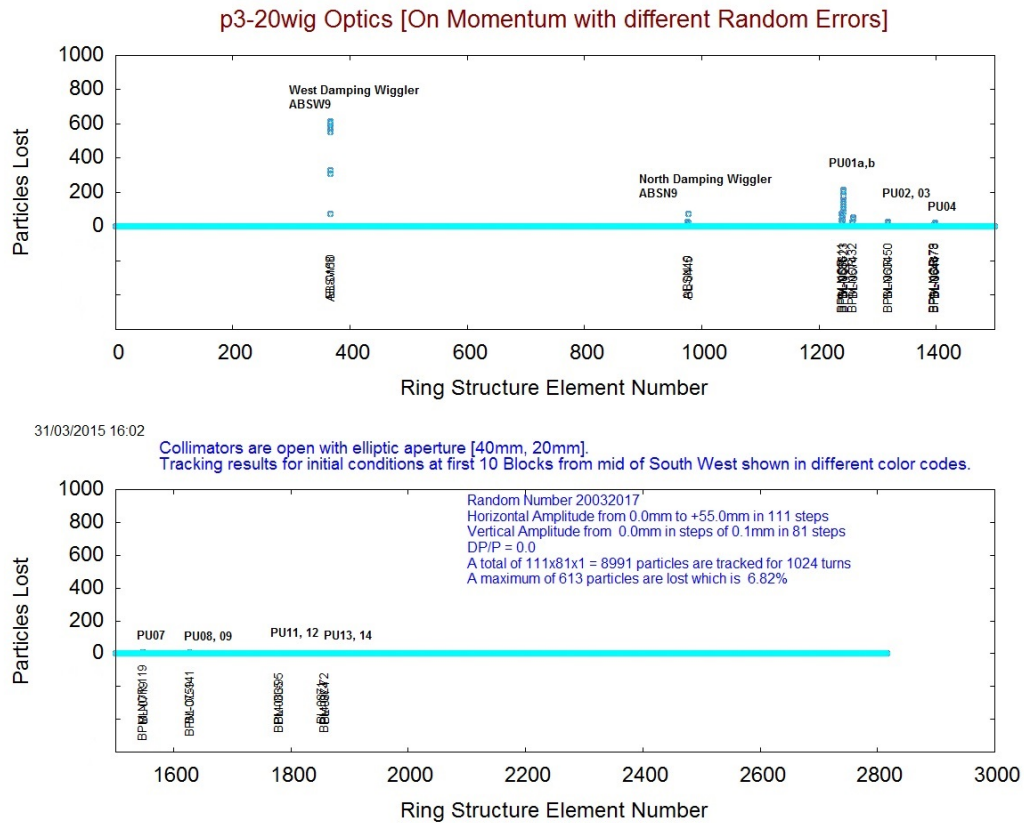


Figure 26b: Tracking results for on momentum particles with magnetic field errors tracked at 10 different structure element positions starting from South West for 30 random error sets (Collimators are with elliptic aperture of 40mm, 20mm). A maximum of 613 particles are lost out of 8991 near ABSW9, 10, which is 6.82%.

2.4.5.2 Off Momentum Tracking

In many third generation synchrotron light sources the beam lifetime is dominated by the Touschek effect [13, 14]. This is, in particular, also true for timing mode operation at PETRA III where typically 100 mA are stored in 40 evenly spaced bunches. The beam lifetime in this mode of operation is as low as 1.4 h. Typically, Top-Up leads to injections every 50 to 60 seconds when the beam current variation is limited to 1%. Since Touschek scattered particles suffer large longitudinal momentum deviations off momentum tracking studies were performed to gain insight into the local distribution of the lost particles.

Before we head for the details of the tracking simulation, one can ask the natural question whether the inspection of the off momentum optics of PETRA III indicates preferred locations of particle loss.

Using the MAD-X [15] code, where the chromatic functions are defined as

$$\begin{aligned}
W_x &= \sqrt{a_x^2 + b_x^2}, & W_y &= \sqrt{a_y^2 + b_y^2}, \\
a_x &= \frac{\partial \alpha_x}{\partial p_t} - \frac{\alpha_x}{\beta_x} \frac{\partial \beta_x}{\partial p_t}, & a_y &= \frac{\partial \alpha_y}{\partial p_t} - \frac{\alpha_y}{\beta_y} \frac{\partial \beta_y}{\partial p_t}, \\
b_x &= \frac{1}{\beta_x} \frac{\partial \beta_x}{\partial p_t}, & b_y &= \frac{1}{\beta_y} \frac{\partial \beta_y}{\partial p_t}, \\
\phi_x &= \frac{1}{2\pi} \tan^{-1} \left(\frac{a_x}{b_x} \right), & \phi_y &= \frac{1}{2\pi} \tan^{-1} \left(\frac{a_y}{b_y} \right),
\end{aligned}$$

one can look at the beta beating as a function of energy:

$$\begin{aligned}
b_x &= W_x \cos(2\pi\phi_x), & b_y &= W_y \cos(2\pi\phi_y), \\
a_x &= W_x \sin(2\pi\phi_x), & a_y &= W_y \sin(2\pi\phi_y).
\end{aligned}$$

Since the apertures are small in the vertical plane, we try to analyze a_y at undulator sections for the standard optics (p3_20wig) of PETRA III. The optical functions together with the chromatic functions a_y and b_y are shown in Figure 25.

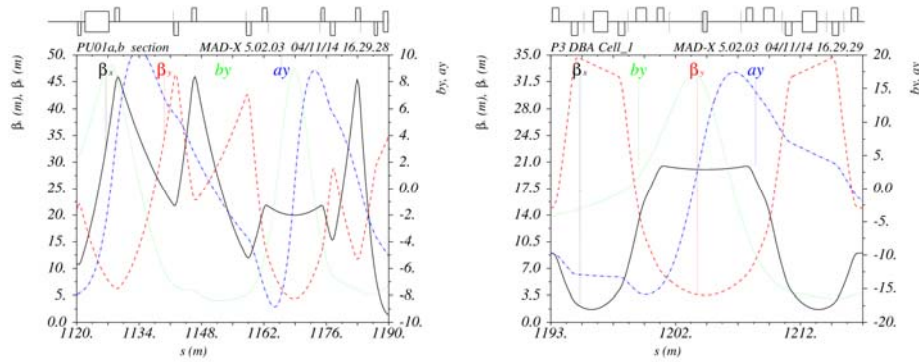


Figure 25: The computed values of a_y and b_y are plotted for the sections for undulator PU01 and PU02. The a_y value is high (negative) at the upstream of PU01 and PU02; as well as (positive) downstream of PU01 and PU02.

High losses are expected at extreme values of a_y . The major contribution of a_y comes from b_y , which is nothing else but the variation of beta with energy. The function a_y changes sign due to α_y . So, the loss of particles occur in vertical plane is due to variation of beta with energy. From these simple optics considerations it may be anticipated that off momentum particles are most likely lost at high a_y values. This matches with the BLMs measurements and is in accordance with the observed radiation damage. Collimators are foreseen in these sections to mitigate the sources of radiation damage.

Beyond linear optics considerations, a more precise treatment of particle losses due to large momentum offset caused by Touschek scattering would take into account the local nature of the physical process. The starting point would then be given by the local phase space distribution of Touschek scattered particles as generated by the stable beam. This takes into account that the scattering rate and distribution of particles depends on the local phase space density around the ring. Then this particle distribution

could be tracked through the ring. Actually, the ring should rather be regarded as beamline in this context, because for a particle with considerable momentum deviation a closed solution might not exist. Touschek scattered particles might survive only a few turns or may even be lost within one turn. Recording the positions where the particles are lost provides the desired information about the beam loss pattern. It should be noted here that such an approach is adopted for the Elegant tracking code [16]. An even more complete picture might arise when one takes into account synchrotron radiation during tracking. A particle with energy excess after Touschek scattering might be recaptured when it radiates off some of its energy while travelling through a section with strong magnetic fields, as it is for instance the case in the damping wiggler section in PETRA III. The bottom line of this discussion is that the locally generated Touschek scattered particles might experience very different histories leading to deviations from the simple loss pattern predicted by scrutinizing the off energy optical functions. For PETRA III, however, this does not seem to be the case.

The approach adopted in the tracking studies here is simply to calculate local momentum apertures by tracking off momentum particles with various initial conditions and record their corresponding loss pattern. This obviously contains less quantitative information, because the mechanism how those particles are generated is ignored. A function, calculating distributions of Touschek scattered particles, is missing in SixTrack. Our main goal is to identify potential locations of cumulated particle loss. As it turns out this approach already provides a reasonable picture of the distribution of lost particles and is in good agreement with the considerations concerning the off momentum optical functions as presented above. The setup for the tracking studies is as follows.

The measured magnetic field errors are introduced to the magnets as thin elements. The particles are tracked with horizontal amplitude of -35 mm to 35 mm in 141 steps, vertical amplitude of 1 step from 0 mm instead of 0.1 mm. The momentum variations considered are $\Delta P/P$ from -0.02 to 0.02 in 41 steps. A total of 5781 particles are tracked with synchrotron oscillations for 8192 turns (damping times for 6.0 GeV operation, $\tau_x = 84.66$ ms, $\tau_y = 84.77$ ms, $\tau_e = 42.41$ ms with revolution time of $T_0 = 7.68$ μ s) with magnetic field errors (with systematic and random), damping wigglers with errors at different initial positions for single random error set, where the collimators at SWL and SWR are open. The results of such tracking are shown in Figure 27. The results are shown in different colors for tracking at 384 different initial block positions starting from South West of the ring. A maximum of 606 particles are lost out of 5781 near PU1a, b, which is 10.48%. Similar to the on momentum tracking, here the simulation shows also that the losses are localized at certain positions and are independent of tracking starting block position and are independent of random error sets, only the numbers of loss particles are changing. This means the loss of particles at local position PU01a is fixed for any random error sets or any start point of tracking, but only different number of particles lost are seen. The obvious point of high loss is at PU01a, b which is experimentally seen. Similar is the case for damping wiggler section where most of the particles are lost. It is quite noticeable from Figure 27 that a comparable number of particles are lost at sextupoles locations. The severe losses are observed at longitudinal position of S2_NR_118. We have no monitoring system at this location. We have seen radiation damage at up and downstream locations of PU02 which is reproduced in tracking results. The tracking results shows severity at PU04 as

mentioned in integrated TLD dose rate, unfortunately we do not have field measurement data for PU04.

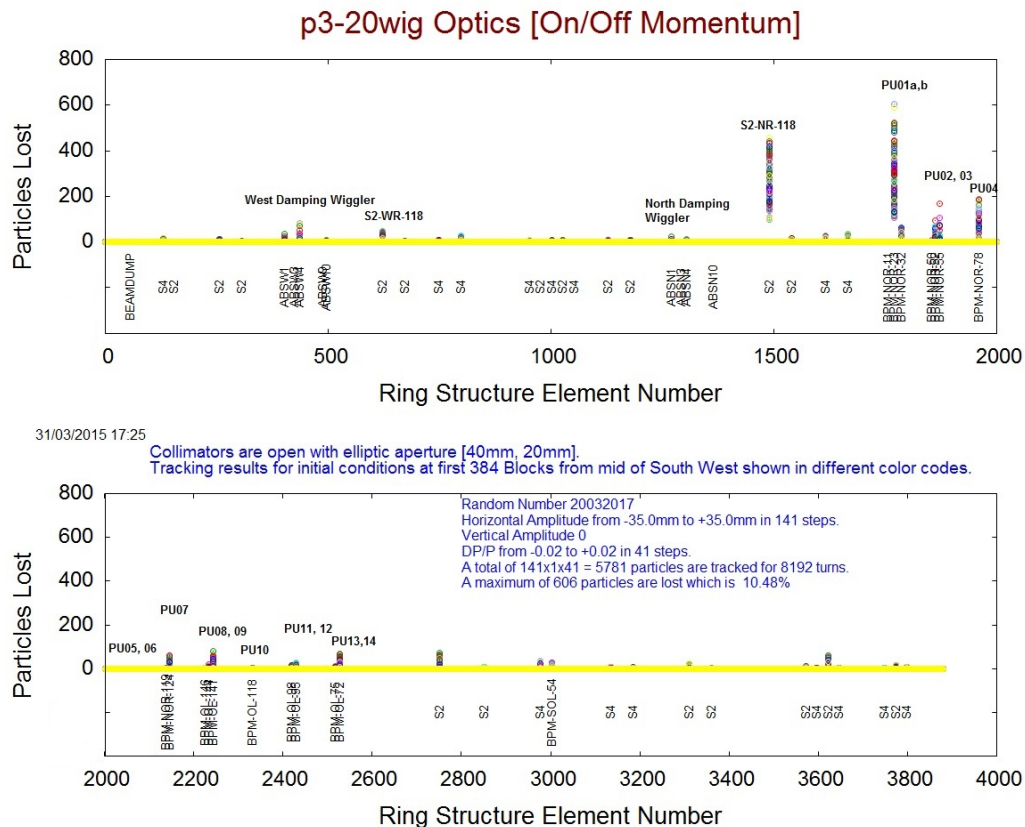


Figure 27: Tracking results for off momentum ($\Delta P/P = -0.02$ to 0.02) particles with magnetic field errors tracked at 384 different structure element positions starting from South West for a single random number (Collimators are open). A maximum of 606 particles are lost out of 5781 near PU1a, b, which is 10.48%.

Now, it is time to vary the collimator settings to observe the influence on beam losses at different positions. We have observed during earlier experiments that the BLMs show less count rates with collimator settings closed to some minimum positions (say ± 4 mm). This suggests that the particles are lost somewhere else! In the following Figures 28(a,b,c) the tracking results with off momentum particles are shown for different closing positions of collimators at COLL2 and COLL1. If the vertical closing apertures becomes smaller and smaller (6 mm to 3.5 mm) the loss of particles increases at the collimators from 12.35% to 24.72% which explains effective scrapping by the collimators. The loss rate is drastically reduced at all undulator locations except PU04 which is blind to these collimators. Still appreciable loss is observed at S2_NR_118 even with closed collimators. The radiation doses measured in the inner side of the ring on 22.01.2014 in the PETRA III tunnel are produced herewith (Table 1) from the PETRA eLogbook for comparison with the tracking results. It may be noted that tracking shows heavy loss at S2_NR_118 which is clearly seen in the measured data. Figure 28d shows that the losses of particles are at S2_WR_118, S2_NR_118, S2_SOR_83 is also in the inner side.

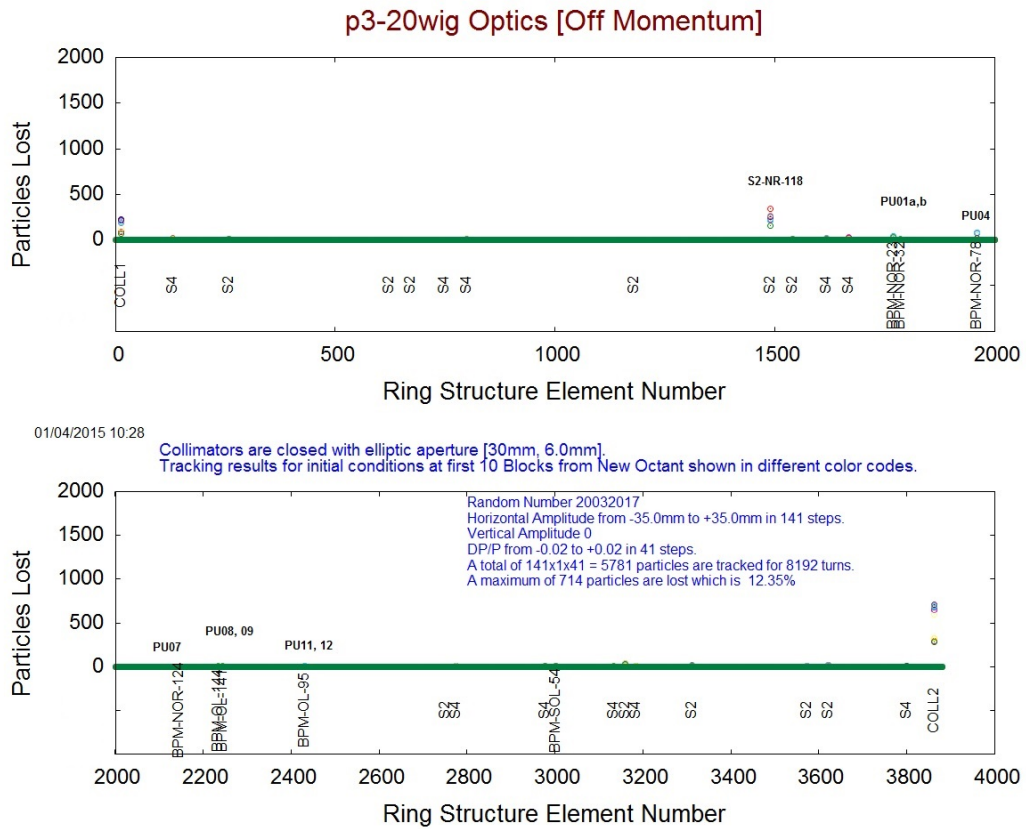


Figure 28a: Tracking results for off momentum ($\Delta P/P = -0.02$ to 0.02) particles with magnetic field errors tracked at 20 different longitudinal positions starting from New Octant for a single random number (Collimators are closed at 6.0 mm, maximum of 714 particle lost at COLL2 which is 12.35%).

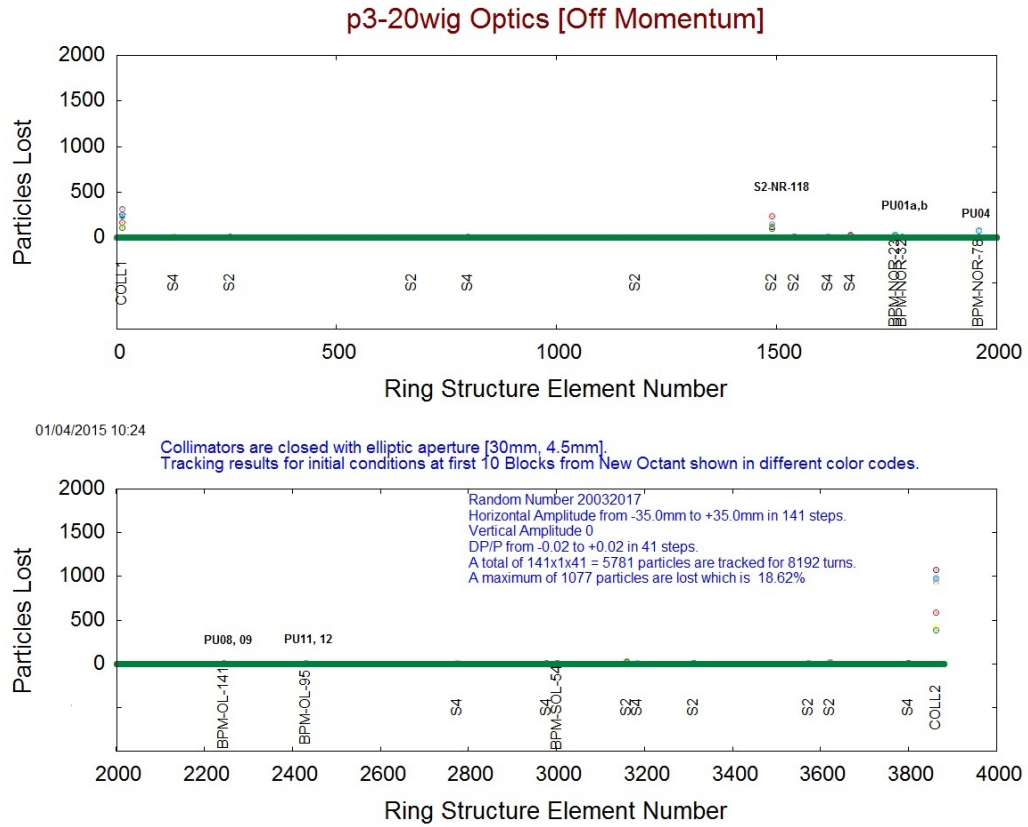


Figure 28b: Tracking results for off momentum ($\Delta P/P = -0.02$ to 0.02) particles with magnetic field errors tracked at 20 different longitudinal positions starting from New Octant for a single random number (Collimators are closed at 4.5 mm, maximum of 1077 particle lost at COLL2 which is 18.62%).

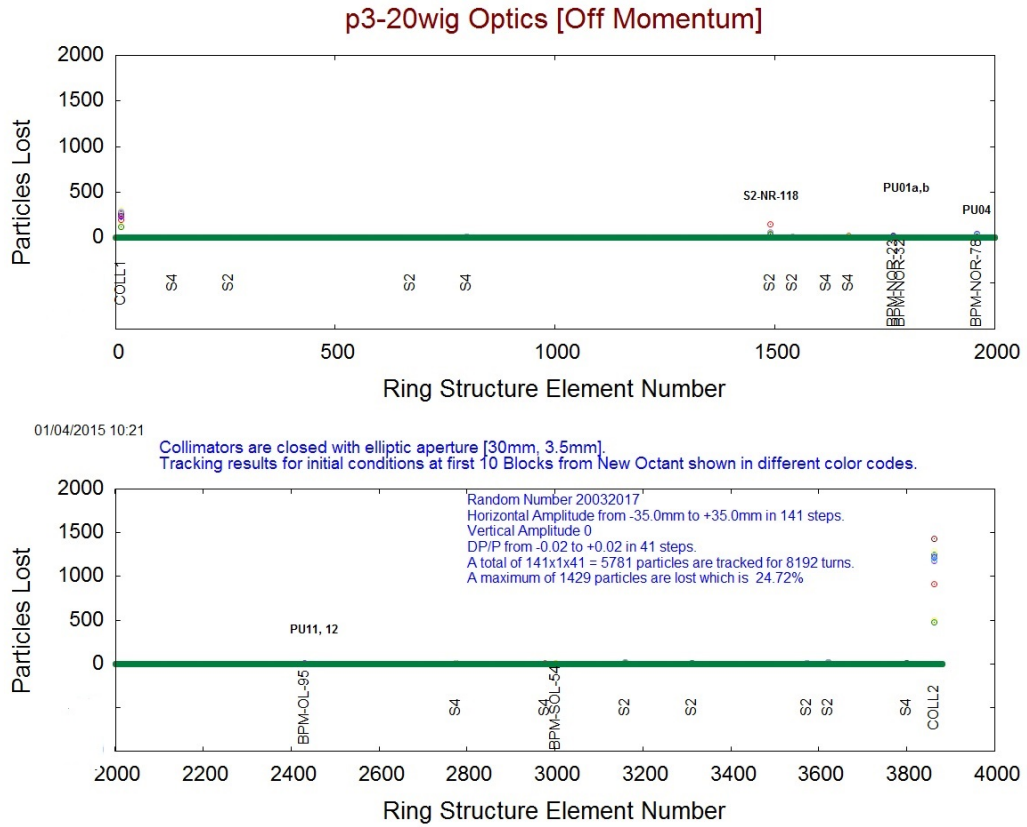


Figure 28c: Tracking results for off momentum ($\Delta P/P = -0.02$ to 0.02) particles with magnetic field errors tracked at 20 different structure element positions starting from New Octant for a single random number (Collimators are closed at 3.5 mm, maximum of 1429 particle lost at COLL2 which is 24.72%).

Table 1: Logbook entry on 22.01.2014 which is reproduced here along with tracking results.

Location	Rate [μ Sv]	Particles Lost
NR_118	100	456
WR_118	17	49
NWR_83	20	2
OR_118	9	
SOR_83	80	38

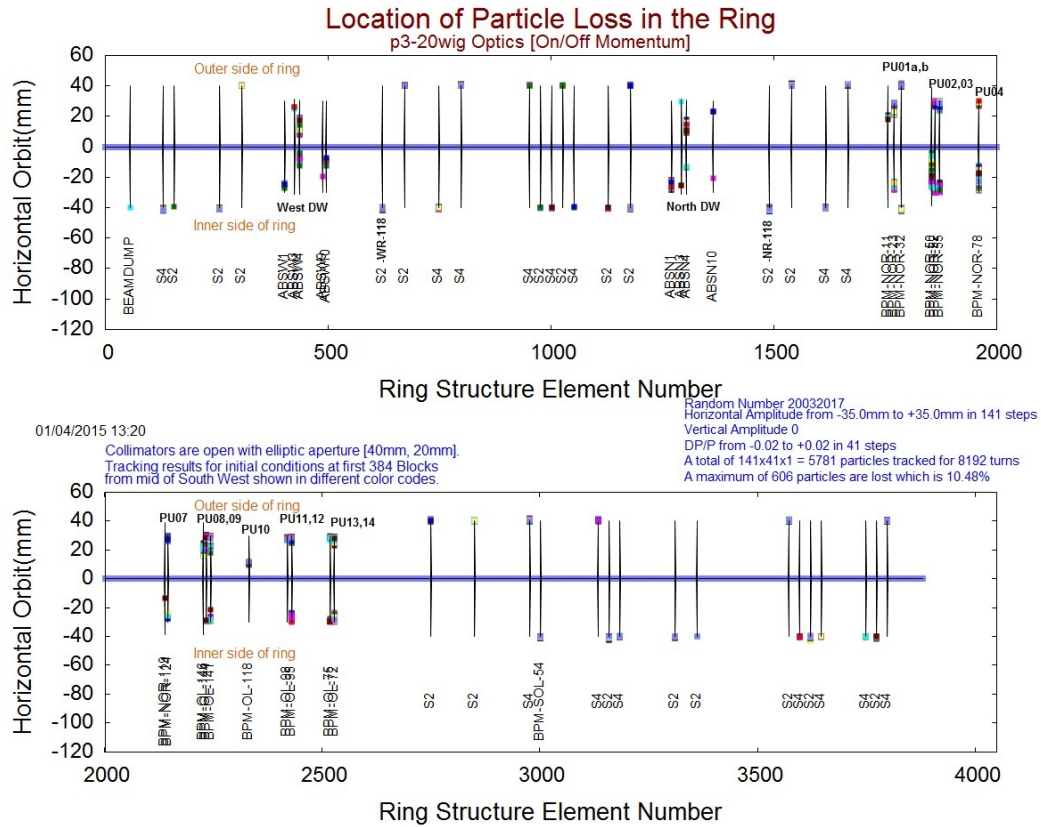


Figure 28d: Tracking results for off momentum ($\Delta P/P = -0.02$ to 0.02) particles with magnetic field errors tracked at 384 different longitudinal positions starting from south west for a single random number (Collimators are open). Here the end horizontal orbits are shown at loss points to indicate in/out side of the ring. The solid lines indicate the available physical apertures.

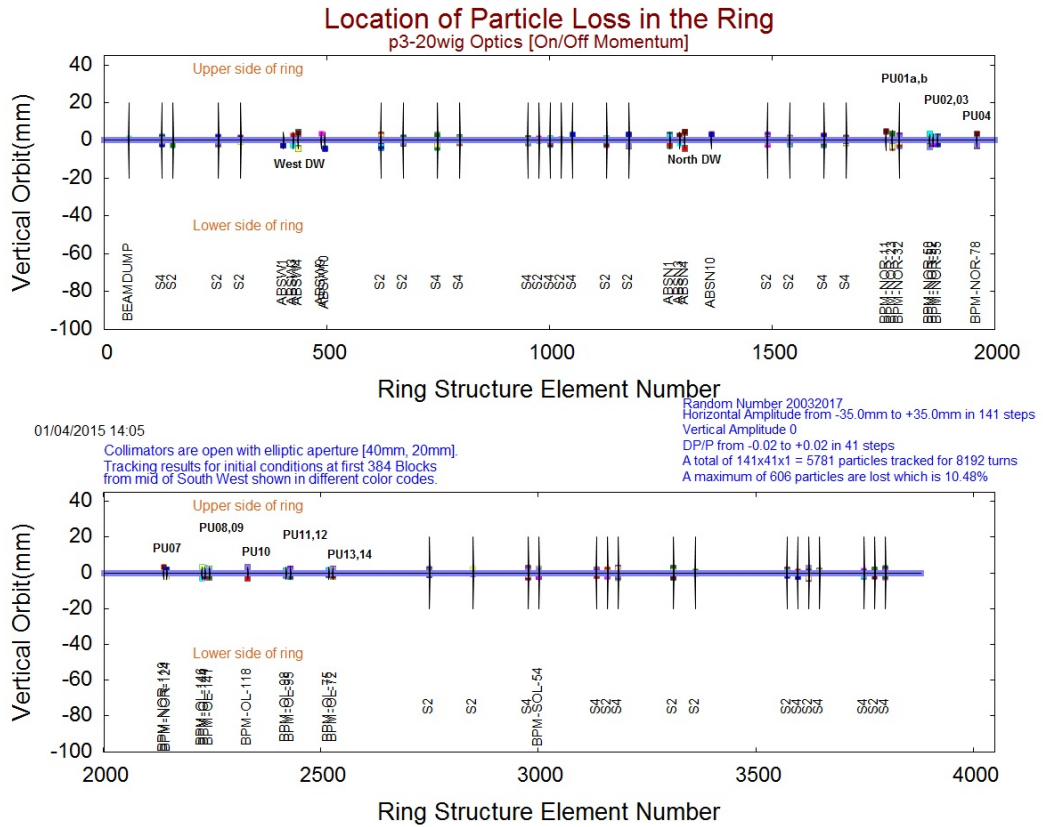


Figure 28e: Tracking results for off momentum ($\Delta P/P = -0.02$ to 0.02) 5781 particles with magnetic field errors tracked at 384 different longitudinal positions starting from south west for a single random number (Collimators are open). Here the end vertical orbits are shown at loss points to indicate up/down side of the ring. The solid lines indicate the available physical apertures.

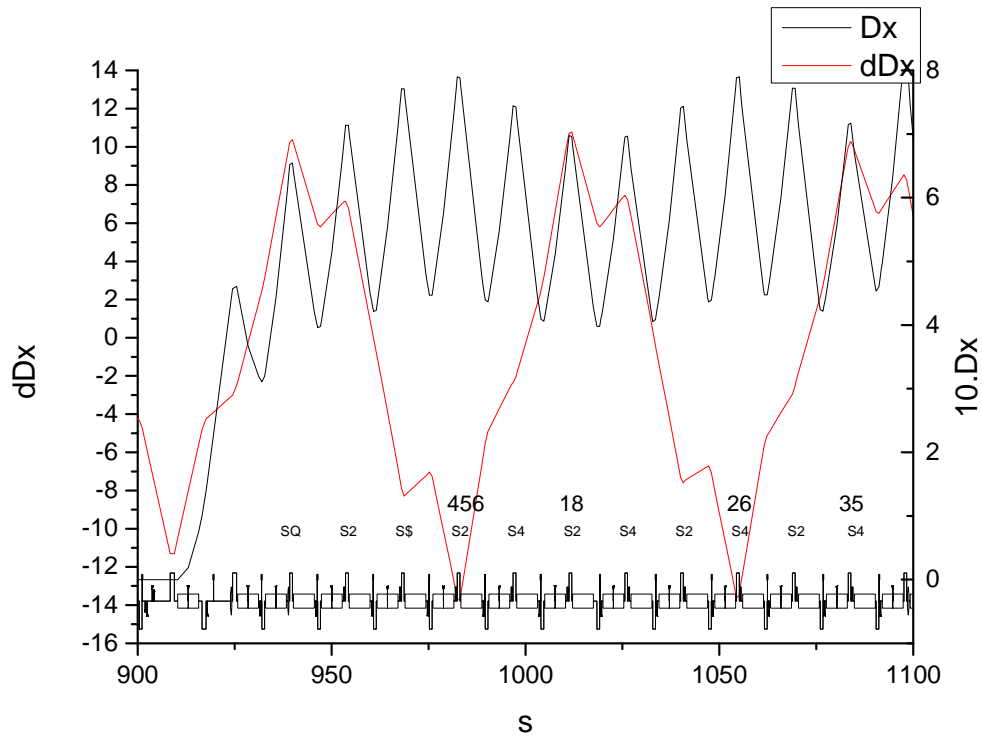


Figure 29: The horizontal dispersion function D_x magnified by a factor of 10 and its chromatic derivative dD_x plotted in the achromat section just after the north damping wiggler section for p3_20wig optics of PETRA III as computed by MAD-X. The particle losses from tracking simulations with SixTrack are shown along with the sextupole names.

In this achromat section some correlation is seen between the loss of particles in the tracking and the measured data in the PETRA tunnel that we have already mentioned above. But, as shown in the Figure 29, the losses are at high dispersion and its high chromatic derivative of D_x locations. For positive chromatic derivative D_x the loss is outside of the ring and for negative chromatic derivative D_x the loss is inner side of the ring. The radiation activation at S2_NR_118 which was measured in the inner side of the tunnel is corresponding to negative dD_x . At other sextupole locations S2, S4 and S4 the radiation activation is outside, inside and outside of the ring corresponding to positive or negative of dD_x . The loss of particles at S2_WR_118 and S2_SOR_83 is also at the inner side which is explained in a similar way.

2.4.6 Conclusions

Radiation damage of insertion devices is observed in several places of the PETRA III undulators. It follows a general pattern that devices located at the entrance of a straight section are damaged at the upstream end while undulators installed at the exit of a straight sections show signs of demagnetization at the downstream end. This seems to indicate that particle losses occur in the vertical plane at locations where the beta functions become large while the physical aperture limits are still very small. The tracking results showed the losses at the beam line positions where severe demagnetization had occurred confirming that this might have avoided by proper

collimation. The optics studies shows major contribution to the losses at the location of high a_y resulting from high b_y , which is nothing but higher beta beating with energy at very low physical aperture. So, one could say that the large beta beat for particles with energy deviation at the limiting vertical apertures in these straight sections are consistent with primarily off-momentum particle loss in those regions, supported by the measured indication of losses in those areas as Touschek scattered particles suffer large longitudinal momentum deviations. For a better protection the IDs against radiation damage additional collimators at high β_y values have been recently installed in April 2015.

2.4.7 Acknowledgements

The authors gratefully acknowledge and would like to thank Nicholas John Walker for reading the manuscript, suggestions to improve the content of the paper and constant encouragements and guidance. The authors also acknowledge and thank colleagues involved in measurements from FS-PE and M-Division for their fruitful contributions.

2.4.8 References

1. K. Balewski, W. Brefeld, et al., "PETRA III: A new high brilliance synchrotron radiation source at DESY", EPAC-2004, Lucerne, 2004, pp.2302-2304.
2. K. Balewski et al., "PETRA III, A low emittance Synchrotron Radiation Source", Technical Design Report, DESY 2004-035.
3. K. Balewski, M Bieler, et al., "PETRA III Upgrade", Proceedings of 2nd International Particle Accelerator Conference (IPAC11), San Sebastian, Spain, 4-9, September 2011, pp. 2948-2950.
4. N. Simos, P. K. Job, et al., "An experimental study of radiation-induced demagnetization of insertion device permanent magnets", BNL-81453-2008-CP, 2008.
5. J. Chavanne, P. Elleaume, et al., "Partial demagnetization of ID6 and dose measurements on certain IDs", ESRF Machine Technical Note 1-1996/ID, 1996.
6. E.R. Moog, P.K. DenHartog, et al., "Radiation doses to insertion devices at the advanced photon source", The 10th United States national conference on synchrotron radiation instrumentation. AIP Conference Proceedings, Volume 417, pp. 219-223 (1997).
7. P. Vagin, O. Bilani, et al., "Radiation Damage of Undulators at PETRA III", Proceedings of IPAC2014, Dresden, Germany, 2014.
8. P. Vagin, S. Francoual, J. Keil, O. H. Seeck, J. Stempfer, A. Schöps, M. Tischer "Commissioning Experience with Undulators at PETRA III", Proceeding of SRI2012, Lyon, July 2012, <http://iopscience.iop.org/1742-6596/425/3>
9. M. Tischer, P. Vagin, "Demagnetization Effects PETRA III Undulators", this Beam Dynamics Newsletter
10. F. Schmidt, "SixTrack User's Reference Manual", CERN/SL/94-56 (AP), CERN, Geneva, 2012.
11. A. Kling, R. Wanzenberg , "Beam Dynamics Activities at PETRA III", Published in ICFA Beam Dyn.Newslett.62, pp. 235-243, 2013.
12. W. Decking, O. Kaul, et al., "Treatment of wiggler and undulator field errors in tracking codes", IEEE PAC 1995, pp. 2874-2876.
13. A. Piwinski, "The Touschek Effect in Strong Focusing Storage Rings", DESY 98-179. 1998.
14. F. Wang, "Touschek Lifetime Calculations for the NSLS-II Electron Storage Ring", MIT-Bates Linear Accelerator Center, Middleton , MA 01949, 2006.

15. H. Grote, F. Schmidt, et al., “The MAD-X Program (User's Reference Manual)”, CERN, Geneva, 2015.
16. M. Borland, “elegant: A Flexible SDDS-compliant Code for Accelerator Simulation”, APS LS-287, September 2000.
17. K. Wittenburg, “The PIN-Diode Beam Loss Monitor System at HERA“, Proc. BIW2000, Cambridge, MA (2000).
18. W. Goettmann et al., "Beam Loss Position Monitor using Cerenkov Radiation in Optical Fibers", Proc. DIPAC 2005, Lyon, France (2005), POW026.
19. A. Kaukher et al., „XFEL Beam Loss Monitor Sytem“, Proc. BIW2012, Newport News, VA (2012) MOPG007.
20. A. Klett, A. Leuschner, „A Pulsed Neutron Monitor“, IEEE 2007 Nuclear Science Symposium, Conf. Records, Oct. 27 -Nov 3, 2007, Honolulu, Hawaii, US

3 Workshop and Conference Reports

3.1 ICFA Advanced Beam Dynamics Workshop “AOC2015” enables accelerator experts to meet optics challenges of future machines

M. Giovannozzi, R. Tomás, F. Zimmermann, CERN

Mail to: Massimo.Giovannozzi@cern.ch

About 50 experts attended the ICFA beam dynamics workshop on Advanced Optics Control (AOC) hosted at CERN in February 2015 (Thursday 5th and Friday 6th), in order to discuss the frontiers and future directions of accelerator optics control for colliders, light sources, and other specialized storage rings. The details of the program as well as a collection of all talks are available on the indico web site <http://indico.cern.ch/event/349643>

In addition to ICFA, the AOC workshop was also sponsored and supported by EuCARD-2 XBEAM, EuCARD-2 XRING, HIC for FAIR, ICFA, CERN PS MTE, HiLumi LHC, LIU, and CERN. The large number of sponsoring organizations reflects the importance of the topics addressed and their relevance for many future projects.

AOC2015 was the third workshop devoted to optics measurements, corrections, and control, following two earlier workshops organized in the frame of EuCARD-AccNet, i.e. the 2011 EuCARD-AccNet workshop on Optics Measurements, Corrections and Modeling for High-Performance Storage Rings (<http://indico.cern.ch/event/132526>) and the LHC Optics Measurement and Corrections review (<http://indico.cern.ch/event/246159>) in 2013.

One key topic of AOC2015 was the lessons from LHC Run-1 and the preparation for the LHC Run-2. Interesting new diagnostics and modelling approaches were reported from various state-of-the-art light sources. Optics challenges for future machines were also reviewed, including the High-Luminosity LHC, the Future Circular Colliders for hadron and leptons, new light sources like the ESRF upgrade, special storage rings dedicated to measuring the electric dipole moment of protons or deuterons.

The AOC2015 workshop was organized by CERN, together with GSI and FZ Jülich in Germany. The scientific program of the workshop had been set up following suggestions by an Organizing Committee composed of M. Bai (FZ Jülich), G. Franchetti (GSI), M. Giovannozzi (CERN), M. Lamont (CERN), R. Tomás CERN), and F. Zimmermann (CERN). Four scientific secretaries helped during the sessions A. Huschauer (TU Vienna & CERN), R. Martin (Humboldt U. Berlin & CERN), Ewen H. Maclean (Manchester U. & CERN), and Tobias Persson (CERN). Also the workshop secretary D. Rivoiron (CERN) should be acknowledged for a fantastic job. Among the 50 participants of AOC2015, 27 came from CERN, 1 from PSI in Switzerland, 3 from France, 7 from Germany, 1 from Japan, 1 from Russia, 2 from Spain, 5 from the UK, and 3 from the USA.

The program was composed of 24 oral contributions and addressed the following topics, corresponding to the four sessions: (1) Current and future colliders (RHIC, LHC, HiLumi LHC, FCC); (2) Advanced techniques (resonance driving terms, automatic tuning, resonance mapping, advanced diagnostics); (3) Lepton machines (SLS, SPEAR, ESRF upgrade, DIAMOND upgrade, SuperKEKB, FCC-ee, MICE); (4) Exotics (FNAL IOTA, EDM ring, PS islands, septum-less injection, fixed lines, nonlinear alpha buckets)

The talks and discussions at this workshop and the subsequent discussions have drawn attention to several critical issues. A few of the key highlights of the meeting are as follows:

- Excellent optics performance of the LHC is the result of advances in the understanding of beam optics, and improvements in the tools and methodologies available for measurement and control.
- LHC achieved a record low β beating for colliders, but the latter is still not as good as for light sources.
- β^* levelling has been successfully implemented at RHIC.
- Future machines like HL-LHC, upgrades of existing light sources, FCC etc. will require even better optics and orbit control; this is especially true for a proposed EDM storage ring.
- MOGA has become a preferred technique for optics control at many light sources.
- Chromatic and nonlinear corrections become ever more important.
- Nonlinear optics is being specifically designed and exploited, e.g. for multi-turn extraction (CERN PS), more stable dynamics (IOTA), septum-less extraction/injection, or bunch shortening.
- Close collaboration of accelerator physicists and computer scientists is essential for advancing the optics control of cutting-edge accelerators, as is illustrated by the remarkable progress at the LHC, compared with earlier colliders.
- AOC workshop brought together tools and expertise from around the world and has helped enabling the accelerator community to meet the challenges posed by current and future machines.

Advanced Optics Control Workshop

5-6 February 2015, CERN

The Advanced Optics Control workshop aims at reviewing recent advancements in optics measurement, correction, and understanding from colliders and synchrotrons around the world. This workshop may be regarded as the third of a series after the meeting in [OMCM \(2011\)](#) and [OMC \(2013\)](#).

Organizers

- Mei Bai
- Giuliano Franchetti
- Massimo Giovannozzi
- Mike Lamont
- Rogelio Tomas Garcia
- Frank Zimmermann

Secretary: Delphine Rivoiron

web site
<http://indico.cern.ch/e/AOC>

Logos on the right: HIC FAIR, ICFA, EUCARD², BEAM COLL, BEAM RING, OMC, CERN, and others.

Figure 1: Workshop poster. The background shows a detail of the AD ring at CERN combined with a drawing of Newton’s “Optics”. On the right, the logos of the workshop partners and sponsors are displayed, including EuCARD-2, XBEAM XCOLL and XBEAM XRING.



Figure 2: Photos of AOC2015 participants during a dinner on 5 February 2015.

4 Recent Doctorial Theses

4.1 Optics Design and Optimization of Electron Bunch Compressor Transfer Line (with a Case Study of CTF3 Bunch Compressor)

Amalendu Sharma

Mail to: amalendu@rrcat.gov.in

Graduation date: September 25, 2014
 Institution: Raja Ramanna Centre for Advanced Technology, Indore, India
 (Homi Bhabha National Institute, Mumbai, India)
 Supervisor: Prof. Pitambar Singh

Abstract:

CLIC (Compact Linear Collider) project at CERN is an upcoming electron positron collider in the TeV energy range. This collider will be based on high gradient linear accelerator operating at high RF frequency. Here, high RF frequency will be generated using an another electron beam known as “drive beam”. To demonstrate this scheme of acceleration, CTF3 (CLIC Test Facility 3) has been developed at CERN. The work carried out in the thesis is the beam optics design of a transfer line (Transfer Line-2) for CTF3 drive beam with the ability to compress the electron bunch length from 8.3 ps to ~ 1.5 ps, under the given constraints. The optics design covers a wide range of tuning in R_{56} parameter (-0.30 m to +0.30 m) with the constraints of utilization of available magnets and installation of the line in a given geometry of the pre existing building. At such short bunch length, second order effect, mainly T_{566} of the magnetic optics also become important. In order to correct T_{566} , a new sextupole scheme has been evolved and has been applied successfully in entire range of R_{56} tuning in this transfer line, keeping dilution in transverse emittance below 10%. Detailed simulation studies are carried out to quantify the effect of CSR on bunch length and transverse emittance in TL-2, which is found to be insignificant in the domain of operation of this line.

Thesis also consists of a study of different optics usually employed for bunch length compression. By including quadrupole magnets in chicane optics, tuning range of R_{56} is analyzed along with its chromatic behavior. Thesis also includes similar studies of two different arcs, in which beam at the exit is shifted parallel to the axis of the incoming beam.

In an optics, the magnetic element which contributes in R_{56} , mainly is a dipole magnet. Therefore, thesis also includes a detailed analysis of dipole magnets from beam optics point of view. An exact analytical expressions of transfer functions of a hard edge dipole magnet using a basic geometrical approach has been derived, which otherwise in literature is derived using complex higher order perturbation techniques. This new formulation shows that higher order effects are more pronounced in longitudinal plane and therefore have more importance for the optics of bunch compressors. Application of these expressions to chicane type bunch compressors

shows deviation in results for bunch length obtained using computer codes which simulate up to third order. This expression can be used in quick estimation of bunch length and emittance more accurately.

5 Forthcoming Beam Dynamics Events

5.1 The 9th International Accelerator School for Linear Colliders

The 9th International Accelerator School for Linear Colliders will take place at the **Delta Whistler Village Suites, Whistler, British Columbia, Canada from October 26 to November 6, 2015**. This school is a continuation of the series of schools which began nine years ago: Japan 2006, Italy 2007, United States 2008, China 2009, Switzerland 2010, United States 2011, India 2012 and Turkey 2013. The school is organized by the Linear Collider Collaboration (LCC) and the International Committee for Future Accelerators (ICFA) Beam Dynamics Panel. It will be hosted by TRIUMF and sponsored by a number of funding agencies and institutions around the world including the U.S. NSF, the U.S. DOE, Fermilab, SLAC, CERN, DESY, INFN, IHEP and RRCAT.

We will offer an 11-day program, including an excursion, a site visit to TRIUMF and an examination. There will be 8 days of lectures and 1/2 day for a joint session with the Linear Collider Workshop (which takes place at the same time and same town). The first 2-1/2 days will be an introductory course with an overview of future lepton colliders (ILC, CLIC and advanced accelerators) and XFEL, as well as introductions to linac and beam instrumentation basics. This will be followed by three elective courses in parallel, one on linear collider beam physics, one on linear collider technology, and the third one on XFEL. The XFEL is a new addition to this year's school. It is an important application of the ILC/CLIC technology. Each student is required to take the introductory course and one of the three electives. A complete program can be found on the school web site (www.linearcollider.org/school/2015/). There will be homework assignments and a final examination but no university credits.

We encourage young physicists (graduate students, post doctoral fellows, junior researchers) to apply. In particular we welcome those physicists who are considering changing to a career in accelerator physics and technology. This school uses an in-depth approach. An elective course on the XFEL has been added; therefore, former students are welcome to apply if they have a compelling reason to do so. The school will accept a maximum of 60 students from around the world. There will be a registration fee to cover local expenses (lodging, meals, excursion, local transportation, school supplies, etc.). Financial support for a limited number of students is available. Each applicant should complete the online registration form (which can be found on the school web site) and submit a curriculum vita as well as a letter of recommendation from his/her supervisor (in electronic form, either PDF or MS WORD). **The application deadline is August 20, 2015.**

Organizing Committee

Lyn Evans (CERN, Chair)
Alex Chao (SLAC)
Hesheng Chen (IHEP)
Weiren Chou (Fermilab)
Paul Grannis (Stony Brook U.)
P. D. Gupta (RRCAT)
Mike Harrison (BNL)
In Soo Ko (PAL)
Shin-ichi Kurokawa (KEK)
Hermann Schmickler (CERN)
Steinar Stapnes (CERN)
Nobuhiro Terunuma (KEK)
Nick Walker (DESY)

Curriculum Committee

Weiren Chou (Fermilab, Chair)
William Barletta (USPAS)
Alex Chao (SLAC)
Jie Gao (IHEP)
Shane Koscielniak (TRIUMF)
Srinivas Krishnagopal (BARC)
Lia Merminga (TRIUMF)
Carlo Pagani (Milano U. & INFN)
Joerg Rossbach (Hamburg U.)
Takayuki Saeki (KEK)
Hermann Schmickler (CERN)
Nobuhiro Terunuma (KEK)

Local Committee

Lia Merminga (TRIUMF, Chair)
Shane Koscielniak (TRIUMF)
Jana Thomson (TRIUMF)
G. Roy (TRIUMF)

Ninth International Accelerator School for Linear Colliders – Curriculum (v.2, 06/24/2015)

26 October – 6 November, 2015, Delta Whistler Village Suites, Whistler, British Columbia, Canada

Daily Schedule

Breakfast 07:30 – 09:00
 Morning 09:00 – 12:30, including 1/2-hour break
 Lunch 12:30 – 14:00
 Afternoon 14:00 – 17:30, including 1/2-hour break
 Tutorial & homework 17:30 – 18:30
 Dinner 19:00 – 20:00
 Tutorial & homework 20:00 – 22:00

List of Courses (black: required, red, blue and purple: elective)

	Morning	Afternoon	Evening
Mon 26 Oct		<i>Arrival, registration</i>	<i>Reception</i>
Tues 27 Oct	Introduction to science and XFEL	Introduction to science, ILC and CLIC	Tutorial & homework
Wed 28 Oct	Introduction to science and XFEL	Joint lecture: Linac basics	Tutorial & homework
Thurs 29 Oct	Joint lecture: Instrumentation basics	Course A: Linear collider physics Course B: Linear collider technology Course C: XFEL physics & technology	Tutorial & homework
Fri 30 Oct	<i>Excursion: TRUMF site visit and Vancouver sightseeing</i>		
Sat 31 Oct		Course A: Linear collider physics Course B: Linear collider technology Course C: XFEL physics & technology	Tutorial & homework
Sun 1 Nov		Course A: Linear collider physics Course B: Linear collider technology Course C: XFEL physics & technology	Tutorial & homework
Mon 2 Nov		Course A: Linear collider physics Course B: Linear collider technology Course C: XFEL physics & technology	Tutorial & homework
Tues 3 Nov		Course A: Linear collider physics Course B: Linear collider technology Course C: XFEL physics & technology	Tutorial & homework
Wed 4 Nov	Course A: Linear collider physics Course B: Linear collider technology Course C: XFEL physics & technology	Joint session with LCWS	Tutorial & homework
Thurs 5 Nov	Course A: Linear collider physics Course B: Linear collider technology Course C: XFEL physics & technology	Study time	Study time
Fri 6 Nov	Final exam	Free time	<i>Banquet;</i>
Sat 7 Nov	<i>Departure</i>		
			<i>Student Award Ceremony</i>

Program

	Tuesday, 27 October	Wednesday, 28 October	Thursday, 29 October	Friday, 30 October
Morning 09:00 – 12:30	<p>Welcome – <i>L. Merminiga (TRIUMF)</i> Introduction – <i>W. Chou (Fermilab)</i></p> <p>Lecture 11 – Introduction to linear colliders (1.5 hrs)</p> <p>Lecture 12 – ILC (3 hrs)</p>	<p>Lecture 14 – Introduction to XFEL (3 hrs)</p>	<p>Joint lecture AB2 – Instrumentation basics (3 hrs) <i>Hermann Schmickler (CERN)</i></p>	<p>Excursion: <i>TRIUMF site visit</i> <i>Vancouver sightseeing</i></p>
Afternoon 14:00 – 17:30	<p>Lecture 12 – ILC (cont'd)</p> <p>Lecture 13 – CLIC (1.5 hrs) <i>Frank Tecker (CERN)</i></p>	<p>Joint lecture AB1 – Linac basics (3 hrs) <i>Daniel Schulte (CERN)</i></p>	<p>Lecture A1 – Linac (9 hrs) <i>Daniel Schulte (CERN)</i></p> <p>Lecture B1 – NC RF (9 hrs) <i>Walter Wuensch (CERN)</i></p> <p>Lecture C1 – FEL theory (9 hrs)</p>	
Evening 19:00 – 22:00	Tutorial & homework	Tutorial & homework	Tutorial & homework	Tutorial & homework

Program (cont'd)

	Saturday, 31 October	Sunday, 1 November	Monday, 2 November	Tuesday, 3 November
Morning 09:00 – 12:30	Lecture A1 – Linac (cont'd) <i>Daniel Schulte (CERN)</i> Lecture B1 – NC RF (cont'd) <i>Walter Wuensch (CERN)</i> Lecture C1 – FEL theory (cont'd)	Lecture A2 – Sources (6 hrs) <i>Masao Kuriki (Hiroshima Univ.)</i> Lecture B2 – SC RF (12 hrs) <i>Takayuki Saeki (KEK)</i> Lecture C2 – FEL beam physics (9 hrs)	Lecture A3 – Damping rings (12 hrs) <i>Yannis Papaphillipou (CERN)</i> Lecture B2 – SC RF (cont'd) <i>Takayuki Saeki (KEK)</i> Lecture C2 – FEL beam physics (cont'd)	Lecture A3 – Damping rings (cont'd) <i>Yannis Papaphillipou (CERN)</i> Lecture B2 & C3b – Instrumentation (3 hrs) <i>Hermann Schmickler (CERN)</i>
Afternoon 14:00 – 17:30	Lecture A1 – Linac (cont'd) <i>Daniel Schulte (CERN)</i> Lecture B1 – NC RF (cont'd) <i>Walter Wuensch (CERN)</i> Lecture C1 – FEL theory (cont'd)	Lecture A2 – Sources (cont'd) <i>Masao Kuriki (Hiroshima Univ.)</i> Lecture B2 – SC RF (cont'd) <i>Takayuki Saeki (KEK)</i> Lecture C2 – FEL beam physics (cont'd)	Lecture A3 – Damping rings (cont'd) <i>Yannis Papaphillipou (CERN)</i> Lecture B2 – SC RF (cont'd) <i>Takayuki Saeki (KEK)</i> Lecture C3a – FEL technology: NC RF (3 hrs)	Lecture A3 – Damping rings (cont'd) <i>Yannis Papaphillipou (CERN)</i> Lecture B4 – LL/HP RF (9 hrs) <i>Stefan Simrock (ITER)</i> Lecture C3c – FEL technology: SC RF (3 hrs)
Evening 19:00 – 22:00	Tutorial & homework	Tutorial & homework	Tutorial & homework	Tutorial & homework
	Wednesday, 4 November	Thursday, 5 November	Friday, 6 November	Saturday, 7 November
Morning 09:00 – 12:30	Lecture A4 – BDS & beam-beam (6 hrs) <i>Andrei Seryi (John Adams Inst.)</i> Lecture B4 – LL/HP RF (cont'd) <i>Stefan Simrock (ITER)</i> Lecture C3d – FEL technology: undulators (3 hrs)	Lecture A4 – BDS & beam-beam (cont'd) <i>Andrei Seryi (John Adams Inst.)</i> Lecture B4 – LL/HP RF (cont'd) <i>Stefan Simrock (ITER)</i> Lecture C3e – FEL technology: seeding lasers (3 hrs)	08:00 – 12:30 Final exam (4.5 hrs)	Departure
Afternoon 14:00 – 17:30	Joint session with LCWS	Study time	Free time	
Evening 19:00 – 22:00	Tutorial & homework	Study time	Banquet at 19:00; Student Award Ceremony	

Notes on the Program:

1. There are a total of 11 school days in this year's program, excluding the arrival day (October 26) and the departure day (November 7). The time is divided as follows: 2-1/2 days for required courses, 5-1/2 days for elective courses, one day for excursion and site visit, 1/2 day for a joint session with the Linear Collider Workshop (LCWS), 1/2 day for study time and a final examination day.
2. The required course consists of six lectures: introduction, ILC, CLIC, XFEL, linac basics and instrumentation basics. Every student must take this course.
3. There are three elective courses: Course A (the red course) is linear collider beam physics, Course B (the blue course) is linear collider technology, and Course C (the purple course) is XFEL beam physics and technology. They will run in parallel. Each student will choose one of these.
4. The linear collider beam physics course consists of lectures on four topics: (1) linac, (2) sources, (3) damping rings, and (4) beam delivery system and beam-beam effects.
5. The linear collider technology course also consists of lectures on four topics: (1) normal conducting RF, (2) superconducting RF, (3) instrumentation, and (4) LLRF and high power RF.
6. The XFEL course is a new addition to this year's school. It has three parts: (1) FEL theory, (2) FEL beam physics, and (3) FEL technology, which consists of five 3-hour lectures: NC RF, SRF, instrumentation, undulators and seeding lasers.
7. There will be homework assignments, but homework is not counted in the grade. There will be a final examination. Some of the exam problems will be taken from variations of the homework assignments. The exam papers will be graded immediately after the exam and results announced in the evening of November 6 at the student award ceremony.
8. There is a tutorial and homework period every evening. It is part of the curriculum and students are required to attend. Lecturers will be available in the evening of their lecture day during this period.
9. Lecturers have been asked to cover the basics as well as possible. Their teaching material will be made available online to the students ahead of time (a few weeks prior to the school). Students are strongly encouraged to study this material prior to the beginning of the school.
10. Lecturers of the elective courses are required to provide lecture syllabus as soon as possible in order to help students make their selection.
11. All lecturers are responsible for the design of homework and exam problems as well as the answer sheet. They are also responsible for grading the exams.
12. The award ceremony will honor the top (~10) students based on their exam scores.

5.2 ICFA Mini-Workshop on "High Field Superconducting Magnets for *pp* Colliders"

An ICFA mini-workshop on "high field superconducting magnets for *pp* colliders" will be held at Shanghai Jiaotong University, Shanghai, China from **June 14th to 17th, 2015**. This workshop is motivated by the upcoming needs of the 20-T level accelerator magnets for recently proposed circular *pp* colliders, i.e., the Super proton proton Collider (SppC) and the Future Circular Collider (FCC). The purpose of this workshop is to review the present related technologies on high field accelerator magnets, with special emphasis on the high J_c Nb₃Sn and HTS conductors, the design study of the 20-T accelerator magnets and the fabrication methods of the high field coils and magnets. The R&D roadmap for the next years and possible collaborations between labs will be discussed, to make sure we are able to realize the 20-T dipole and quadrupole magnets in time. Any institutes or companies working on these issues are welcome to participate in this workshop, to give presentations, exchange information and to have fruitful discussions there.

The International Advisory Committee" for this workshop is listed below.

Naoyuki Amemiya (Kyoto U., Japan)
 Emanuela Barzi (FNAL, USA)
 Weiren Chou (FNAL, USA)
 Ramesh Gupta (BNL, USA)
 Steve Gourlay (LBNL, USA)
 Zhenghe Han (Tsinghua U., China)
 Guangli Kuang(HMFL, China)
 Vadim Kashikhin (FNAL, USA)
 Yijie Li (SJTU, China)
 Lizhen Ma (IMP, China)
 Toru Ogitsu (KEK, Japan)
 Qing Qin (IHEP, China)
 GianLuca Sabbi (LBNL, USA)
 Jingyu Tang (IHEP, China)
 Jiuqing Wang (IHEP, China)
 Peter Wanderer (BNL, USA)
 Guo Yan (WST, China)

5.3 The 37th International Free Electron Laser (FEL) Conference

The 37th International Free Electron Laser (FEL) conference is hosted by the Korea Atomic Energy Research Institute (KAERI) and the Pohang Accelerator Laboratory (PAL) and will be held in Daejeon, Korea, from **23th to 28th of August 2015**. The FEL conference series is dedicated to all scientific, technological, and user aspects of free-electron lasers. Detailed information on the conference is available and regularly updated on the conference website:

<http://www.qrc.or.kr/fel2015>

Registration will open in March 2015. An exhibition for companies with FEL related products and services, is an integral part of the conference.

The important dates are listed:

On-line registration : 9th Mar. - 12th Jun. (early), 13th Jun. -15th Aug. (Late)
 Student Grant request : No later than 5th Jun.
 Abstract Submission : 9th Mar. - 30th May.
 Paper Submission : No later than 21st Aug.

Further information about this exhibition is available on the conference website.

Conference chairs:

Nikolay A. Vinokurov and In Soo Ko

LOC chair: Y.U. Jeong

Contact:

kleegle@gmail.com

5.4 13th International Conference on Heavy Ion Accelerator Technology (HIAT2015)

The 13th International Conference on Heavy Ion Accelerator Technology will take place from **September 7-11, 2015** in Yokohama, Japan. Details for registering for the conference can be found on the conference web site at <http://www.rarf.riken.jp/hiat2015/registration.html>. In order to qualify for the early registration reduced fee the full payment must be received prior to 24:00 JST, July 1, 2015. Details for uploading of abstracts can be found on the conference web site at <http://www.rarf.riken.jp/hiat2015/author/abstract.html>. The abstract submission closing date is May 27, 2015. Information on financial support for students can be found at <http://www.rarf.riken.jp/hiat2015/program/student.html>.

Industry partners are invited to register as Exhibitors and/or Sponsors for the HIAT2015 conference. Details of the exhibition and sponsorship opportunities can be found at <http://www.rarf.riken.jp/hiat2015/sponsor/exhibitor.html> and <http://www.rarf.riken.jp/hiat2015/sponsor/sponsorship.html>, respectively.

HIAT2015 Conference Chair: Osamu Kamigaito

Conference website: <http://www.rarf.riken.jp/hiat2015/>

Conference email: hiat2015@ribf.riken

5.5 4th International Beam Instrumentation Conference (IBIC 2015)

The 4th International Beam Instrumentation Conference, IBIC 2015, will be held in Melbourne, Australia, from **13-17 September 2015**. Like its predecessors, BIW and DIPAC, this conference is dedicated to exploring the physics and engineering challenges of beam diagnostics and measurement techniques for charged particle accelerators.

Abstract submissions will be considered on the following topics:

- Overview and Commissioning
- BPMs and Beam Stability
- Time Resolved Diagnostics and Synchronization
- Beam Loss Detection
- Transverse Profile Monitors

- Beam Charge Monitors and Other Instruments
- Machine Parameter Measurements

IBIC 2015 is hosted by the Australian Synchrotron. The 3.5 day scientific program will include tutorials, invited orals, and contributed talks and three poster sessions. Following the conference there will be the opportunity for tours of the Australian Synchrotron light source.

An exhibition for vendors of beam instrumentation and diagnostics related products is an integral part of the conference. Further information about the industrial exhibition will be available on the conference website. Exhibitor registration opens on 21 April 2015 on a first-come, best-dressed basis.

All the necessary information on abstract submission and registration, paper preparation as well as travel and accommodation can be found on the conference website: <http://www.ibic2015.org>.

Chair of the IBIC2015 Program Committee: Mark Boland

5.6 The 17th International Conference on RF Superconductivity (SRF2015)

Registration is now available for SRF2015. The 17th International Conference on RF Superconductivity will take place from **September 13-18, 2015** in the Whistler Conference Centre in Whistler, British Columbia, Canada.

Details for registering for the conference can be found on the conference web site at <http://srf2015.triumf.ca/generalreg.html>.

Details for uploading abstracts can be found on the conference web site at <http://srf2015.triumf.ca/abstracts.html>. The abstract submission closing date is now June 15, 2015.

Following tradition, SRF2015 tutorial sessions will be held prior to the conference from Sept. 10-12 at the Delta Whistler Village Suites. Registration details can also be found at <http://srf2015.triumf.ca/generalreg.html>

SRF 2015 Conference Chair : Robert Laxdal,

Conference email: srf2015@conferences.triumf.ca

5.7 International Workshop on Beam Cooling and Related Topics (COOL'15)

The COOL'15 - International Workshop on Beam Cooling and Related Topics, will take place at Thomas Jefferson National Accelerator Facility (Jefferson Lab), Newport News, Virginia, USA, **September 28 to October 3, 2015**. This is the 10th workshop in the series that was first held at Karlsruhe, Germany in 1984 and has been a bi-annual event since 1999.

The COOL'15 workshop will highlight the latest developments in the field of particle beam cooling, including:

- Electron cooling
- Stochastic cooling
- Laser cooling
- Muon cooling
- Optical Stochastic cooling and coherent electron cooling

- Storage and cooling of particles in antiproton and heavy ion traps
- Other methods of phase space manipulation
- Cooled beam dynamics

It will provide a perfect opportunity for accelerator physicists, engineers and students to meet and interact in a quiet and relaxed environment. The oral (invited and contributed) and poster sessions will be organized for the workshop. The proceedings will be published electronically on the JACoW site.

Workshop Co-Chairs: Yaroslav Derbenev (derbenev@jlab.org)

Yuhong Zhang (yzhang@jlab.org)

Workshop website: <https://www.jlab.org/conferences/cool15/index.html>

5.8 12th International Computational Accelerator Physics Conference (ICAP'15)

The 12th International Computational Accelerator Physics Conference, ICAP'15, will take place in Shanghai, China, from **October 12 to 16, 2015**. ICAP'15 is jointly organized by the the Shanghai Institute of Applied Physics (SINAP), SLAC National Accelerator Laboratory (SLAC) and Tsinghua University, and SINAP is the host of the conference.

Conference website:

<http://icap2015.csp.escience.cn>

The ICAP'15 conference follows the series of meetings in La Jolla, USA (1988), Los Alamos, USA (1990), Pleasanton, USA (1993), Williamsburg, USA (1996), Monterey, USA (1998), Darmstadt, Germany (2000), East Lansing, USA (2002), St. Petersburg, Russia (2004), Chamonix, France (2006), San Francisco, USA (2009) and Rostock-Warnemunde, Germany (2012).

ICAP'15 will focus on advances in Computational Accelerator Physics and their application to existing machines and future facilities. It will provide a forum and the opportunity for researchers in modeling and simulation to exchange information and discuss new ideas that benefit a wide area of accelerator science and technology. Topics of interest will include, but not be limited to, computational needs and challenges, beam dynamics and electromagnetic field calculations, code development and validation, data processing and visualization, high performance computing as well as emerging technologies that will impact computing for accelerator design.

The Scientific Program for ICAP'15 will consist of invited and contributed oral, and poster presentations, representing the computational efforts in accelerator physics worldwide. ICAP is a JACoW conference and JACoW's Scientific Programme Management System (SPMS) will be open for abstract submission in the coming weeks. The deadline for abstract submission is: July 15, 2015.

ICAP'15 Co-Chairs: Zhentang Zhao, SINAP

Kwok Ko, SLAC

Chuanxiang Tang, Tsinghua University

6 Announcements of the Beam Dynamics Panel

6.1 ICFA Beam Dynamics Newsletter

6.1.1 Aim of the Newsletter

The ICFA Beam Dynamics Newsletter is intended as a channel for describing unsolved problems and highlighting important ongoing works, and not as a substitute for journal articles and conference proceedings that usually describe completed work. It is published by the ICFA Beam Dynamics Panel, one of whose missions is to encourage international collaboration in beam dynamics.

Normally it is published every April, August and December. The deadlines are 15 March, 15 July and 15 November, respectively.

6.1.2 Categories of Articles

The categories of articles in the newsletter are the following:

1. Announcements from the panel.
2. Reports of beam dynamics activity of a group.
3. Reports on workshops, meetings and other events related to beam dynamics.
4. Announcements of future beam dynamics-related international workshops and meetings.
5. Those who want to use newsletter to announce their workshops are welcome to do so. Articles should typically fit within half a page and include descriptions of the subject, date, place, Web site and other contact information.
6. Review of beam dynamics problems: This is a place to bring attention to unsolved problems and should not be used to report completed work. Clear and short highlights on the problem are encouraged.
7. Letters to the editor: a forum open to everyone. Anybody can express his/her opinion on the beam dynamics and related activities, by sending it to one of the editors. The editors reserve the right to reject contributions they judge to be inappropriate, although they have rarely had cause to do so.

The editors may request an article following a recommendation by panel members. However anyone who wishes to submit an article is strongly encouraged to contact any Beam Dynamics Panel member before starting to write.

6.1.3 How to Prepare a Manuscript

Before starting to write, authors should download the template in Microsoft Word format from the Beam Dynamics Panel web site:

<http://www-bd.fnal.gov/icfabd/news.html>

It will be much easier to guarantee acceptance of the article if the template is used and the instructions included in it are respected. The template and instructions are expected to evolve with time so please make sure always to use the latest versions.

The final Microsoft Word file should be sent to one of the editors, preferably the issue editor, by email.

The editors regret that LaTeX files can no longer be accepted: a majority of contributors now prefer Word and we simply do not have the resources to make the conversions that would be needed. Contributions received in LaTeX will now be returned to the authors for re-formatting.

In cases where an article is composed entirely of straightforward prose (no equations, figures, tables, special symbols, etc.) contributions received in the form of plain text files may be accepted at the discretion of the issue editor.

Each article should include the title, authors' names, affiliations and e-mail addresses.

6.1.4 Distribution

A complete archive of issues of this newsletter from 1995 to the latest issue is available at

<http://icfa-usa.jlab.org/archive/newsletter.shtml>.

This is now intended as the primary method of distribution of the newsletter.

Readers are encouraged to sign-up for electronic mailing list to ensure that they will hear immediately when a new issue is published.

The Panel's Web site provides access to the Newsletters, information about future and past workshops, and other information useful to accelerator physicists. There are links to pages of information of local interest for each of the three ICFA areas.

Printed copies of the ICFA Beam Dynamics Newsletters are also distributed (generally some time after the Web edition appears) through the following distributors:

Weiren Chou	chou@fnal.gov	North and South Americas
Rainer Wanzenberg	rainer.wanzenberg@desy.de	Europe ⁺⁺ and Africa
Toshiyuki Okugi	toshiyuki.okugi@kek.jp	Asia ^{**} and Pacific

⁺⁺ Including former Soviet Union.

^{**} For Mainland China, Jiu-Qing Wang (wangjq@mail.ihep.ac.cn) takes care of the distribution with Ms. Su Ping, Secretariat of PASC, P.O. Box 918, Beijing 100039, China.

To keep costs down (remember that the Panel has no budget of its own) readers are encouraged to use the Web as much as possible. In particular, if you receive a paper copy that you no longer require, please inform the appropriate distributor.

6.1.5 Regular Correspondents

The Beam Dynamics Newsletter particularly encourages contributions from smaller institutions and countries where the accelerator physics community is small. Since it is impossible for the editors and panel members to survey all beam dynamics activity worldwide, we have some Regular Correspondents. They are expected to find interesting activities and appropriate persons to report them and/or report them by themselves. We hope that we will have a "compact and complete" list covering all over the world eventually. The present Regular Correspondents are as follows:

Liu Lin	Liu@ns.lnls.br	LNLS Brazil
---------	--	-------------

Sameen Ahmed Khan
Jacob Rodnizki
Rohan Dowd

Rohelakan@yahoo.com
Jacob.Rodnizki@gmail.com
Rohan.Dowd@synchrotron.org.au

SCOT, Oman
Soreq NRC, Israel
Australian Synchrotron

We are calling for more volunteers as Regular Correspondents.

6.2 ICFA Beam Dynamics Panel Members

Name	eMail	Institution
Rick Baartman	baartman@lin12.triumf.ca	TRIUMF, 4004 Wesbrook Mall, Vancouver, BC, V6T 2A3, Canada
Marica Biagini	marica.biagini@lnf.infn.it	INFN-LNF, Via E. Fermi 40, C.P. 13, Frascati, Italy
John Byrd	jmbyrd@lbl.gov	Center for Beam Physics, LBL, 1 Cyclotron Road, Berkeley, CA 94720-8211, U.S.A.
Yunhai Cai	yunhai@slac.stanford.edu	SLAC, 2575 Sand Hill Road, MS 26 Menlo Park, CA 94025, U.S.A.
Swapan Chattopadhyay	swapan@cockcroft.ac.uk	The Cockcroft Institute, Daresbury, Warrington WA4 4AD, U.K.
Weiren Chou (Chair)	chou@fnal.gov	Fermilab, MS 220, P.O. Box 500, Batavia, IL 60510, U.S.A.
Wolfram Fischer	wfischer@bnl.gov	Brookhaven National Laboratory, Bldg. 911B, Upton, NY 11973, U.S.A.
Yoshihiro Funakoshi	yoshihiro.funakoshi@kek.jp	KEK, 1-1 Oho, Tsukuba-shi, Ibaraki-ken, 305-0801, Japan
Jie Gao	gaoj@ihep.ac.cn	Institute for High Energy Physics, P.O. Box 918, Beijing 100039, China
Ajay Ghodke	ghodke@cat.ernet.in	RRCAT, ADL Bldg. Indore, Madhya Pradesh, 452 013, India
Ingo Hofmann	i.hofmann@gsi.de	High Current Beam Physics, GSI Darmstadt, Planckstr. 1, 64291 Darmstadt, Germany
Sergei Ivanov	sergey.ivanov@ihep.ru	Institute for High Energy Physics, Protvino, Moscow Region, 142281 Russia
In Soo Ko	isko@postech.ac.kr	Pohang Accelerator Lab, San 31, Hyoja-Dong, Pohang 790-784, South Korea
Elias Metral	elias.metral@cern.ch	CERN, CH-1211, Geneva 23, Switzerland
Yoshiharu Mori	mori@rri.kyoto-u.ac.jp	Research Reactor Inst., Kyoto Univ. Kumatori, Osaka, 590-0494, Japan
George Neil	neil@jlab.org	TJNAF, 12000 Jefferson Ave., Suite 21, Newport News, VA 23606, U.S.A.
Toshiyuki Okugi	toshiyuki.okugi@kek.jp	KEK, 1-1 Oho, Tsukuba-shi, Ibaraki-ken, 305-0801, Japan
Mark Palmer	mapalmer@fnal.gov	Fermilab, MS 221, P.O. Box 500, Batavia, IL 60510, U.S.A.
Chris Prior	chris.prior@stfc.ac.uk	ASTeC Intense Beams Group, STFC RAL, Chilton, Didcot, Oxon OX11 0QX, U.K.
Yuri Shatunov	Yu.M.Shatunov@inp.nsk.su	Acad. Lavrentiev, Prospect 11, 630090 Novosibirsk, Russia
Jiu-Qing Wang	wangjq@ihep.ac.cn	Institute for High Energy Physics, P.O. Box 918, 9-1, Beijing 100039, China
Rainer Wanzenberg	rainer.wanzenberg@desy.de	DESY, Notkestrasse 85, 22603 Hamburg, Germany

*The views expressed in this newsletter do not necessarily coincide with those of the editors.
The individual authors are responsible for their text.*